AD/A-003 582

RESEARCH ON MOLECULAR LASERS

G. J. Wolga, et al

Cornell University

Prepared for:

Office of Naval Research
Advanced Research Projects Agency

November 1974

DOCUMENT CONTROL DATA - R&D

(Security classification of title, body of abstract and indexing annotation must be entered when the overall report is classified)

1. ORIGINATING ACTIVITY (Corporate author)	2a. REPORT SECURITY CLASSIFICATION
Cornell University Ithaca, N.Y. 14850	Unclassified
	2b. GROUP N/A

3. REPORT TITLE

STUDY OF MOLECULAR LASERS

4. DESCRIPTIVE NOTES *(Type of report and inclusive dates)*

Annual Report - 1974

5. AUTHOR(S) *(Last name, first name, initial)*

G.J. Wolga
Simon H. Bauer

Ross A. McFarlane
T.A. Cool

6. REPORT DATE	7a. TOTAL NO. OF PAGES	7b. NO. OF REFS
November 1974	112	31

8a. CONTRACT OR GRANT NO. N00014-67-A-0077-0006	9a. ORIGINATOR'S REPORT NUMBER(S) N/A
b. PROJECT NO.	
c.	9b. OTHER REPORT NO(S) (Any other numbers that may be assigned this report) N/A
d.	

10. AVAILABILITY/LIMITATION NOTICES

11. SUPPLEMENTARY NOTES	12. SPONSORING MILITARY ACTIVITY
	Office of Naval Research

13. ABSTRACT

Research concerning molecular and chemical lasers was conducted in the following areas:

1. Measurement of vibrational energy transfer rates in the HF, DF, HF-DF, HF-CO_2, and DF-CO_2 systems over the temperature range 200-350K.

2. Experimental design and testing of experiments to measure vibration to rotation energy transfer in HF.

3. Vibrational relaxation measurements at T = 300K of HF(v=1), DF(v=1) and $CO_2(00°1)$ by atoms including H,D,O,N,F,Cl, and Br.

4. Vibrational relaxation measurements at T = 300K of CO(v=1) by atoms with initial work centering on oxygen atoms.

5. Chemical laser studies in the following areas:
   a) Bending mode relaxation of CO_2
   b) Computer model for the CS_2-O_2-He chemical laser
   c) Alternate hydrogen sources for HF and DF lasers
   d) Laser heating initiated chemical reactions
   e) CO v=1-0 pulsed chemical laser
   f) C_3O_2 + O_2 + He chemical CO laser
   g) Model for the C_3O_2 + O_2 + He laser
   h) Laser initiated reactions in mixtures of B_2H_6

Security Classification

14. KEY WORDS	LINK A		LINK B		LINK C	
	ROLE	WT	ROLE	WT	ROLE	WT
Molecular Lasers						
Chemical Lasers						
Vibrational Relaxation						
Energy Transfer						
Chemical Reaction Rates						
Vibrational Energy Transfer						
CO Chemical Lasers						

INSTRUCTIONS

1. ORIGINATING ACTIVITY: Enter the name and address of the contractor, subcontractor, grantee, Department of Defense activity or other organization (*corporate author*) issuing the report.

2a. REPORT SECURITY CLASSIFICATION: Enter the overall security classification of the report. Indicate whether "Restricted Data" is included. Marking is to be in accordance with appropriate security regulations.

2b. GROUP: Automatic downgrading is specified in DoD Directive 5200.10 and Armed Forces Industrial Manual. Enter the group number. Also, when applicable, show that optional markings have been used for Group 3 and Group 4 as authorized.

3. REPORT TITLE: Enter the complete report title in all capital letters. Titles in all cases should be unclassified. If a meaningful title cannot be selected without classification, show title classification in all capitals in parenthesis immediately following the title.

4. DESCRIPTIVE NOTES: If appropriate, enter the type of report, e.g., interim, progress, summary, annual, or final. Give the inclusive dates when a specific reporting period is covered.

5. AUTHOR(S): Enter the name(s) of author(s) as shown on or in the report. Enter last name, first name, middle initial. If military, show rank and branch of service. The name of the principal author is an absolute minimum requirement.

6. REPORT DATE: Enter the date of the report as day, month, year; or month, year. If more than one date appears on the report, use date of publication.

7a. TOTAL NUMBER OF PAGES: The total page count should follow normal pagination procedures, i.e., enter the number of pages containing information.

7b. NUMBER OF REFERENCES: Enter the total number of references cited in the report.

8a. CONTRACT OR GRANT NUMBER: If appropriate, enter the applicable number of the contract or grant under which the report was written.

8b, 8c, & 8d. PROJECT NUMBER: Enter the appropriate military department identification, such as project number, subproject number, system numbers, task number, etc.

9a. ORIGINATOR'S REPORT NUMBER(S): Enter the official report number by which the document will be identified and controlled by the originating activity. This number must be unique to this report.

9b. OTHER REPORT NUMBER(S): If the report has been assigned any other report numbers (*either by the originator or by the sponsor*), also enter this number(s).

10. AVAILABILITY/LIMITATION NOTICES: Enter any limitations on further dissemination of the report, other than those imposed by security classification, using standard statements such as:

   (1) "Qualified requesters may obtain copies of this report from DDC."

   (2) "Foreign announcement and dissemination of this report by DDC is not authorized."

   (3) "U. S. Government agencies may obtain copies of this report directly from DDC. Other qualified DDC users shall request through
_____."

   (4) "U. S. military agencies may obtain copies of this report directly from DDC. Other qualified users shall request through
_____."

   (5) "All distribution of this report is controlled. Qualified DDC users shall request through
_____."

If the report has been furnished to the Office of Technical Services, Department of Commerce, for sale to the public, indicate this fact and enter the price, if known.

11. SUPPLEMENTARY NOTES: Use for additional explanatory notes.

12. SPONSORING MILITARY ACTIVITY: Enter the name of the departmental project office or laboratory sponsoring (*paying for*) the research and development. Include address.

13. ABSTRACT: Enter an abstract giving a brief and factual summary of the document indicative of the report, even though it may also appear elsewhere in the body of the technical report. If additional space is required, a continuation sheet shall be attached.

It is highly desirable that the abstract of classified reports be unclassified. Each paragraph of the abstract shall end with an indication of the military security classification of the information in the paragraph, represented as (TS), (S), (C), or (U).

There is no limitation on the length of the abstract. However, the suggested length is from 150 to 225 words.

14. KEY WORDS: Key words are technically meaningful terms or short phrases that characterize a report and may be used as index entries for cataloging the report. Key words must be selected so that no security classification is required. Identifiers, such as equipment model designation, trade name, military project code name, geographic location, may be used as key words but will be followed by an indication of technical context. The assignment of links, roles, and weights is optional.
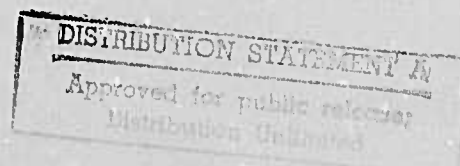
028179

RESEARCH ON MOLECULAR LASERS

ANNUAL REPORT
1 November, 1974

Cornell University
Ithaca, N.Y. 14853

Sponsored by:

Advanced Research Projects Agency

ARPA Order No. 660

Reporting Period

1 October 1973 - 30 September 1974

1. ARPA Order	660
2. Program Code Number	0173-7-006252
3. Name of Contractor	Cornell University
4. Effective Date of Contract	1 October 1968
5. Contract Expiration Date	30 September 1974
6. Amount of Contract for Current Period	$170,000
7. Contract Number	N00014-67-A-0077-0006
8. Principal Investigator	Professor G.J. Wolga
9. Telephone Number	(607)-256-3962
10. Project Scientists	Professor S.H. Bauer (607)-256-4028
	Professor T.A. Cool (607)-256-4191
	Professor R.A. McFarlane (607)-256-4075
11. Title of Work	RESEARCH ON MOLECULAR LASERS

Sponsored by

ADVANCED RESEARCH PROJECTS AGENCY

ARPA Order No. 660

The views and conclusions contained in this document are those of the authors and should not be interpreted as necessarily representing the official policies, either expressed or implied, of the Advanced Research Projects Agency or the U.S. Government.

Technical Report Summary

This report describes research conducted at Cornell University on molecular and chemical lasers. The objective of this work has been to provide precise, quantitative information concerning: the rates with which vibrational and rotational molecular energy in important laser molecules is transferred to other molecules and relaxed by collisions with atoms; the investigation of mechanisms in chemical laser excitation and the development of accurate models for important chemical laser systems; research on new chemical laser systems.

The methodology employed consisted of: laboratory experiments utilizing laser induced fluorescence to study molecular relaxation and energy transfer; double resonance experiments to study vibration to rotation energy transfer; chemical laser initiation and pumping by electrical discharges in gases and by volumetric heating of gas mixtures with external lasers; literature survey of known reaction rates appropriate to the modelling of a chemical laser system; computer code development for selected chemical lasers.

Specific technical results obtained were:

1. Vibrational energy transfer rates in the HF, DF, HF-DF, $HF-CO_2$ and $DF-CO_2$ systems over the temperature range 200-350K.

2. Vibrational relaxation rates of HF(v=1) by H, D, O, F, Cl, and Br atoms at T = 300K.

3. Vibrational relaxation rates of $CO_2(00°1)$ by H,O,N,F,cl atoms at T=300K.

4. Vibrational relaxation rate of CO(v=1) by O atoms at T=300K.

5. Vibrational relaxation rates of $CO_2(010)$ by CO_2, N_2 and He.

6. A computer model for the CS_2-O_2-He chemical laser.

7. A model for the $C_3O_2-O_2$-He CO chemical laser.

8. Development of a CO v=1-0 pulsed chemical laser.

The studies of vibrational relaxation by atoms provide the first comprehensive data for the HF, CO_2 and CO lasers. To accomplish this a new experimental technique, microwave paramagnetic resonance of atoms, was added to the laser induced fluorescence method to enable accurate determination of atom concentration to be made in the low temperature region appropriate to laser operation. These results should be extended over a range of temperature to assist the development of adequate theories to explain these important processes.

The rates experimentally determined in these studies can be directly utilized in the comprehensive modeling that is required for the development and scaling of important high power chemical and molecular lasers.
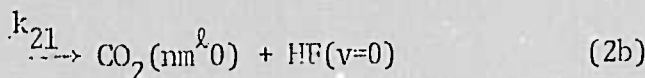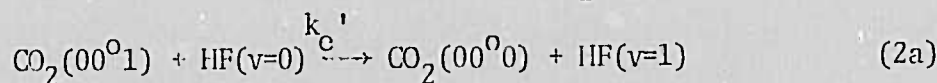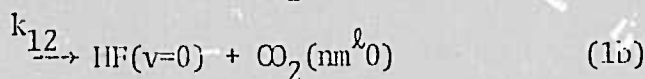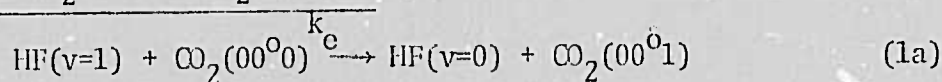
INDEX

ARPA Final Report

Professor T.A. Cool

Two primary tasks have been performed during the period from 10-1-73 to 9-30-74. Laser-induced fluorescence measurements of vibrational energy transfer rates for the HF, DF, HF-DF, HF-CO_2, and DF-CO_2 systems have been performed over the temperature range from 200 to 350°K to extend our previous work in the range from 300-700°K. A second investigation has been the design and preliminary testing of a sophisticated experiment designed to measure vibration to rotation energy transfer rates in HF. Progress on each of these tasks is summarized in the following.
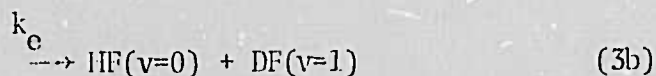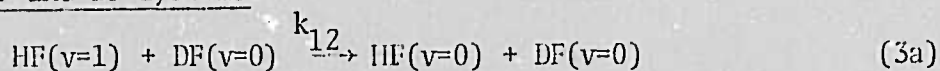
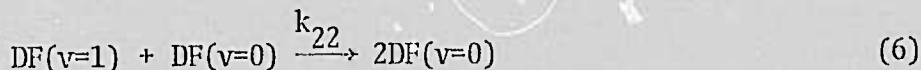## I. Low Temperature Vibrational Relaxation Rate Measurements

The measured rate constants for the HF, DF, HF-DF, HF-CO_2 and DF-CO_2 systems are summarized in Table and Figures 1 and 2. This work is in preparation for publication in the Journal of Chemical Physics. The rate constants and probabilities refer to the processes:

A. HF-CO_2 and DF-CO_2 Systems:

$$HF(v=1) + CO_2(00^00) \xrightarrow{k_e} HF(v=0) + CO_2(00^01) \qquad (1a)$$

$$\xrightarrow{k_{12}} HF(v=0) + CO_2(nm^\ell0) \qquad (1b)$$

$$CO_2(00^01) + HF(v=0) \xrightarrow{k_e'} CO_2(00^00) + HF(v=1) \qquad (2a)$$

$$\xrightarrow{k_{21}} CO_2(nm^\ell0) + HF(v=0) \qquad (2b)$$

B. HF and DF Systems:

$$HF(v=1) + DF(v=0) \xrightarrow{k_{12}} HF(v=0) + DF(v=0) \qquad (3a)$$

$$\xrightarrow{k_e} HF(v=0) + DF(v=1) \qquad (3b)$$

$$HF(v=1) + HF(v=0) \xrightarrow{k_{11}} 2HF(v=0) \qquad (4)$$

$$DF(v=1) + HF(v=0) \xrightarrow{k_{21}} DF(v=0) + HF(v=0) \qquad (5a)$$

$$\xrightarrow{k'_e} DF(v=0) + HF(v=1) \qquad (5b)$$

$$DF(v=1) + DF(v=0) \xrightarrow{k_{22}} 2DF(v=0) \qquad (6)$$
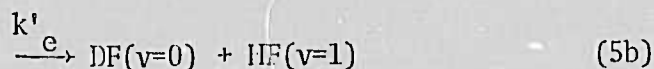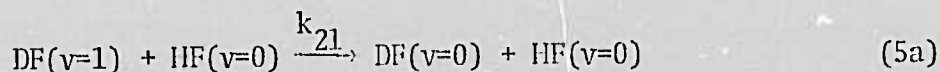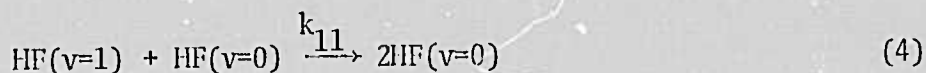
Two important features of the experimental data should be noted. Figures 1 and 2 reveal that the probabilities have inverse temperature dependences approximately described by the relationship $P \propto T^{-n}$ where $1.25 \lesssim n \lesssim 2.0$. Secondly, at the lowest temperatures (200-220°K) the influence of polymers of the HF and DF was easily discernable. The rates for deactivation by HF dimers and tetramers are very large and dominate other processes in the temperature range from 200 to 220°K. It was possible to separate out the contribution from the monomer in each case; the data of Table I and Figs.1 and 2 include only the monomer effects.

II. Vibration to Rotation Energy Transfer in HF

Apparatus are being assembled for a double-resonance experiment designed to measure the rates for vibration to rotation energy transfer in HF. The processes of interest are

$$HF(v=1,J_1) + HF(v=0,J_2) \rightarrow HF(v=0,J_1') + HF(v=0,J_2'). \qquad (7)$$
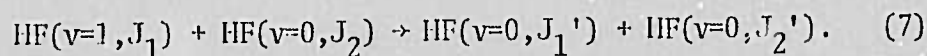
The experiment consists of the use of one HF laser to pump the $HF(v=1,J_1)$ molecules in less than 500 nanoseconds and the use of a second probe laser to monitor the populations of $HF(v=0,J_1')$ and $HF(v=0,J_2')$ at later times.

Figure 3 illustrates the experimental technique. The detection of R-branch fluorescence in process (9b) (below) provides the means for

TABLE I

Rate Constant Measurements for $HF-CO_2$ and $DF-CO_2$ Mixtures

Rate Constants ($10^4 sec^{-1} Torr^{-1}$), and Probabilities

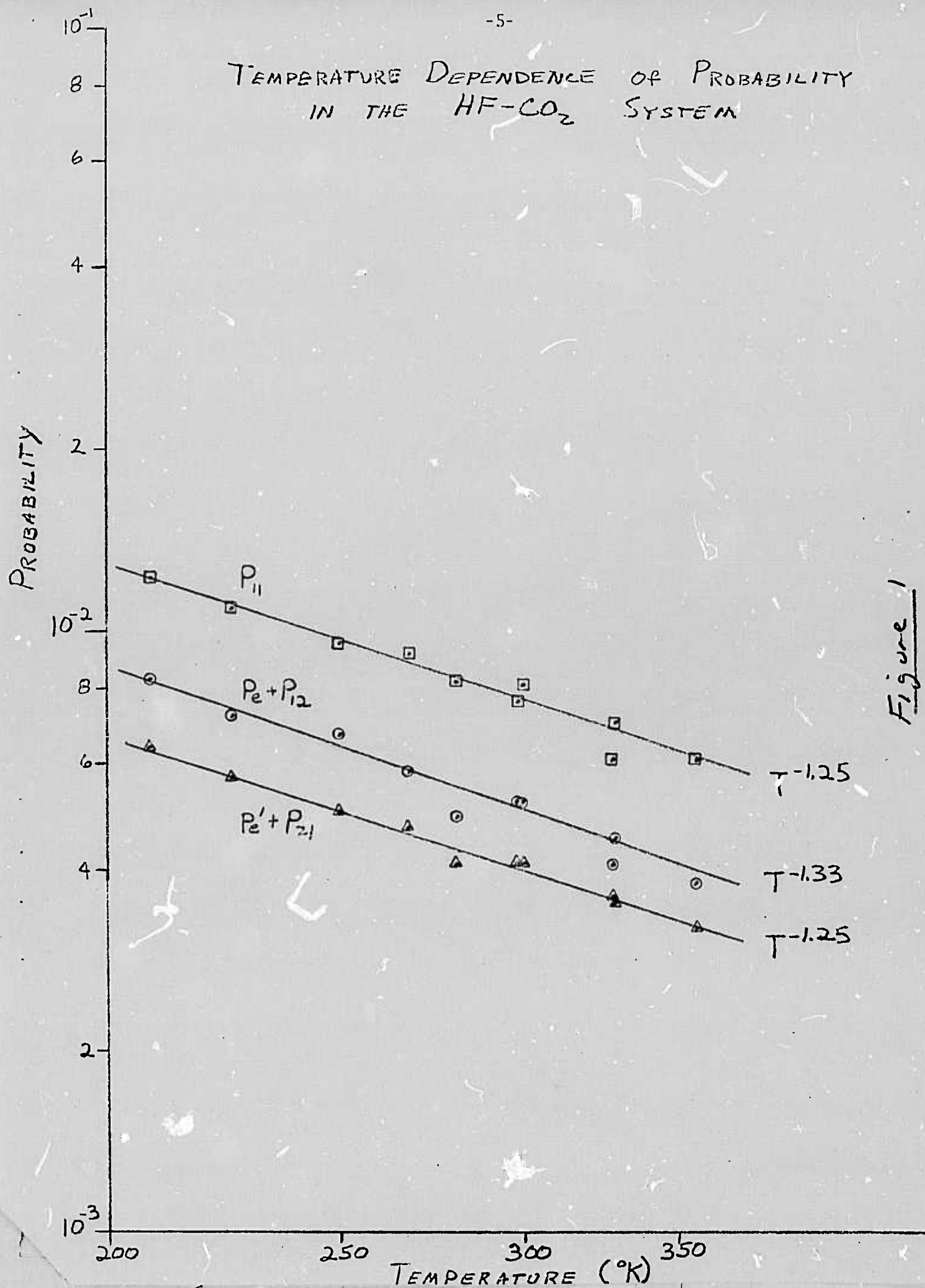| System	Temperature (°K)	k_{11}	P_{11}	$k_e + k_{12}$	$P_e + P_{12}$	$k_e' + k_{21}$	$P_e' + P_{21}$
$HF-CO_2$	357	4.0	.0061	2.8	.0038	2.55	.0034
$HF-CO_2$	327	4.2	.0061	3.2	.0041	2.8	.0036
$HF-CO_2$	328	4.8	.0070	3.5	.0045	2.7	.0035
$HF-CO_2$	300	5.85	.0081	4.25	.0052	3.3	.0041
$HF-CO_2$	298	5.45	.0076	4.2	.0052	3.3	.0041
$HF-CO_2$	280	6.1	.0082	4.1	.0049	3.45	.0041
$HF-CO_2$	268	6.9	.0091	4.95	.0058	4.0	.0047
$HF-CO_2$	250	7.5	.0095	5.9	.0067	4.4	.0050
$HF-CO_2$	225	9.0	.0108	6.7	.0072	5.3	.0057
$HF-CO_2$	208	10.5	.0122	8.1	.0083	6.2	.0064
$DF-CO_2$	357	1.15	.0018	13.5	.0185	1.11	.0015
$DF-CO_2$	328	1.50	.0022	15.0	.0187	1.30	.0017
$DF-CO_2$	300	1.80	.0026	16.5	.0207	1.60	.0020
$DF-CO_2$	281	2.10	.0029	--	--	--	--
$DF-CO_2$	275	2.20	.0030	19.4	.0233	1.75	.0021
$DF-CO_2$	250	2.90	.0038	22.8	.0262	2.10	.0024
$DF-CO_2$	228	3.50	.0044	29.6	.0324	2.80	.0031
$DF-CO_2$	214	3.60	.0044	--	--	--	--
$DF-CO_2$	207	4.6	.0053	31.0	.0368	3.3	.0039

TEMPERATURE DEPENDENCE OF PROBABILITY IN THE HF-CO$_2$ SYSTEM
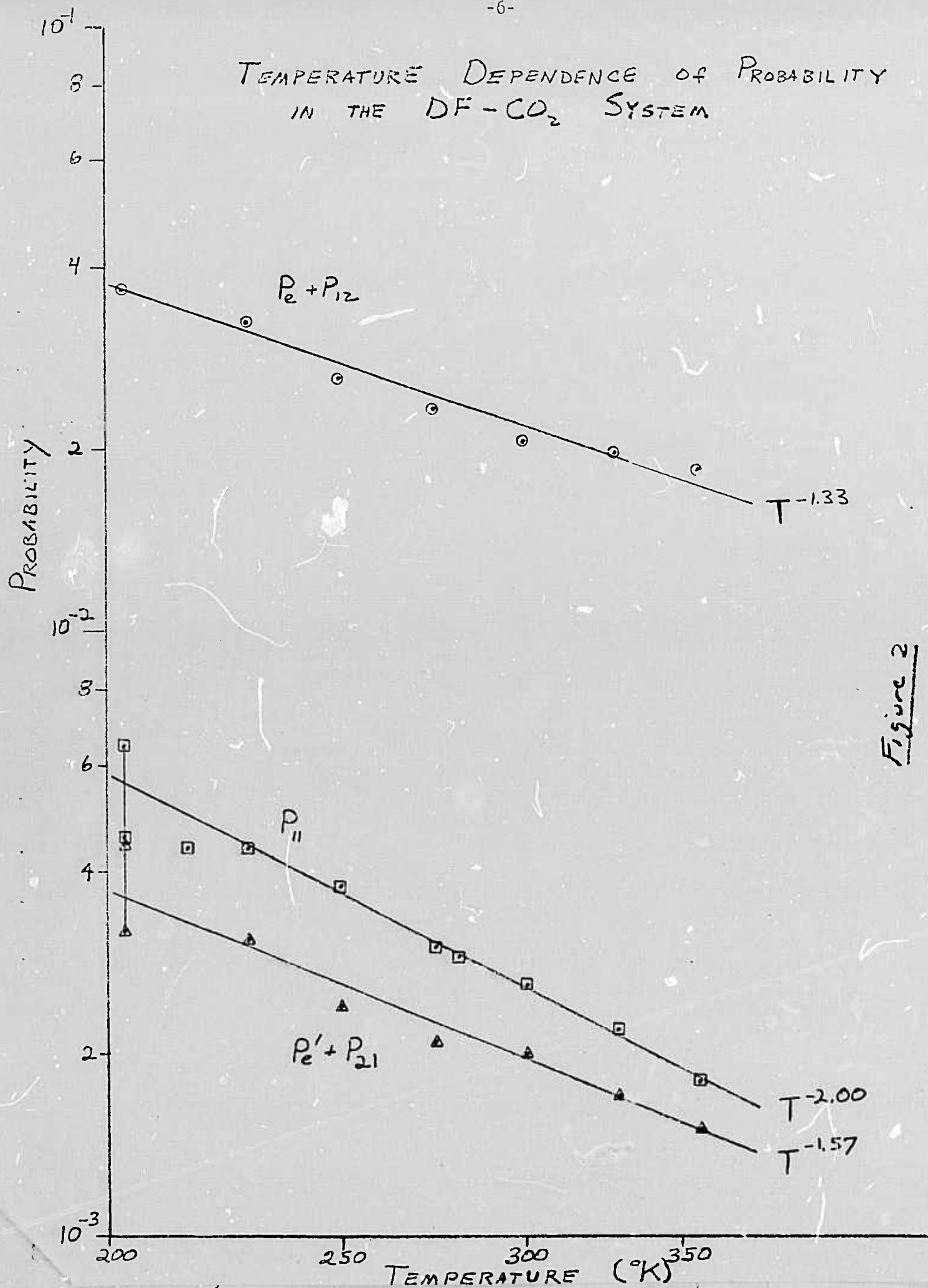
Figure 2

determination of the HF(v=0,J') population of eqn. (7); that is,

$$HF(v=0,J') + n^o \rightarrow HF(v=1,J'-1) \qquad\qquad (8)$$
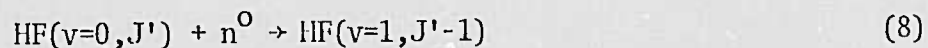
(where n^o is provided by the probe laser),

followed by the fluorescences:

$$HF(v=1,J_1'-1) \rightarrow HF(v=0,J_1'-1) + n^o \qquad\qquad (9a)$$

$$\rightarrow HF(v=0,J_1'-2) + n^o \qquad\qquad (9b)$$
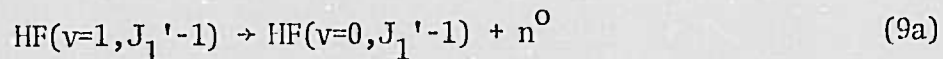
The apparatus and instrumentation for initial experiments have been nearly completed. These studies will be our primary task during the coming year.
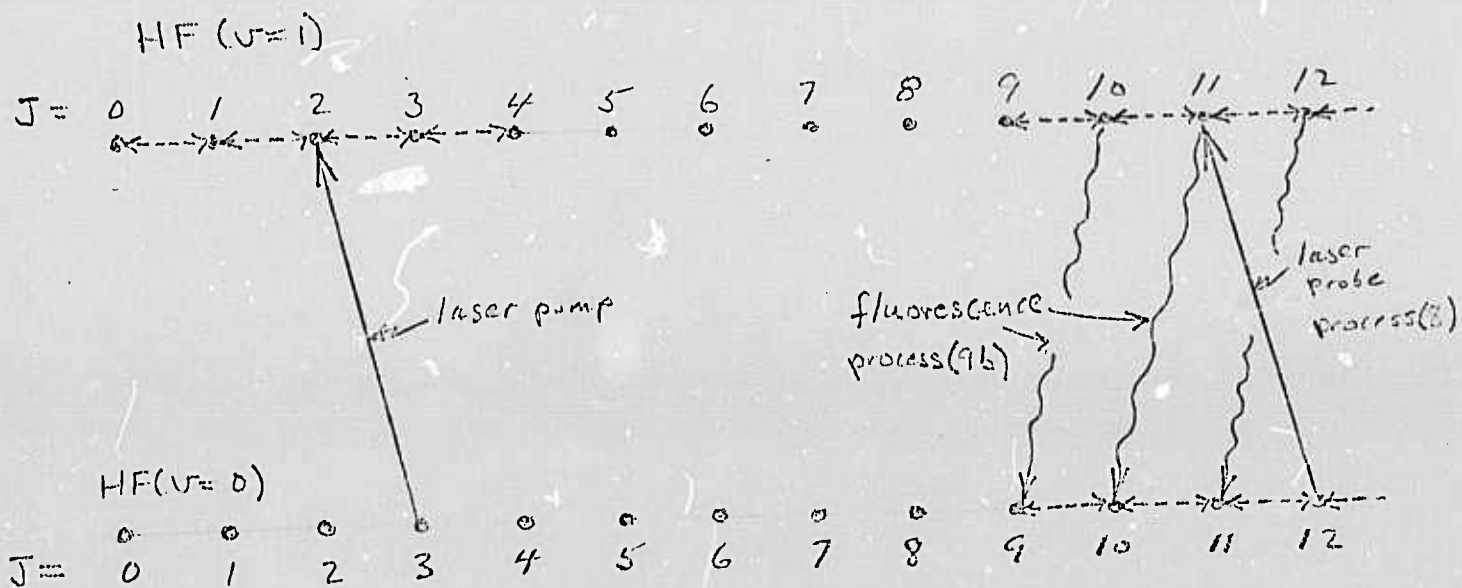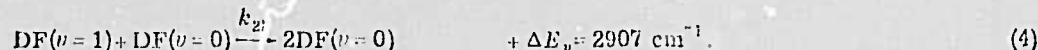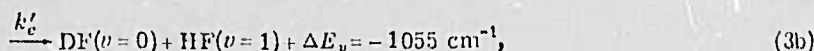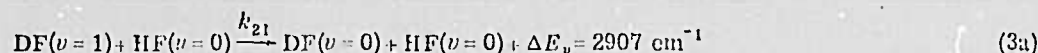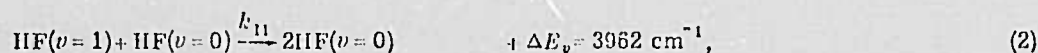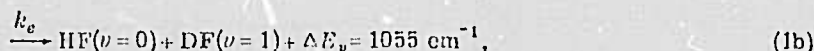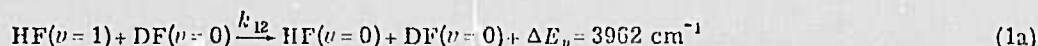
Figure 3

NOTES

Vibrational relaxation in HF and DF mixtures

Roy A. Lucht and Terrill A. Cool

School of Applied and Engineering Physics, Cornell University, Ithaca, New York 14850
(Received 20 November 1973)

The laser-excited fluorescence method has been employed to determine rate constants for vibrational energy transfer $(V \to V, R)$ and deactivation $(V - R, T)$ processes in HF–DF mixtures at temperatures from 297 to 673 °K. The importance of an understanding of vibrational energy transfer processes in HF and DF chemical lasers has led to several recent rate measurements for

the HF and DF systems in this temperature range.[1-8] Although good qualitative agreement exists as to the variations in energy transfer probabilities with temperature and isotopic composition, there are some important systematic discrepancies between the available data. For this reason, we report here the results of careful recent measurements of the rates for the processes

$$HF(v=1) + DF(v=0) \xrightarrow{k_{12}} HF(v=0) + DF(v=0) + \Delta E_v = 3962 \text{ cm}^{-1} \tag{1a}$$

$$\xrightarrow{k_e} HF(v=0) + DF(v=1) + \Delta E_v = 1055 \text{ cm}^{-1}, \tag{1b}$$

$$HF(v=1) + HF(v=0) \xrightarrow{k_{11}} 2HF(v=0) \qquad + \Delta E_v = 3962 \text{ cm}^{-1}, \tag{2}$$

$$DF(v=1) + HF(v=0) \xrightarrow{k_{21}} DF(v=0) + HF(v=0) + \Delta E_v = 2907 \text{ cm}^{-1} \tag{3a}$$

$$\xrightarrow{k'_e} DF(v=0) + HF(v=1) + \Delta E_v = -1055 \text{ cm}^{-1}, \tag{3b}$$

$$DF(v=1) + DF(v=0) \xrightarrow{k_{22}} 2DF(v=0) \qquad + \Delta E_v = 2907 \text{ cm}^{-1}. \tag{4}$$

The present apparatus and gas handling techniques have been described in detail elsewhere.[1,6,8] HF and DF were introduced separately into the flow through
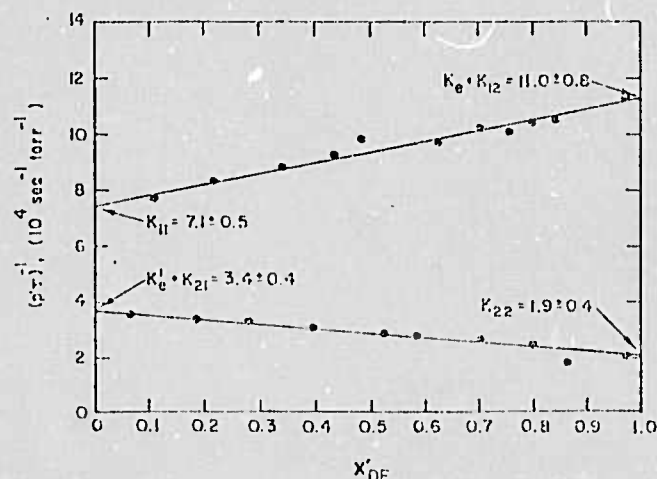

FIG. 1. Observed HF and DF single experimental decay rates for HF–DF–argon mixtures at $T = 321 \pm 2$ °K as a function of the reduced mole fraction of DF; $X'_{DF} = X_{DF}/(X_{DF} + X_{HF})$. The upper curve is for HF fluorescence; the lower curve for DF fluorescence.

choked values as described in Ref. 1. The $P_1(5)$ transition from an HF chemical laser pulsed at 200 Hz with a pulse energy of less than 0.04 mJ and a pulse width of 0.5 μsec FWHM was used to excite HF in HF/DF argon mixtures. The HF(DF) partial pressures ranged from 0.10 to 1.5 torr; the argon partial pressure was fixed at 30 torr. A cold gas filter of HF(DF) was used to ascertain that no appreciable component ($< 2\%$) of $2-1$ band fluorescence was present. Interference filters were routinely used to separate HF and DF fluorescences.[1] Oven temperatures were read to ± 3 °K accuracy with thermocouples.[8]

TABLE I. Rate constant measurements for mixtures of HF and DF.

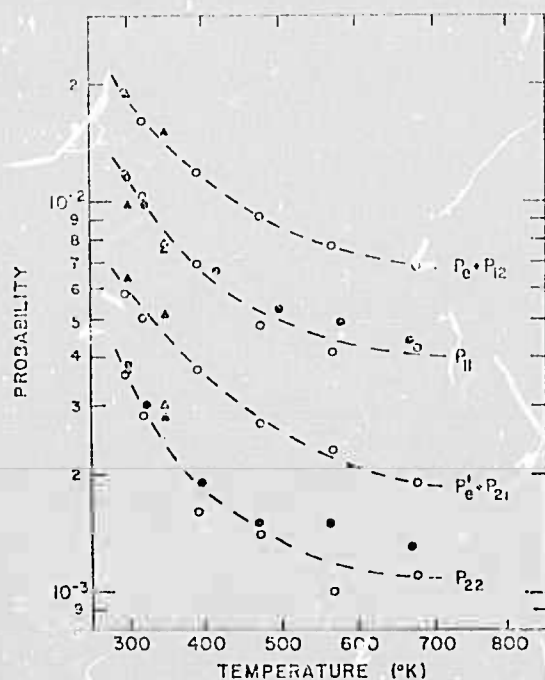| Temperature	Rate constants (10^4 sec^{-1} torr^{-1})			
	k_{11}	$k_e + k_{12}$	k_{22}	$k'_e + k_{21} = k_{21}$
297	8.4 ± 1.0	13.5 ± 1.0	2.5 ± 0.4	4.1 ± 0.4
321	7.1 ± 0.5	11.0 ± 0.8	1.9 ± 0.4	3.4 ± 0.4
395	4.3 ± 0.5	7.3 ± 0.5	1.0 ± 0.3	2.3 ± 0.3
475	2.7 ± 0.3	5.1 ± 0.3	0.8 ± 0.1	1.5 ± 0.2
570	2.1 ± 0.3	3.9 ± 0.4	0.5 ± 0.2	1.2 ± 0.2
673	2.0 ± 0.3	3.2 ± 0.3	0.5 ± 0.2	0.9 ± 0.2

FIG. 2. Temperature dependences for the probabilities for the energy transfer processes of Eqs. (1)–(4). The probabilities P have been calculated as discussed in Ref. 8: $\triangle$, Ref. 1; $\blacktriangle$, Ref. 6; $\bullet$, Ref. 8; $\bigcirc$, present work.

In Fig. 1, the observed HF and DF single exponential fluorescence decay rates $(p'\tau)^{-1}$ are given for a complete range of compositions at the fixed temperature of 321 ± 2 °K (p' is the sum of HF and DF partial pressures). The intercepts $X'_{DF} = 0$ and $X'_{DF} = 1.0$ for the lower curve (DF fluorescence) give the values indicated for the respective rate constants $k'_e + k_{21}$ and k_{22} when a

small correction is made for the deactivation by argon.[9] Similarly, values for $k_e + k_{12}$ and k_{11} are obtained from the intercepts for the HF fluorescence decay rates of Fig. 1 (upper curve). The values for $k_e + k_{12}$ could alternatively be determined from observations of the rise of DF fluorescence; such measurements always agreed well with those obtained from the decay of HF fluorescence.

The measured rate constants are tabulated in Table I. The strong inverse temperature dependence of the vibrational energy transfer and deactivation probabilities for Processes (1)–(4) are indicated in Fig. 2. Additional data obtained in this laboratory with three different experimental apparatus are included with the present data in Fig. 2. It should be noted that though the different data sets of Fig. 2 are nicely self-consistent, the values of $k_e + k_{12}$ given here exceed other reported values[5,7] by nearly a factor of 2 at the lower temperatures.

[1]D. H. Stephens and T. A. Cool, J. Chem. Phys. 56, 5863 (1972).

[2]J. K. Hancock and W. H. Green, J. Chem. Phys. 57, 4515 (1972).

[3]R. M. Osgood, Jr., A. Javan, and P. B. Sackett, Appl. Phys. Lett. 20, 469 (1972).

[4]S. F. Fried, J. Wilson, and R. L. Taylor, IEEE J. Quantum Electron. QE-9, 59 (1973).

[5]J. F. Bott and N. Cohen, J. Chem. Phys. 58, 4539 (1973).

[6]J. L. Ahl and T. A. Cool, J. Chem. Phys. 58, 5540 (1973).

[7]J. J. Hinchen, J. Chem. Phys. 59, 2224 (1973).

[8]R. A. Lucht and T. A. Cool, J. Chem. Phys. 60, 1026 (1974).

[9]Deactivation of HF and DF by argon is slow and difficult to measure accurately. The deactivation rates for both molecules from the argon used here do not exceed 50 and 100 sec^{-1}·Torr^{-1} at 300 and 675 °K, respectively (Ref. 8); in the present data reduction, we have used the value of 65 sec^{-1}·Torr^{-1} at all temperatures.

Temperature dependence of vibrational relaxation in the HF, DF, HF-CO₂, and DF-CO₂ systems*

Roy A. Lucht† and Terrill A. Cool

Department of Applied and Engineering Physics, Cornell University, Ithaca, New York 14850
(Received 13 July 1973)

The laser excited fluorescence method has been employed to determine rate constants for V → V, R and V → R, f relaxation HF($v = 1$) and DF($v = 1$) by CO₂ over the temperature range from 295 to 670 °K. The self-deactivation rates for HF($v = 1$) and DF($v = 1$) by ground state molecules and the rate of V → V, R transfer from HF($v = 1$) and DF($v = 1$) to the CO₂ (00°1) state exhibit a marked decrease with increasing temperature. The results provide additional evidence for the conversion of the large vibrational energy defects of the present systems into rotational motion of the hydrogen halide under the influence of a sizable attractive intermolecular potential well.

I. INTRODUCTION

Recently much effort has been directed toward the development of efficient "transfer chemical lasers" based upon vibrational energy transfer to the upper CO₂ laser level from various hydrogen- and deuterium-halide reaction products.[1] The laser fluorescence method has been applied in several recent studies to the measurement of key rates for vibrational deactivation and vibrational energy transfer for the HX–CO₂ and DX–CO₂ chemical laser systems (X=F, Cl, Br, I).[3-5]

Large rates for energy transfer and deactivation have been observed at room temperature for these systems despite the existence, in most cases, of quite large vibrational energy discrepancies between initial and final molecular states. The large rates for these examples have been attributed to substantial energy transfers to rotation under the influence of sizable attractive intermolecular forces.[2,3] A valid description of these processes has not been achievable within the framework of first order perturbation theories based upon the use of the Born approximation. Recent theoretical work carried to higher order perturbations, consistent with relatively strong multipole moment interactions, has yielded results in good agreement with room temperature measurements on the HF–CO₂, DF–CO₂ and HCl–CO₂ systems.[6]

In the present work, comprehensive rate measurements on the HF–CO₂ and DF–CO₂ systems have been performed from 295 to 670 °K. The results exhibit the pronounced inverse temperature dependence associated with systems subject to strong attractive interactions. An accurate description of the observed temperature dependences for the vibrational energy transfer rates should provide a sensitive check on successful theoretical approaches.

II. EXPERIMENTAL APPARATUS AND TECHNIQUES

The laser fluorescence apparatus and measurement techniques used in this work have been described in detail elsewhere.[3,7,8] The following discussion is limited to a description of several important modifications which have been made to facilitate the present measurements. A schematic diagram of the experimental apparatus is given in Fig. 1.

A. Laser source

A repetitively pulsed transverse-pin-discharge chemical laser was substituted for the chopper modulated cw chemical laser used previously.[7] The pulsed laser utilized a premixed high speed (100 m/sec) flow of He, SF₆, and H₂(D₂) to provide laser pulses of approximately 0.5 μsec FWHM at repetition frequencies as high as 2000 Hz. The flow direction was transverse (see Fig. 1) to a row of 80 tungsten pin cathodes spaced 5 mm apart and operated with individual ballast resistors of 250 ohms. A 6 mm diameter aluminum rod anode was positioned parallel to the cathode row with a gap spacing of 15 mm. The discharge was driven by a thyratron controlled resonant-charging circuit connected to 16 discharge capacitors of 250 pF each. Each capacitor fed live discharge pins in parallel.

A diffraction grating was employed to permit single line laser operation. Both the diffraction grating and a dielectric-coated germanium output mirror were mounted internally and purged with dry nitrogen to prevent the accumulation of ground state HF(DF) in the space between the optical surfaces and the discharge region. The $P_1(5)$ and $P_1(7)$ transitions for HF and DF, respectively, were employed at typical laser pulse energies of 0.04 mJ. Respective pulse repetition rates of 500 Hz and 50 Hz represented optimum compromises between pulse energy and data acquisition rates for the HF and DF systems.

B. Heated absorption cell

The fluorescence cell shown schematically in Fig. 1 was machined from solid nickel. Cell windows of sapphire were employed to accommodate the passage of the laser beam through the cell. A double window construction was employed in which the inner and outer windows were separated by means of an evacuated tube of 1 cm i.d. and 15 cm length. This acted as a heat shield to maintain the inner window at the temperature of the interior of the cell. Temperatures were read to an accuracy of ±3 °K with a thermocouple immersed in the absorption cell gas flow. This thermocouple was checked periodically against a mercury-glass thermometer inserted into wells located along the cell body. The gases entering the cell were premixed by passage
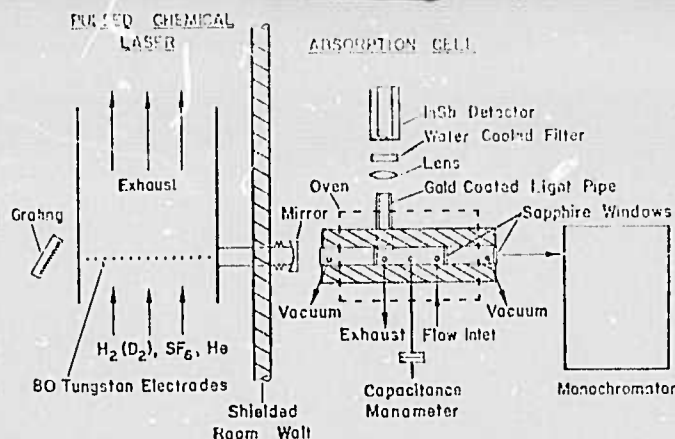
FIG. 1. Schematic diagram of experimental apparatus.

through passivated stainless steel tubing of 3 mm i.d. and 2.5 m length. The cell contained a plenum chamber and flow baffling to permit uniform heating of the gases to the cell temperature before passage into the laser absorption region. The absorption region consisted of a cylindrical chamber of 1 cm diameter and 8 cm length into which the entering flow was introduced in a laminar fashion without recirculation or separation. The flow passed uniformly along the cell axis and was removed around the periphery of the window through which the laser beam entered. An additional sapphire window (see Fig. 1) was placed at right angles to this window to pass fluorescence from the absorption region into a gold coated light pipe leading to the detector and infrared filters. The light pipe could be filled with HF or DF when desired to act as a cold gas filter. The fluorescence from HF and DF could be attenuated by a factor of about 100 by this means, which demonstrated the absence of appreciable 2→1 band fluorescence.

Fluorescence was observed with an InSb detector and associated circuitry with a time response of 2μ sec. Narrow band interference filters[3,7] were used for observations of fluorescence from the $CO_2(00^01)$ →$CO_2(00^00)$ band and for R-branch fluorescence from HF $(v=1)$ and DF $(v=1)$. The high background radiation associated with cell temperatures above 600 °K dictated the water cooling of the filters and the use of a Au:Ge detector at the highest temperatures.

The gas handling procedures and apparatus described previously[3,8] were employed in the present work. The major impurities (in parts per million) of the gases used in this study were as follows: argon: Air Products UHP grade, typical analysis ($O_2 < 2$, $N_2 < 4$, $CO_2 < 1$, $H_2O < 3$); HF: Air Products CP grade, typical analysis ($H_2SiF_6 = 30$, $SO_2 = 40$, $H_2 = 300$); DF: Merck, Sharp and Dohme, CP grade, guaranteed minimum isotopic purity of 98%; CO_2: Air Products, ($O_2 + N_2 = 10$, $CO < 10$, $CH_4 = 1.4$, $H_2O < 1.5$).

A dry ice cold trap was employed in the argon flow to minimize the water vapor impurity. The HF(DF) was purified by repeated trap to trap distillation between 77 °K and 195 °K. In each stage of distillation, the middle 90% of the sample was retained. The distilled sample was condensed and pumped on at 77 °K to remove any residual H_2 or D_2. The sample was finally held at room temperature for 3 to 4 hours before use. This ensured that the sample did not contain an excess nonequilibrium fraction of associated HF(DF).
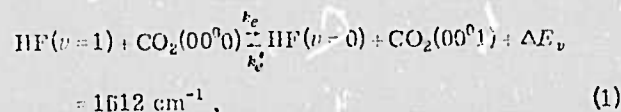
A continuous flow system was employed to minimize the effects of surface reactions in causing adsorption, decomposition, and contamination of the gas samples.[3] The residence time for gases within the absorption cell was 0.2 sec. The passivation of the cell and connecting lines was accomplished by an initial exposure of the entire system to 600 torr of ClF_3 for 24 h followed by the passivation procedures previously described.[3,8] The entire process was repeated between HF–CO_2 and DF–CO_2 data sets.

All measurements were performed with an argon pressure within the cell of 30 torr to act as an inert buffer gas to prevent excessive diffusion to the walls and to ensure rotational thermalization of HF and DF. Typical partial pressures of HF, DF and CO_2 ranged from 0.05 to 3 torr.
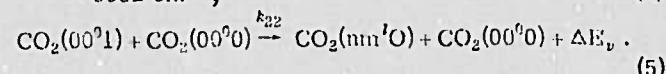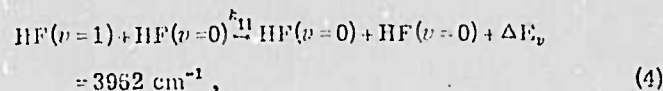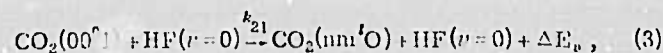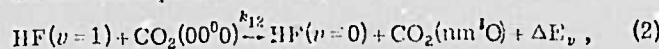
III. EXPERIMENTAL RESULTS

A. Vibrational relaxation processes

The processes of importance in describing vibrational relaxation in the HF–CO_2 and DF–CO_2 systems include vibration to vibration and rotation (V→V, R) energy transfer

$$HF(v=1) + CO_2(00^00) \underset{k_v'}{\overset{k_v}{\rightleftharpoons}} HF(v=0) + CO_2(00^01) + \Delta E_v$$
$$= 1612 \text{ cm}^{-1}, \tag{1}$$

and the vibration to rotation and translation (V→R, T) deactivation processes:

$$HF(v=1) + CO_2(00^00) \overset{k_{12}}{\rightarrow} HF(v=0) + CO_2(nm^10) + \Delta E_v, \tag{2}$$

$$CO_2(00^01) + HF(v=0) \overset{k_{21}}{\rightarrow} CO_2(nm^10) + HF(v=0) + \Delta E_v, \tag{3}$$

$$HF(v=1) + HF(v=0) \overset{k_{11}}{\rightarrow} HF(v=0) + HF(v=0) + \Delta E_v$$
$$= 3962 \text{ cm}^{-1}, \tag{4}$$

$$CO_2(00^01) + CO_2(00^00) \overset{k_{22}}{\rightarrow} CO_2(nm^10) + CO_2(00^00) + \Delta E_v. \tag{5}$$

Analogous processes apply for the DF–CO_2 system with the vibrational energy discrepancies $\Delta E_v = 553$ cm^{-1} for Process (1) and $\Delta E_v = 2907$ cm^{-1} for Process (4). Processes (1) through (5) are implicitly summed over all possible rotational quantum number changes.

Vibrational deactivation by the argon diluent is described by the process

$$HF(v=1) + Ar \overset{k_{1m}}{\rightarrow} HF(v=0) + Ar + \Delta E_v = 3962 \text{ cm}^{-1} \tag{6}$$
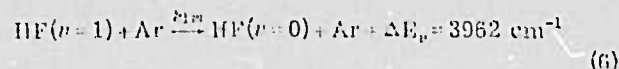
(and an analogous expression for DF), and the process

$$CO_2(00^01) + Ar \overset{k_{2m}}{\rightarrow} CO_2(nm^10) + Ar + \Delta E_v. \tag{7}$$
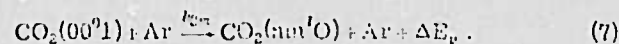
Experiments were performed at high enough pressures that the influences of radiative decay could be neglected. Moreover, the presence of the argon buffer acted to en-

sure that rotational equilibration of HF and DF was achieved on a time scale short compared to that for vibrational relaxation. When rotational equilibrium at the temperature T exists, then the forward and reverse rates for the overall process (1) (summed on J) are related by the expression

$$k_e/k_e' = \exp(\Delta E_v/kT) . \qquad (8)$$

Solutions to the rate equations for the Processes (1)–(7) describing the temporal variations in HF($v=1$) or DF($v=1$) and CO₂(00^01) populations in response to a laser-induced population $[HF]_0$ or $[DF]_0$ have been given[9,10] in terms of two exponential decay constants

$$\lambda_{1,2} = \tfrac{1}{2}\{a_1 + b_2 \pm [(a_1-b_2)^2 + 4a_2b_1]^{1/2}\} \qquad (9)$$

where

$$a_1/p = (k_e + k_{12}) X_{CO_2} + k_{11} X_{HF} + k_{1m} X_{Ar} ,$$

$$b_1/p = k_e' X_{HF} ,$$

$$a_2/p = k_e X_{CO_2} ,$$

and

$$b_2/p = (k_e' + k_{21}) X_{HF} + k_{22} X_{CO_2} + k_{2m} X_{Ar} .$$

The method we have employed in data reduction is based upon the determination of the decay constants, λ_1 and λ_2, for limiting cases when the concentration of one of the molecules HF(DF) or CO₂ approaches zero.[3,11] The expressions for the relaxation times for the fluorescence in the limiting cases have the two possible forms given in equations (10) and (11):

$$(p'\tau)^{-1} = k_e + k_{12} + k_{1m}(p_m/p') \text{ when } X_{HF(DF)} \to 0 , \qquad (10a)$$

$$(p'\tau)^{-1} = k_{11} + k_{1m}(p_m/p') \text{ when } X_{CO_2} \to 0 , \qquad (10b)$$

or

$$(p'\tau)^{-1} = k_{22} + k_{2m}(p_m/p') \text{ when } X_{HF(DF)} \to 0 , \qquad (11a)$$

$$(p'\tau)^{-1} = k_e' + k_{21} + k_{2m}(p_m/p') \text{ when } X_{CO_2} \to 0 . \qquad (11b)$$

In these expressions p' is the sum of the partial pressures of HF(DF) and CO₂; p_m is the partial pressure of argon; τ is the measured single exponential time constant for the situations described in Table I.

B. Self-deactivation of HF and DF

Measurements were made of the single exponential decay of fluorescence from HF($v=1$) and DF($v=1$) in mixtures of HF or DF with 30 torr of argon buffer gas. Values of the relaxation rates, $(p\tau)^{-1}$, were adequately described by the relationship (10b):

$$(p\tau)^{-1} = k_{11} X_{HF(DF)} + k_{1m} X_{Ar}$$

TABLE I. Limiting conditions on measured single experimental time constant τ.

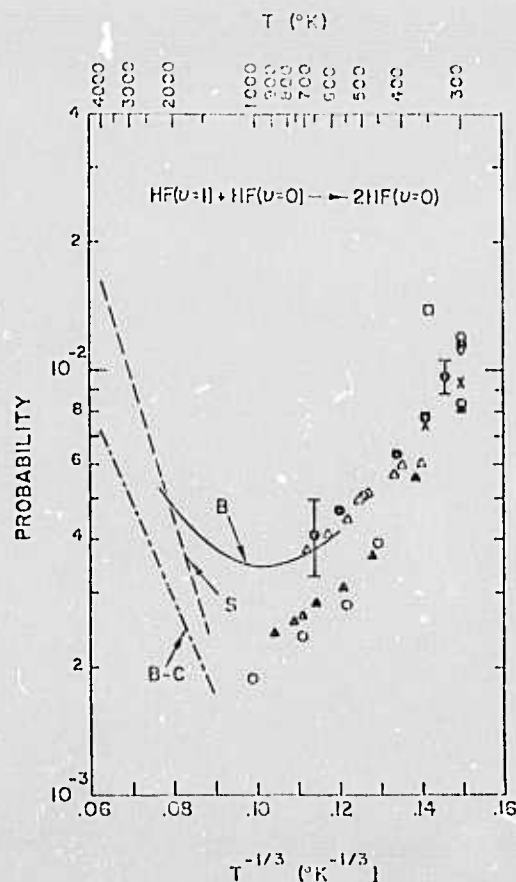| Measured characteristic time, τ	Equation describing limiting conditions when $a_1 > b_2$	Equation describing limiting conditions when $b_2 > a_1$
Decay Time of HF(DF) Fluorescence	(10a) and (10b)	(11a) and (11b)
Rise Time of CO₂ Fluorescence	(10a) and (10b)	(11a) and (11b)
Decay Time of CO₂ Fluorescence	(11a) and (11b)	(10a) and (10b)

FIG. 2. Temperature dependence of the probability for self-deactivation of HF: line B-C, Bott and Cohen Ref. 14; line S, Solomon, et al., Ref. 12; line B, Blair, et al., Ref. 17; □, Airey and Fried, Ref. 20; O, Hancock and Green, Ref. 4; ∇, Blair, et al., Ref. 17; ×, Ahl and Cool, Ref. 11; △, Fried, et al., Ref. 18; ▲, Bott, Ref. 16; O, Hinchen, Ref. 19; ⊟, Stephens and Cool, Ref. 3; O, present work.

Values of k_{1m} were too small to be accurately measured; however, values of 50 sec⁻¹ torr⁻¹ and 100 sec⁻¹ torr⁻¹ are reasonable upper bounds on k_{1m} at 295 and 675 °K, respectively, for both HF and DF.

The temperature dependences of the measured probabilities for deactivation of HF($v=1$) are presented in Figs. 2 and 3 along with the previous measurements of several authors.

High temperature data have been obtained with the shock tube by Solomon et al.,[12] Blauer et al.,[13] by Bott and Cohen,[14,15] Bott[15] and Blair, et al.[17] Bott[16] and Blair et al.[17] have combined the use of a shock tube with the laser induced fluorescence technique to obtain data for HF deactivation at intermediate temperatures. Two other studies, besides the present one, have employed heated ovens and the laser fluorescence method for measurements at temperatures below 1000 °K. Fried, et al.[18] have presented measurements of HF self-deactivation for temperatures from 300 to 730 °K. Hinchen[19] has measured the deactivation rates for both HF and DF in the temperature range from 295 to 1000 °K. Previous studies of HF self-deactivation near room temperature include the original measurement of Airey and Fried at 350 °K,[20] the subsequent work of Stephens and Cool[3] at
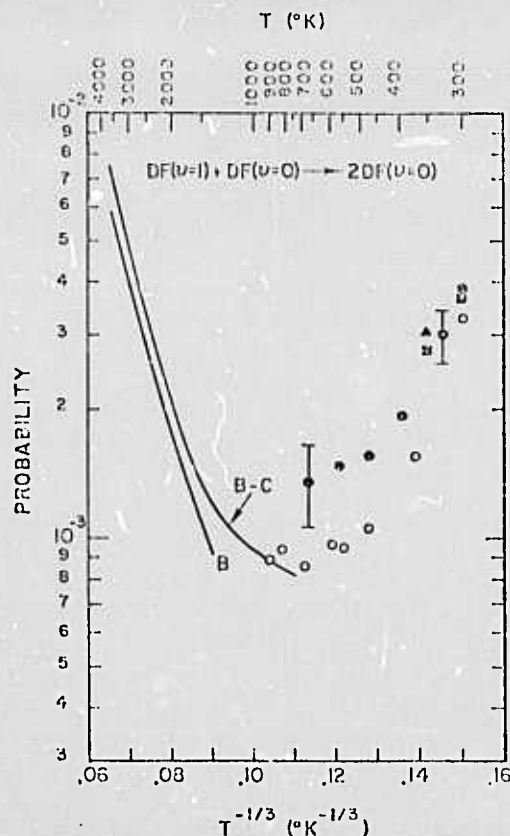
FIG. 3. Temperature dependence of the probability for self-deactivation of DF: line B-C, Bott and Cohen, Ref. 15; line B, Blauer, *et al.*, Ref. 13; O, Hinchen, Ref. 19; △, Stephens and Cool, Ref. 3; □, Ahl and Cool, Ref. 11; ⊙, present work.

350 °K, the measurements of Hancock and Green[4] at 295 °K, and the results of Ahl and Cool[11] at 300 and 350 °K. Stephens and Cool[3] have given a value for the self-deactivation rate of DF($v=1$) at 350 °K.

Discrepancies of factors of two exist between measurements made by the several groups. Evidently systematic differences in experimental technique exist because the discrepancies are somewhat beyond the respective experimental uncertainties quoted by the various investigators. The most likely sources of such systematic differences would appear to stem from the difficulties in precise determination of sample pressures and in the minimization of the effects of surface adsorption and degassing of HF and DF. Hinchen[19] observed possible effects of degassing from the cell walls under conditions of low flow rates for undiluted HF and DF samples. To minimize these effects, the present experiments were performed at cell pressures above 30 torr with a combined gas flow (HF or DF and argon) of 0.015 mM/sec at a mean flow velocity of about 6 cm/sec. These flow conditions approximate the maximum flow rates used by Hinchen.[19] Variations in flow rate up or down by a factor of two had little effect on measured relaxation rates except at the highest temperature of 670 °K. At this temperature the apparent deactivation rate decreased by 20% (to a value within the probable error limit shown in Fig. 2) when the flow rate was increased by a factor of three. At such high flow rates pressure fluctuations were encountered which made ac-

curate rate measurements difficult. The deactivation probabilities for HF and DF obtained in the present work are consistently higher at all temperatures than those reported by Hinchen. For several reasons cell degassing does not appear to explain these discrepancies: (a) measured rates of cell degassing for HF and DF at the end of a given run did not exceed 0.930 torr/min even at the highest cell temperatures, (b) linear variations in $(p\tau)^{-1}$ with $X_{HF(DF)}$ were observed for all HF (DF) mole fractions ($0 \le X_{HF(DF)} \le 0.1$), (c) the intercepts for $X_{HF(DF)} \to 0$ did not exceed 100 sec^{-1} torr^{-1}, (d) the discrepancies do not increase markedly with cell temperature.

While the discrepancies among the various data shown in Figs. 2 and 3 are probably not unreasonable for measurements of this nature, perhaps some of the differences can be resolved as more experience is gained with the use of the various techniques.

C. Vibrational energy transfer and deactivation in the HF-CO$_2$ system

The transfer of energy from HF($v=1$) to the CO$_2$(00^{0}1) upper laser level is believed to occur primarily by the single-step mechanism of process (1),[3] rather than by an initial coupling to the CO$_2$(10^{0}1) or CO$_2$(02^{0}1) levels as was initially suggested.[21] Evidently energy transfer to rotation of HF upon recoil results in an over-all internal energy discrepancy for process (1) which is substantially less than the vibrational energy defect of 1612 cm^{-1}.

For the HF-CO$_2$ system, the value of k_{11} is always sufficiently large compared to values for the sums $k_e + k_{12}$ and $k_e' + k_{21}$ that $a_1 > b_2$ for all mixture compositions and cell temperatures. Moreover, the large vibrational energy defect for process (1) ensures that $(a_1 - b_2)^2 \gg 4a_2 b_1$. Therefore, measured values of $(p'\tau)^{-1}$ vary linearly with the composition of HF-CO$_2$ mixtures and exhibit the limiting behavior for small mole fractions specified in the first column of Table I.

The experimental procedure followed here consisted of two parts. In the first case, fluorescence from HF($v=1$) molecules was monitored to determine the variation in the fluorescence decay rate, $(p'\tau)^{-1}$, as a function of the reduced CO$_2$ mole fraction, $X'_{CO_2} = X_{CO_2}/(X_{HF} + X_{CO_2})$. The intercepts at $X'_{CO_2} = 0$ and $X'_{CO_2} = 1$ of such data plots yielded values of $k_{11} + k_{1n}(p_m/p')$ and $k_e + k_{12} + k_{1n}(p_m/p')$, respectively. Secondly, the decay of fluorescence from CO$_2$(00^{0}1) molecules was monitored to establish the variation of the CO$_2$(00^{0}1) deactivation rates, $(p'\tau)^{-1}$, as a function of the reduced CO$_2$ mole fraction, X'_{CO_2}. In this case the respective intercepts at $X'_{CO_2} = 0$ and $X'_{CO_2} = 1$ provided values for the quantities $k'_e + k_{2l} + k_{2n}(p_m/p')$ and $k_{22} + k_{2n}(p_m/p')$.

Fig. 4 shows relaxation rate data for the decay of HF($v=1$) molecules as a function of the reduced mole fraction, X'_{CO_2}, for temperatures ranging from 297 to 670 °K. The line drawn at 350 °K corresponds to the data previously presented by Stephens and Cool.[3] The solid data points at $X'_{CO_2} = 0$ are the values of $k_{11} = k_{11} + (p_m/p') \times k_{1n}$ obtained from the measurements of the decay of
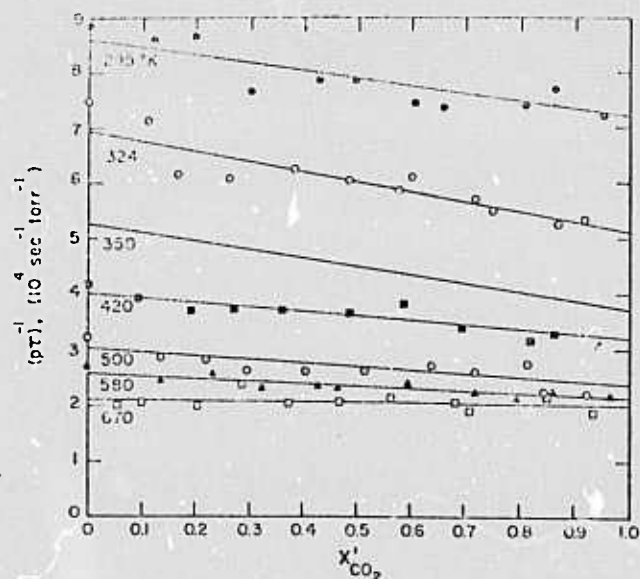
FIG. 4. Observed HF fluorescence decay rates for HF-CO₂-argon mixtures for several temperatures as a function of the reduced mole fraction of CO₂; $X'_{CO2} = X_{CO2}/(X_{HF} + X_{CO2})$.

FIG. 6. Same as Fig. 5 after normalization for effects of deactivation by argon (see text).

HF($v=1$) fluorescence in HF-argon mixtures. After subtraction of a small correction for the $(p_m/p')k_{1m}$ term,[22] the intercepts of Fig. 4 yield values for the rate constants k_{11} and $k_e + k_{12}$ as a function of temperature.

Values for the rate constant sum, $k'_e + k_{21}$, were obtained from $CO_2(00^01)$ fluorescence decay data. The data reduction procedure is illustrated by consideration of the data of Fig. 5 obtained at the temperature of 500 °K. Because $k_{2m}(p_m/p')$ was not negligibly small and since p_m/p' varied from point to point, each data point in Fig. 5 had to be individually corrected before an accurate value of $k'_e + k_{21}$ could be deduced from the left-hand intercept. Initial data reduction was accomplished with use of the published values[23] of k_{2m} and k_{22} for normalization of the relaxation data to a mean value of $p_m/$
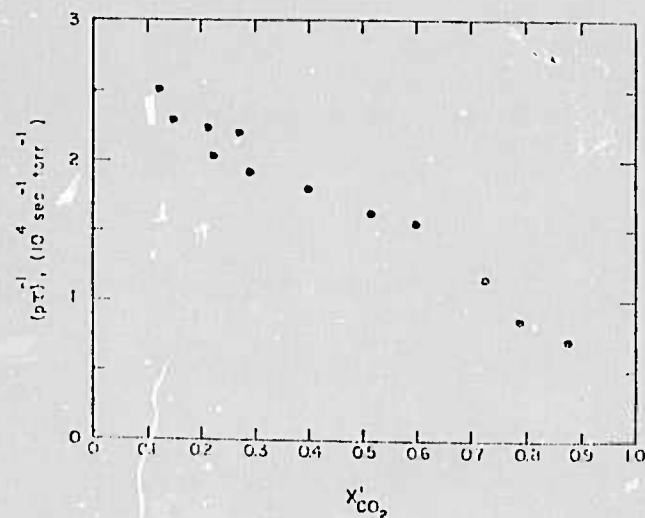

FIG. 5. Observed CO₂ fluorescence decay rates for the latter stages of relaxation for HF-CO₂-argon mixtures at 500 °K as a function of the reduced mole fraction of CO₂; $X'_{CO2} = X_{CO2}/(X_{HF} + X_{CO2})$.

p'. The results of such normalization for the data of Fig. 5 to a value of $p_m/p' = 18.0$ are given in Fig. 6. Notice that the right-hand intercept of Fig. 6 is about 50% higher than the value of 3730 sec⁻¹·torr⁻¹ expected from the published values[23] of k_{22} and k_{2m}. All CO₂ fluorescence data at other temperatures for both the HF-CO₂ and DF-CO₂ systems exhibited similar discrepancies with the expected values for the right hand intercepts of such data plots. Impurities in the argon might explain this behavior; cell degassing could not contribute enough deactivation to account for these observations. In any case these discrepancies were not of serious concern since they were always small compared to the magnitudes of the measured rate constants and could not have introduced appreciable uncertainties in the results. Data similar to those of Fig. 5 were obtained at other temperatures ranging from 297 °K to 670 °K; in all cases a linear variation in the relaxation rate with X'_{CO2} was observed and values of $k'_e + k_{21}$ were deduced at each temperature from the value of $(p'\tau)^{-1}$ for $X'_{CO2} \to 0$ after corrections for the $k_{2m}(p_m/p')$ term were made with the k_{2m} values of Stephenson et al.[23]

D. Vibrational energy transfer and deactivation in the DF-CO₂ system

The decay of DF($v=1$) fluorescence obeyed the relationships (10a) and (10b) for limiting cases $X'_{DF} \to 0$ and $X'_{CO2} \to 0$, respectively. A substantially linear variation of $(p'\tau)^{-1}$ with composition was observed at all temperatures as is illustrated in Fig. 7 for data taken at 299 °K. The intercepts from such data plots were used to determine the temperature dependences of the rate constants k_{11} and $k_e + k_{12}$.

The dependence of the relaxation rate, $(p'\tau)^{-1}$, for the decay of $CO_2(00^01)$ fluorescence upon the reduced CO₂ mole fraction, X'_{CO2}, was determined for several temperatures ranging from 297 to 670 °K. In contrast to the linear dependence (see Fig. 5) found at all temperatures for the HF-CO₂ system, a pronounced nonlinear variation of $(p'\tau)^{-1}$ with X'_{CO2} was observed for all tem-

FIG. 7. Observed DF fluorescence decay rates for DF–CO$_2$–argon mixtures at 299 °K as a function of the reduced mole fraction of CO$_2$; $X'_{CO_2} = X_{CO_2}/(X_{DF} + X_{CO_2})$.
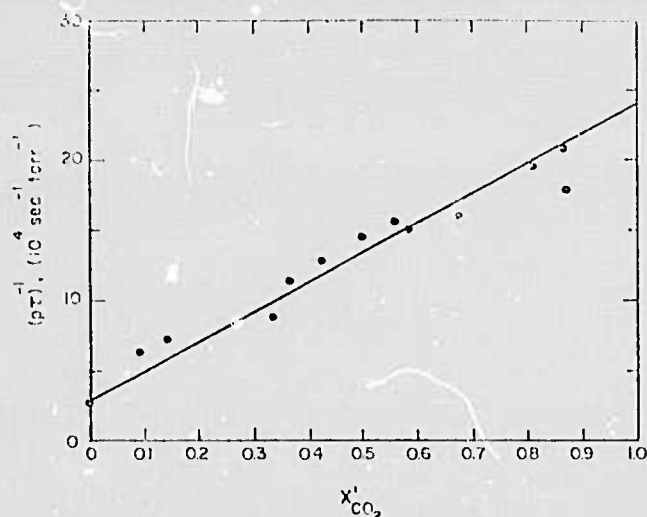
peratures above 325 °K for the DF–CO$_2$ system. Fig. 8 illustrates this nonlinear behavior for the data taken at $T = 470$ °K. The relaxation data of Fig. 8 have been normalized to the value $(p_m/p') = 12.0$ in the manner discussed in connection with Fig. 6.

The explanation for the curvature of data plots typified by Fig. 8 is found by consideration of the magnitudes of the several rate constants of Eqs. (9). For the DF–CO$_2$ system the present measurements indicate that $(k'_e + k_{21})$ > k_{11} for all temperatures investigated here. In contrast, for the HF–CO$_2$ system the large value of k_{11} ensured that the above inequality was reversed at all temperatures investigated. Examination of Eqs. (9) reveals that for the DF–CO$_2$ case b_2/p becomes larger than a_1/p for sufficiently small values of X'_{CO_2}; however, for the HF–CO$_2$ case the relationship $a_1 < b_2$ holds at all values of X'_{CO_2}. Therefore, the relationships (10b) and (11a) are applicable to the analysis of the decay of $CO_2(00^01)$ fluorescence from DF–CO$_2$ mixtures; for HF–CO$_2$ mixtures the relationships (10a) and (10b) are applicable, as has been stated.

The curves shown with the data of Fig. 8 indicate calculated variations of the decay rate $\lambda_2/p = (p'\tau)^{-1}$ for three different assumed values of the rate constant sum $k'_e + k_{21}$. An effective value of $k_{2m} = 185$ sec^{-1}·torr^{-1} was used in the calculations to force the calculated curves to fit the measured right-hand intercept $[(p'_\tau)^{-1} = 2600$ sec^{-1}·torr$^{-1}]$ rather than the intercept $[(p'_\tau)^{-1} = 2269$ sec^{-1}·torr$^{-1}]$ calculated with the value of $k_{2m} = 140$ sec^{-1}·torr^{-1} of reference (23). The solid curve gives a best fit with the experimental data for the value $k'_e + k_{21}$ = 3.1×10^4 sec^{-1}·torr^{-1}. The upper and lower dashed curves are for $k'_e + k_{21} = 3.4$×10^4 sec^{-1}·torr^{-1} and 2.8 ×10^4 sec^{-1}·torr^{-1}, respectively; these curves represent reasonable upper and lower bounds on $k'_e + k_{21}$. The uncertainty concerning the right hand intercepts of data plots like that of Fig. 8 did not have an important effect on the ultimate selection of values for the rate constant sum $k'_e + k_{21}$ at all temperatures investigated. The larg-

est uncertainty in $k'_e + k_{21}$ arising from this cause occurred for the data taken at the highest temperature of 670 °K and was estimated to be ±10%.

E. Summary of rate constant measurements for the HF–CO$_2$ and DF–CO$_2$ systems

1. Deactivation of HF and DF by CO$_2$

The measured probabilities for vibrational deactivation of HF or DF by the processes (1) and (2), with the combined rate constants $k_e + k_{12}$, are given as a function of temperature in Fig. 9. The previous measurements of Hancock and Green[4] at 294 °K, Stephens and Cool[3] at 350 °K, Airey and Smith[21] at 300 °K, and Bott[25] are also indicated in Fig. 9.

For the DF–CO$_2$ case a simple comparison of the magnitudes of the probabilities of Figs. 3 and 9 indicates process (2) is negligible as compared to process (1). That is, the rate constants, k_{11}, for self-deactivation of HF and DF ought to greatly exceed the rate constants, k_{12}, for deactivation by process (2) because of the relatively weaker interaction in the latter case. Thus, the inequality $k_e + k_{12} - k_{11} < k_e < k_e + k_{12}$ can provide useful bounds on the true values of k_e for the DF–CO$_2$ case. The bounds on the values of k_e and k'_e inferred in this manner are summarized in Table II. Table II indicates that the V–V process (1) entirely dominates the V–R, T process (2) in the DF–CO$_2$ case.

Unfortunately, however, for the HF–CO$_2$ case the values of k_{11} are so large that the above inequality is not useful and it is difficult to estimate the contribution of k_{12} to the rate constant sum, $k_e + k_{12}$.

A pronounced inverse temperature dependence of the deactivation probabilities is evident in Fig. 9. This dependence cannot be represented in a simple fashion; however, if the probability were to be expressed as

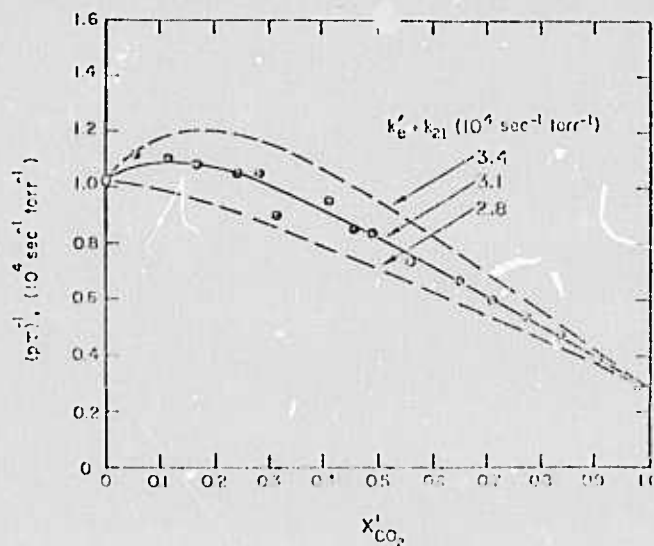FIG. 8. Observed CO$_2$ fluorescence decay rates for the latter stages of relaxation for DF–CO$_2$–argon mixtures at 470 °K as a function of the reduced mole fraction of CO$_2$: X'_{CO_2}, $X_{CO_2}/(X_{DF} + X_{CO_2})$; O, from DF fluorescence decay.
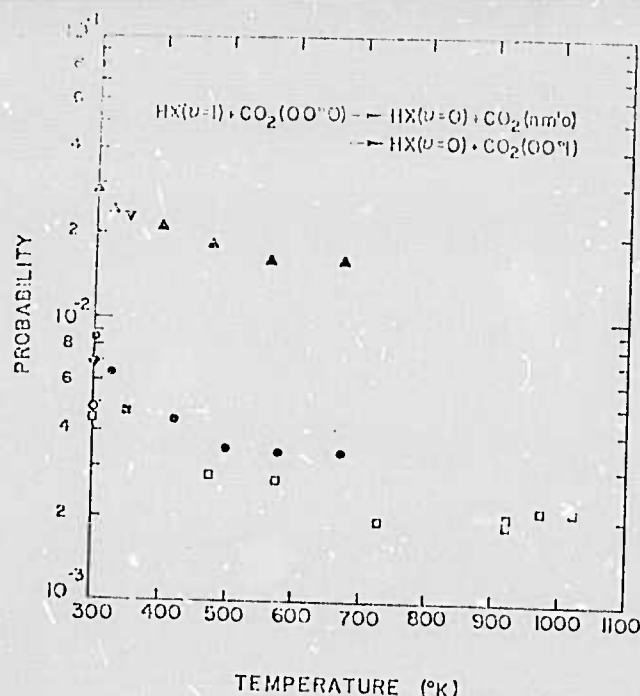
FIG. 9. Temperature dependence of the probability for deactivation of HF and DF by CO_2 by processes (1) and (2): ▾, Stephens and Cool, Ref. 3; ○, DF–CO_2, Airey and Smith, Ref. 24; ▲, DF–CO_2, present work; □, HF–CO_2, Bott, Ref. 25; ○, HF–CO_2, Airey and Smith, Ref. 24; ◇, HF–CO_2, Hancock and Green, Ref. 4; ○, HF–CO_2, present work; ⊡, HF–CO_2, Stephens and Cool, Ref. 3.

$p \propto T^{-n}$ then values of n would vary from about $\frac{3}{2}$ at 300 °K to less than $\frac{1}{2}$ at 650 °K.

2. Deactivation of CO_2 (00°1) by HF and DF

Rate constants for deactivation of $CO_2(00^0 1)$ molecules by HF and DF have been previously given by Chang, et al.[5] Hancock and Green,[4] and Stephens and Cool.[3] For the HF–CO_2 system $k_e' + k_{21} \approx k_{21}$, and thus deactivation measurements yield k_{21} directly. In the DF–CO_2 case k_e' may be estimated with reasonable accuracy (see Table II), and therefore the contribution of k_{21} to the measured overall rate of deactivation can be determined.

Measured probabilities for deactivation of $CO_2(00^0 1)$ by process (3) for HF and DF are presented in Fig. 10 along with the results of the previous measurements. Here again a marked decrease in probability for deactivation accompanies a temperature increase over the

TABLE II. Bounds on the values of k_e and k_e'.

Temperature (°K)	Rate Constants (DF–CO_2) (10^4 sec^{-1} torr^{-1})		
	k_e'/k_{12}	k_e	k_e'
300	21.0 ± 5	16 < k_e < 20	1.1 < k_e' < 1.9
325	19.6 ± 3	14 < k_e < 22	1.3 < k_e' < 1.8
555	14.6 ± 2.5	11 < k_e < 17.2	1.5 < k_e' < 2.3
575	11.7 ± 3.5	8.3 < k_e < 14.2	1.5 < k_e' < 2.6
636	9.7 ± 4.0	6.9 < k_e < 11.7	1.6 < k_e' < 2.8
679	8.6 ± 1.5	6.5 < k_e < 10.1	1.9 < k_e' < 3.0

temperature range investigated.

All of the rate constants and associated probabilities of the present work given in Figs. 2, 3, 9 and 10 are summarized along with estimated error limits in Table III.

IV. DISCUSSION

The primary interest in the present measurements lies in what they reveal concerning the nature of the intermolecular potential for HF–CO_2 and DF–CO_2 collision pairs. Evidence has been cited[3] for the existence of moderately deep attractive intermolecular potential wells for the HF–CO_2, DF–CO_2, HCl–CO_2 and DCl–CO_2 systems. Conceivably these systems are similar to the HX–HX systems in which forces of a hydrogen bonding nature, strongly sensitive to intermolecular orientation, are thought to be influential in energy transfer processes.[20,25] That is, because the electron charge distribution in CO_2 is strongly localized in the vicinity of the oxygen atoms[27] the collinear configuration, F–H··O=C=O, with the hydrogen atom adjacent to an oxygen atom, may possess an associative potential minimum. The opposite collinear configuration, with the fluorine atom centrally located, should lead to an essentially repulsive interaction. At low temperatures, and for collisions with impact parameters small enough
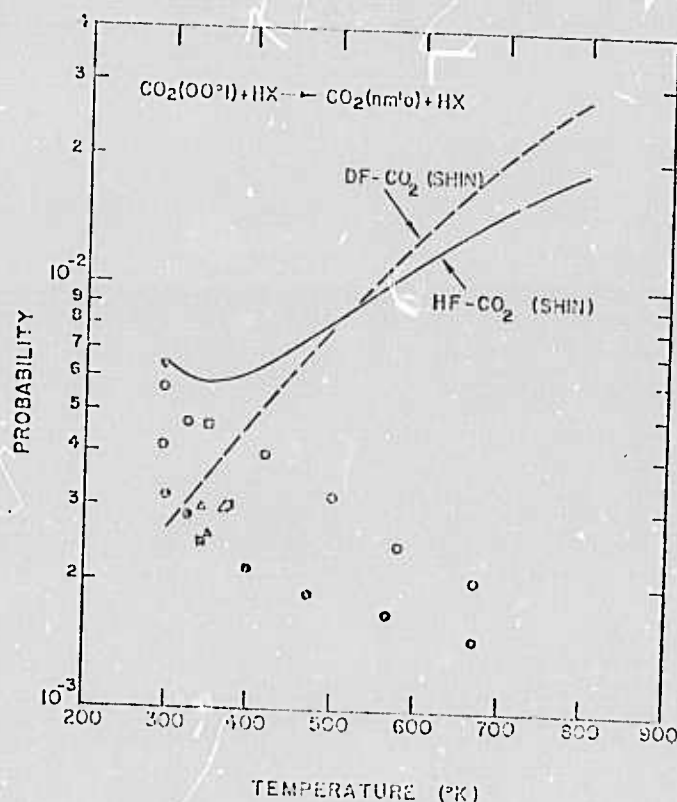
FIG. 10. Temperature dependence of the probability for deactivation of $CO_2(00^0 1)$ molecules by HF and DF by process (3). ▾, CO_2–HF, Hancock and Green, Ref. 4; ○, CO_2–HF, Bott, Ref. 25; △, CO_2–HF, Chang, et al., Ref. 5; □, CO_2–HF, Stephens and Cool, Ref. 3; ○, CO_2–HF, present work; solid curve, CO_2–HF, calculated by Shin, Ref. 29; ⊡, CO_2–DF, Chang, et al., Ref. 5; ▲, CO_2–DF, Stephens and Cool, Ref. 3; ○, CO_2–DF, present work; dashed curve, CO_2–DF, calculated by Shin, Ref. 29.

TABLE III. Summary of rate constants and probabilities.

System	Temperature (°K)	Rate constants (10^4 sec^{-1} torr^{-1}), and probabilities[a]					
		k_{11}	P_{11}	$k_e + k_{12}$	$P_e + P_{12}$	k_{21}	P_{21}
DF–CO₂	299	2.7±0.3	0.0038	24.0±5	0.030	2.6±0.5	0.0032
DF–CO₂	325	2.1±0.3	0.0030	19.0±3	0.024	2.2±0.3	0.0028
DF–CO₂[b]	350	2.0±0.2	0.0030	17.2±2.5	0.023	1.9±0.4	0.0025
DF–CO₂	399	1.2±0.3	0.0019	14.6±2.5	0.021	1.5±0.4	0.0021
DF–CO₂	473	0.87±0.2	0.0015	11.7±2.5	0.018	1.2±0.3	0.0019
DF–CO₂	566	0.77±0.15	0.0015	9.7±2.0	0.016	1.0±0.2	0.0017
DF–CO₂	670	0.64±0.14	0.0013	8.6±1.5	0.016	0.8±0.2	0.0015
HF–CO₂	295	8.4±0.7	0.0117	7.0±0.5	0.0085	4.7±0.5	0.0057
HF–CO₂	324	6.7±0.4	0.0098	5.0±0.4	0.0062	3.7±0.5	0.0047
HF–CO₂[b]	350	5.2±0.3	0.0078	3.6±0.3	0.0047	3.5±0.5	0.0046
HF–CO₂	420	3.9±0.4	0.0066	3.1±0.3	0.0044	2.7±0.4	0.0039
HF–CO₂	500	2.8±0.4	0.0053	2.2±0.3	0.0035	2.0±0.4	0.0031
HF–CO₂	580	2.4±0.4	0.0049	2.0±0.3	0.0034	1.4±0.3	0.0024
HF–CO₂	670	2.0±0.4	0.0044	1.8±0.3	0.0031	1.1±0.2	0.0020

[a]The probabilities, P, have been calculated from the relationship $P = 4k/n\bar{v}\pi(d_1+d_2)^2$, where d_1 and d_2 are the molecular diameters; k is the measured rate constant (sec^{-1}· torr^{-1}); n is the number density of molecules (cm^{-3}· torr^{-1}); and $\bar{v}$ is the average speed of approach between molecules of a given pair. For HF and DF a collision diameter of 3.0 Å has been assumed; collision diameters of 3.3 Å have been taken for HCl and DCl, and a value of 3.9 Å has been taken for CO₂, see J. O. Hershfelder, C. F. Curtis and R. B. Bird, *Molecular Theory of Gases and Liquids* (Wiley, New York, 1954), pp. 597, 1200.
[b]See Ref. 3.

to come under the influence of a short range potential with such features, there would be a tendency for intermolecular alignment in the relatively stable hydrogen bonded configuration. At larger impact parameters where the intermolecular electron charge overlap is negligible, the interaction potential would be dominated by interactions between the transition dipoles for HF and CO₂ and by the interaction between the permanent dipole moment of HF and the quadrupole moment of CO₂.[6]

There would appear to be three possible sources for the observed existence of an inverse temperature relationship for the transition probabilities for the HF–CO₂ and DF–CO₂ systems at low temperatures:

(a) At large impact parameters, in the region of validity of perturbation calculations based on the Born approximation, an "impact parameter" or "straight-line-trajectory" approach leads to a thermally averaged transition probability for near resonant energy transfer that decreases with increasing temperature independently of the precise nature of the interaction potential.[24]

(b) At moderate impact parameters, somewhat larger than the hypothetical classical distance of closest approach for zero impact parameter, the attractive portion of even a spherically symmetric (orientation averaged) interaction potential can lead to transition probabilities with an inverse temperature dependence.[29]

(c) The short range anisotropy introduced into the intermolecular potential by the hydrogen-bonding interaction could introduce a tendency for a favorable alignment for both V→V, R and V→R, T energy transfers at low temperatures and small impact parameters.[30] That is, vibrational energy transfer will be facilitated

when the collision occurs with the hydrogen atom caught between the massive F atom and the CO₂ molecule.[31] Moreover, energy transfer to or from the rotational motion of HF would be expected to be efficient because of the highly anisotropic nature of the intermolecular potential for molecular orientations near the hydrogen bonded configuration.[28] These effects should be important for the small to moderate impact parameter collisions outside the region of validity of the impact parameter first-order-perturbation theories.

The temperature dependences of vibrational energy transfer and deactivation processes for the HCl–CO₂ and DCl–CO₂ systems have recently been determined in the range from 300 to 510 °K by Stephenson, *et al.*[2] The vibrational relaxation probabilities for the HCl–CO₂ and DCl–CO₂ systems are compared with the present results for the HF–CO₂ and DF–CO₂ systems in Figs. 11 and 12. The V→V transfer probabilities of Fig. 11 correspond to energy transfer in the exothermic direction for the processes

$$HX(v=1) + CO_2(00^00) \underset{k'_e}{\overset{k_e}{\rightleftharpoons}} HX(v=0) + CO_2(00^01) + \Delta E_v,$$

(12)
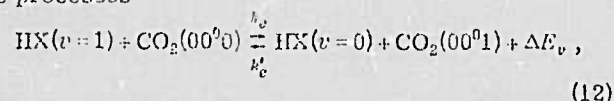
with respective vibrational energy defects of $\Delta E_v = 1612$ cm^{-1}, 558 cm^{-1}, 537 cm^{-1} and -258 cm^{-1} for HX = HF, DF, HCl, and DCl. For the HF–CO₂ case the probabilities of Fig. 11 correspond to the measured values of $k_e + k_{12}$ which provide only an upper bound on the V→V transfer probability for process (12).

Dillon and Stephenson[9] have recently developed a semiclassical nth-order perturbation theoretical approach which appears to provide very satisfactory predictions of the probabilities for the V→V, R processes (1). The theoretical probabilities for the HF–CO₂, DF–CO₂, and HCl–CO₂ systems calculated in reference (5)
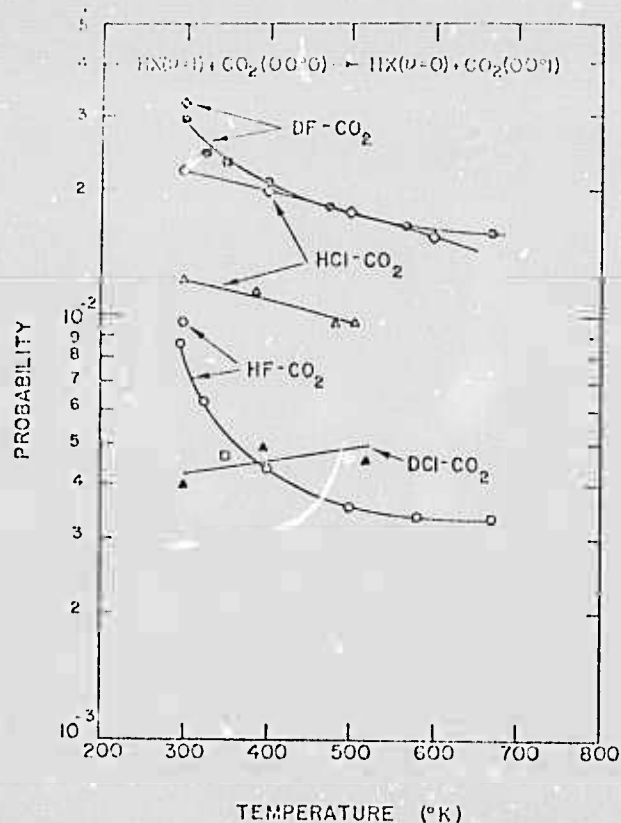
FIG. 11. Comparison of the temperature dependences of the V→V, R transfer probabilities for process (12) for the HCl–CO₂, DCl–CO₂, HF–CO₂ and DF–CO₂ systems: △, HCl–CO₂, Stephenson, *et al.*, Ref. 2; ▲ DCl–CO₂, Stephenson, *et al.*, Ref. 2; ◇, HCl–CO₂, theory of Dillon and Stephenson, Ref. 6; □, HF–CO₂, Stephens and Cool, Ref. 3; ○, HF–CO₂, present work; O, HF–CO₂, theory of Dillon and Stephenson, Ref. 6; ⊡, DF–CO₂, Stephens and Cool, Ref. 3; ○, DF–CO₂, present work; ◇, DF–CO₂, theory of Dillon and Stephenson, Ref. 6.

are included with the experimental data of Fig. 11. Calculations are not yet available for the DCl–CO₂ system.

An important feature of the data of Fig. 11 is the abrupt increase in V→V, R transfer probability as the temperature decreases from 400 to 300 °K for the HF–CO₂ and DF–CO₂ systems. Approximate calculations by Dillon and Stephenson[32] for the HF–CO₂ and DF–CO₂ systems in this temperature range do not indicate the large decrease in probability for increased temperature exhibited by the data in Fig. 11. Nevertheless the agreement between experiment and theory shown in Fig. 11 must be regarded as quite good. The theory while perforce containing computational approximations is independent of *ad hoc* choices of molecular parameters. This agreement lends support to the notion inherent in the theory that the transition probability is approximately proportional to the product of the squared dipole matrix elements for the vibrational transitions involved.

The theory of Dillon and Stephenson describes the V →V, R interaction between HX and CO₂ as a combination of V→V and R→R transfer effects. The V→V transfer is accounted for in terms of a dipole–dipole transition moment interaction; the R→R transfers are described by a permanent moment interaction between the dipole

moment of HX and the quadrupole moment of CO₂. The small perturbation approach based upon use of the Born approximation followed previously by other authors[?,?] has been discarded in favor of a more appropriate description for the relatively strong interactions of present interest. Recognition has been given to the important role played by multiquantum rotational transitions in minimizing the overall conversion of internal energy into translational motion. In the Dillon and Stephenson approach, a proper calculation of the probability for a transition between initial and final states must take account of the efficacy of the time-dependent intermolecular potential in inducing an ordered sequence of virtual transitions along a multiquantum path of intermediate rotational states. The results obtained with the new theory provide a remarkable improvement over the first and second order perturbation theories of multipole moment interactions of Sharma[32] which have been discussed in connection with HX–CO₂ systems by Stephenson, *et al.*[2]

The Dillon and Stephenson theory incorporates the first two of the three explanations offered above for the existence of an inverse temperature dependence for energy transfer probability. That is, the important contributions to the probability come from *n*th-order interactions that are near resonant and involve an anisotropic long range potential; moreover, the temperature dependence associated with curved trajectories at moder-

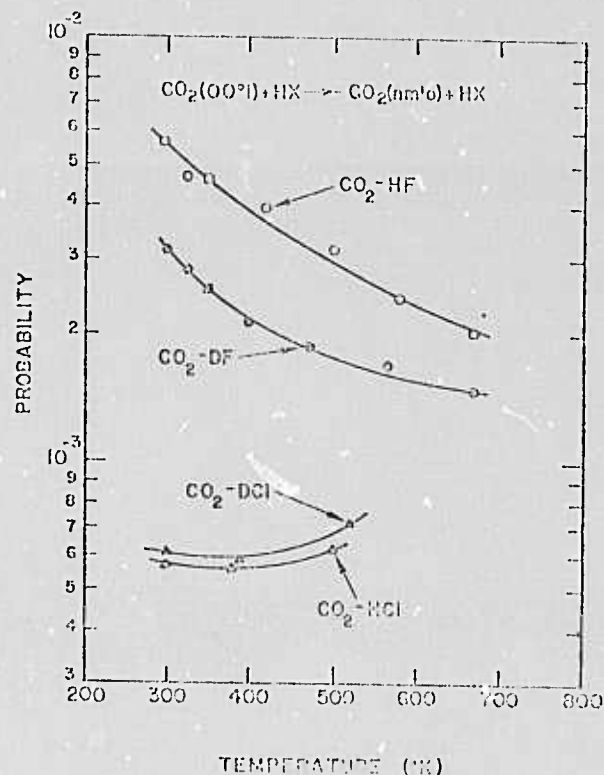

FIG. 12. Comparison of the temperature dependences of the V→R, T deactivation probabilities of CO₂(00°1) molecules by process (3) for HCl, DCl, HF, and DF: △, CO₂–HCl, Stephenson, *et al.*, Ref. 2; ▲, CO₂–DCl, Stephenson, *et al.*, Ref. 2; □, CO₂–HF, Stephens and Cool, Ref. 3; ○, CO₂–HF, present work; ⊡, CO₂–DF, Stephens and Cool, Ref. 3; ○, CO₂–DF, present work.

ately large impact parameters was included since trajectories were calculated with a spherically symmetric potential with an attractive portion (Lennard-Jones). However, the calculations did not include the effects of short range anisotropy in the intermolecular potential and this may be the reason that the calculations do not adequately predict the steep inverse temperature dependence observed in the present experiments.

Further evidence for the existence of strong attractive intermolecular forces in the HF–CO₂ and DF–CO₂ systems is given by the V–R, T relaxation data of Fig. 10 which are replotted in Fig. 12 for comparison with the HCl–CO₂ and DCl–CO₂ systems. The probabilities for HF and DF refer to the process (3) with rate constant k_{21}. The probabilities for the HCl–CO₂ and DCl–CO₂ systems of Fig. 12 refer to the upper bounds on k_{21} given by Stephenson, et al.[2]

A strong inverse temperature dependence is again evident for the deactivation of $CO_2(00^01)$ by both HF and DF, whereas a slight increase in probability with increasing temperature perhaps exists for deactivation by HCl and DCl. The lesser rate of deactivation by DF than that for HF suggests energy transfer to rotation of the collision partner. The deactivation by HCl and DCl does not give as clear evidence of this, although it should be emphasized that the HCl and DCl data are only upper bounds for the actual values of k_{21}.

Semiempirical models of various types have been used to explain the qualitative features of the self-deactivation of HX–HX collision pairs.[14,33,34] An important feature of these models is the inclusion of a substantial attractive intermolecular potential well to account for the observed temperature dependence of deactivation probabilities. Berend and Thommarson[30] have employed an interaction potential designed to explicitly account for hydrogen bonding in the HF and DF systems. Shin[34] and Bott and Cohen[14] have accounted for intermolecular attraction in terms of a dipole–dipole interaction. None of these theoretical results have been included with the data of Fig. 2 and 3 because comparisons of theory and experiment have been adequately discussed elsewhere.[14,30,34] A similar approach has been followed by Shin[35] in calculations of the deactivation of CO₂ by HF and DF. The calculations are compared with experimental results in Fig. 10. The theory does not appear to offer a good description of the deactivation processes as Fig. 10 indicates. The chief difficulty is that the observed temperature dependence of deactivation probabilities is not reproduced in the calculations.

[1] T. A. Cool, IEEE J. Quantum Electron. QE-9, 72 (1973).

[2] J. C. Stephenson, J. Finzi and C. B. Moore, J. Chem. Phys. 56, 5214 (1972).

[3] R. R. Stephens and T. A. Cool, J. Chem. Phys. 56, 5863 (1972).

[4] J. K. Hancock and W. H. Green, J. Chem. Phys. 56, 2474 (1972).

[5] R. S. Chang, R. A. McFarlane and G. J. Wolga, J. Chem. Phys. 56, 667 (1972).

[6] T. A. Dillon and J. C. Stephenson, J. Chem. Phys. 58, 2056 (1973).

[7] R. R. Stephens and T. A. Cool, Rev. Sci. Instrum. 42, 1489 (1971).

[8] R. R. Stephens, Ph.D. thesis, Cornell University, 1971.

[9] C. B. Moore, Fluorescence, edited by C. G. Guilbault (Dekker, New York, 1967), pp. 133–198.

[10] J. C. Stephenson and C. B. Moore, J. Chem. Phys. 56, 1295 (1972).

[11] J. L. Ahl and T. A. Cool, J. Chem. Phys. 58, 5540 (1972).

[12] W. C. Solomon, J. A. Blauer, F. C. Jaye and J. G. Hnat, Intl. J. Chem. Kinet. 3, 215 (1971).

[13] J. A. Blauer, W. C. Solomon and T. W. Owens, Intl. J. Chem. Kinet. 4, 293 (1972).

[14] J. F. Bott and N. Cohen, J. Chem. Phys. 55, 3698 (1971).

[15] J. F. Bott and N. Cohen, J. Chem. Phys. 58, 934 (1973).

[16] J. F. Bott, J. Chem. Phys. 57, 96 (1972).

[17] L. S. Blair, W. D. Breshears, G. L. Schott, J. Chem. Phys. (to be published).

[18] S. S. Fried, J. Wilson and R. L. Taylor, IEEE J. Quantum Electron., QE-9, 59 (1973).

[19] J. J. Hinchen, J. Chem. Phys. (to be published).

[20] J. R. Airey and S. S. Fried, Chem. Phys. Lett. 8, 23 (1971).

[21] T. A. Cool, T. J. Falk and R. R. Stephens, Appl. Phys. Lett., 15, 318 (1971).

[22] This correction amounted to approximately 1500 sec⁻¹ · torr⁻¹ in most cases.

[23] J. C. Stephenson, R. E. Wood and C. B. Moore, J. Chem. Phys. 54, 3097 (1971).

[24] J. R. Airey and I. W. M. Smith, J. Chem. Phys. 57, 1669 (1972).

[25] J. F. Bott, J. Chem. Phys. 58, 4539 (1973).

[26] H. L. Chen and C. B. Moore, J. Chem. Phys. 54, 4072 (1971).

[27] J. E. Lennard-Jones, J. Chem. Phys. 20, 1024 (1952).

[28] R. D. Sharma and C. A. Brau, J. Chem. Phys. 50, 924 (1969).

[29] T. L. Cottrell and J. C. McCoubrey, Molecular Energy Transfer in Gases (Butterworth, London, 1961).

[30] G. C. Berend and R. L. Thommarson, J. Chem. Phys. 58, 3203 (1973).

[31] H. K. Shin, J. Chem. Phys. 49, 3964 (1968).

[32] T. A. Dillon and J. C. Stephenson, J. Chem. Phys. 58, 3849 (1973).

[33] R. D. Sharma and C. W. Kern, J. Chem. Phys. 55, 1171 (1971).

[34] H. K. Shin, Chem. Phys. Lett. 10, 81 (1971).

[35] H. K. Shin, J. Chem. Phys. 57, 3484 (1972).

Vibrational Deactivation of Molecules by Collisions with Atoms

Professor Wolga

The two experimental systems we have constructed for the purpose of measuring deactivation rates of $HF(v=1)$ and $CO_2(00°1)$ have been described in previous reports. During this contract year we have finished the experimental studies of $HF(v=1)$, $DF(v=1)$ and $CO_2(00°1)$ deactivation at room temperature by a variety of atomic species. We shall discuss the individual measurements in separate sections below.

Atom Deactivation of $HF(v=1)$ and $DF(v=1)$

Our data is summarized in Table I below for $HF(v=1)$ and $DF(v=1)$ at $T=300K$.

Table I

X	k_X-HF(sec^{-1}-Torr^{-1})	k_X-DF(sec^{-1}-Torr^{-1})
$O(^3P)$	$1.0 \pm 0.2 \times 10^5$	$2.5 \pm 0.7 \times 10^5$
$F(^2P)$	$0.9 \pm 0.2 \times 10^4$	$2.1 \pm 0.4 \times 10^4$
$Cl(^2P)$	$2.4 \pm 0.5 \times 10^4$	$6.6 \pm 1.0 \times 10^4$
$H(^2S)$	$< 0.5 \times 10^3$	-----
$D(^2S)$	$< 1.5 \times 10^3$	-----
$Br(^2P_{3/2})$	$1.0 \pm 0.5 \times 10^6$	-----

The entries in the DF column for H and D deactivation were not studied because of the very slow deactivation of HF and our belief that no significant change is expected for DF. Several experimental runs were made, however, on the DF-H system to check this hypothesis. No discernable change in the DF self deactivation rate was observed and we therefore did not complete this

data with extensive experimentation.

Several features of this data should be commented upon.

1. In all cases where comparison is possible DF(v=1) was deactivated more rapidly by the same collider than was HF(v=1). This is contrary to what is expected for conventional $V \to R, T$ deactivation. We are therefore led to consider other energy loss mechanisms.

2. Deactivation by oxygen and halogen atoms was very rapid and 1-2 orders of magnitude faster than deactivation by H or D. A principal difference between these two sets of collision partners is that O, F and Cl possess orbital angular momentum degeneracy $(L > 0)$ while H and D are in S states $(L = 0)$. Nikitin has from analysis of molecular vibration data and his calculations postulated that a vibronic mechanism may lead to rapid deactivation when the collider has orbital angular momentum degeneracy. The mechanism he proposes is that during a collision this degeneracy is lifted during the close approach of the colliders and that when the resultant splitting creates an energy difference equal to the vibrational quantum a resonant process of vibrational energy loss is established. Resonant energy exchange processes generally lead to efficient deactivation. The contrast in our data between the rates due to $L = 1$ and $L = 0$ collision partners lends considerable support to Nikitin's hypothesis in the case of atom deactivation. We believe this process is, in fact, generally true and will comment upon it further in our discussion of our CO_2 deactivation data.

3. The rate for the deactivation of HF(v=1) by $Br(^2P_{3/2})$ atoms is extremely fast, $1 \times 10^6 sec^{-1}$ Torr, within a factor of ten of gas kinetic. We attribute this fast rate to a resonant process - Vibrational-Electronic energy transfer schematically described by

$$HF(v=1) + Br(^2P_{3/2}) \xleftrightarrow[k'_e]{k_e} HF(v=0) + Br(^2P_{3/2}).$$
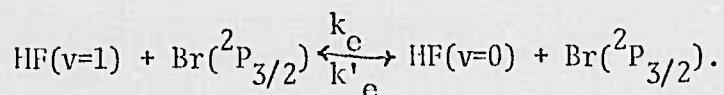
The fine structure splitting in Br is 3685 cm^{-1} while the 1→0, P(6) transition in HF is 3693.5 cm^{-1}. Thus near perfect resonance exists for this process which we believe accounts for the fast rate we observe. We believe that our observation of this fast rate is one of the clearest demonstrations to date that V → E process can be extremely effective when resonantly enhanced. As well, it supports the recent observation[1] by Hon and Novak that the presence of Br enhance: the effectiveness of their HF overtone laser presumably by providing an effective deactivation process for the v=1 state.

We have not repeated this work for DF as yet because no comparable resonance exists in this system.

We are writing up the HF and DF work for publication as well as the V → E transfer studies in the HF-Br system.

Atom Deactivation of $CO_2(00°1)$

Our data is summarized in Table II below for $CO_2(00°1)$ at T = 300K.

Table II

X	k_x-CO_2 $sec^{-1}Torr^{-1}$
$O(^2P)$	$6.7 \pm 1.2 \times 10^3$
$Cl(^2P)$	$4.9 \pm 1.3 \times 10^5$
$F(^2P)$	$1.04 \pm .09 \times 10^5$
$H(^2S)$	$3.3 \pm 3 \times 10^3$
$D(^2S)$	$< 2 \times 10^3$
N	$\leq 9.5 \times 10^2$

These rates describe the collisional process: $CO_2(00°1) + X \rightarrow CO_2(m,n,o)+X$

(1) J.F. Hon and J.R. Novak,"Chemically Pumped Hydrogen Fluoride Overtone Laser" paper TA6, 4th Conf. on Chemical and Molecular Lasers, St. Louis, Mo., 10/21-23/74.

Several features of this data require comment.

1. As with HF(v=1) the relaxation due to collision with halogen atoms possessing orbital degeneracy is much faster than with S state atoms. O atom relaxation is also faster but not by as large a factor.

2. Rate enhancement due to complex formation between CO_2 and O, Cl, or F is tentatively ruled out by our measurements of the broadening coefficient on the atomic ESR lines by CO_2. CO_2 broadens these lines at rates within a factor of two of the broadening rate of argon. Since we anticipate a strong effect on ESR line broadening due to complex formation we feel this mechanism for enhanced deactivation of CO_2 by O, F, and Cl can be ruled out.

3. Chemical reaction of $CO_2(00°1)$ with Cl, F, and O are also ruled out as rate enhancing mechanisms. The reactions with Cl and F are highly endothermic while the reaction with O is ruled out because the reverse rate is extremely slow while the forward reaction is slightly endothermic.

4. V to E transfer from HF(v=1) to the first excited spin-orbit state of Cl, F and O cannot be ruled out. Some near resonant V to E transfers are possible as the following relaxation mechanisms and Table III of spin-orbit splittings reveals.

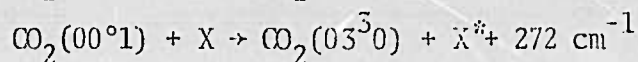$$CO_2(00°1) + X \rightarrow CO_2(11^10) + X^* + 416 \text{ cm}^{-1}$$
$$CO_2(00°1) + X \rightarrow CO_2(03^30) + X^* + 272 \text{ cm}^{-1}$$
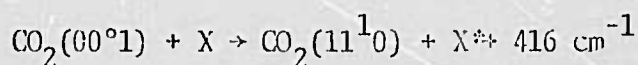
Table III

Specie X	Spin Orbit Splitting, cm^{-1}
O	158.5 (J=1), 226.5 (J=2)
F	404
Cl	881

5. The Nikitin mechanism discussed in regard to our HF measurements may be operative here as well.

6. The Cl and F deactivation rates we have measured are among the fastest $CO_2(00°1)$ deactivation rates yet measured. The effectiveness of F atoms particularly in relaxing $CO_2(00°1)$ must be taken into account in computer codes designed to predict HF-CO_2 and DF-CO_2 chemical transfer lasers which undoubtedly contain F atom relaxers.

This work is being written up in detail for publication.

Continuing Work

During the next contract year we shall concentrate on the following studies mentioned in decreasing order of emphasis.

1. The relaxation of HCl(v=1) and HBr(v=1) by atoms at room temperatures will be studied.

2. The design of apparatus to extend our atom deactivation studies to lower and higher temperatures is being considered. Successful attainment of controllable temperature in our apparatus will be followed by rate measurements with emphasis placed on HF, DF, and HCl.

3. We shall seek to define experimental conditions under which reactive collisions may be studied.

Publications and Conference Papers

1. G.P. Quigley and G.J. Wolga, "Deactivation of HF(v=1) by F, O, and H atoms", Chem. Phys. Lett. 27, 276 (1974).

2. G.P. Quigley and G.J. Wolga, "Vibrational Deactivation of HF(v=1) and DF(v=1) by Collisions with Atoms," Paper MD8- 4th Conference on Chemical and Molecular Lasers., St. Louis, Mo. October 21-23, 1974.

3. M.I. Buchwald and G.J. Wolga, "Vibrational Deactivation of $CO_2(^3\Sigma)$ by Collisions with Atoms," Paper MD9 - ibid. Submitted for publication, J. Chem. Phys.

DEACTIVATION OF HF($v = 1$) BY F, O, AND H ATOMS

G.P. QUIGLEY and G.J. WOLGA

Laboratory of Plasma Studies, Cornell University, Ithaca, New York 14850, USA

The laser induced fluorescence method has been used to measure the rate of deactivation of HF($v = 1$) by F, O, and H atoms at 300° K. The rate for F-atoms was found to be $k_{F-HF} = (0.9 \pm 0.2) \times 10^4$ sec^{-1} torr^{-1}, for O-atoms $k_{O-HF} = (1.0 \pm 0.2) \times 10^5$ sec^{-1} torr^{-1}, and for H-atoms, an upper limit to the rate was found to be $k_{H-HF} < 0.5 \times 10^3$ sec^{-1} torr^{-1}. The results are explained qualitatively in terms of a vibronic to translational energy transfer mechanism.

1. Introduction

A large body of literature exists on experimental studies of vibrational energy transfer processes involving HF [1–9]. The initial motivation for this work was its relevance to the HF chemical laser. Subsequent discovery of anomalous effects such as the unusual temperature dependence for the V → R, T self-relaxation rate and the magnitude of this rate (the absolute magnitude as well as the relative magnitude compared to the V–V rate) have also added to the great interest.

The present study is concerned with the deactivation of HF by reactive atomic species. These rates are of importance because it is thought that atoms of this kind have a substantial effect on the rate of decay of vibrationally excited species. The F and H atom rates are also needed to characterize the HF laser system for the purpose of optimizing efficiency.

2. Experimental

The vibrational relaxation data reported here were obtained in a fast flow system with the laser induced fluorescence technique [10]. The laser source was a pulsed HF chemical laser (SF$_6$:H$_2$ = 16:1) of the transverse electrode type. The laser was operated multiline and the gas flow, SF$_6$ and H$_2$ mixture, and discharge pulse rate were adjusted to give optimum

HF $v = 1 \rightarrow v = 0$ output. The pulse energy was 1 mJ, 55% of which was on the $1 \rightarrow 0$ transitions (P$_6$, P$_7$, P$_8$). The total pulse duration (including $3 \rightarrow 2$, $2 \rightarrow 1$, and $1 \rightarrow 0$ transitions) was less than 1 μsec.

A schematic diagram of the experimental apparatus is shown in fig. 1. There are two distinct parts to this experiment. First, the effect of the atoms on the population of HF($v = 1$) is determined by measuring the change in the decay time of the HF laser induced fluorescence with and without a discharge in the diluent plus parent molecule flow. Second, the atom concentration in the fluorescence cell was measured with an EPR spectrometer by recreating all flow and wall conditions in another section of the flow system (upstream) with an EPR cavity in the same location relative to the discharge as was the fluorescence cell.

The procedure was to set up a flow of diluent (usually argon) plus parent molecule (X$_2$ = F$_2$, O$_2$, H$_2$). This flow is uniquely determined by the pressures P_2 and P_1 (likewise P_4 and P_3) which were measured with a corrosive gas resistant capacitance manometer. A small amount of HF was added downstream (less than 1% of the total flow) through small holes distributed around the circumference of the Teflon tube. The HF is well mixed with the Ar + X$_2$ flow at the fluorescence cell.

The microwave discharge took place in a quartz tube. All other tubes were either Teflon or quartz with a Teflon insert to reduce wall recombination. The HF fluorescence was monitored with an
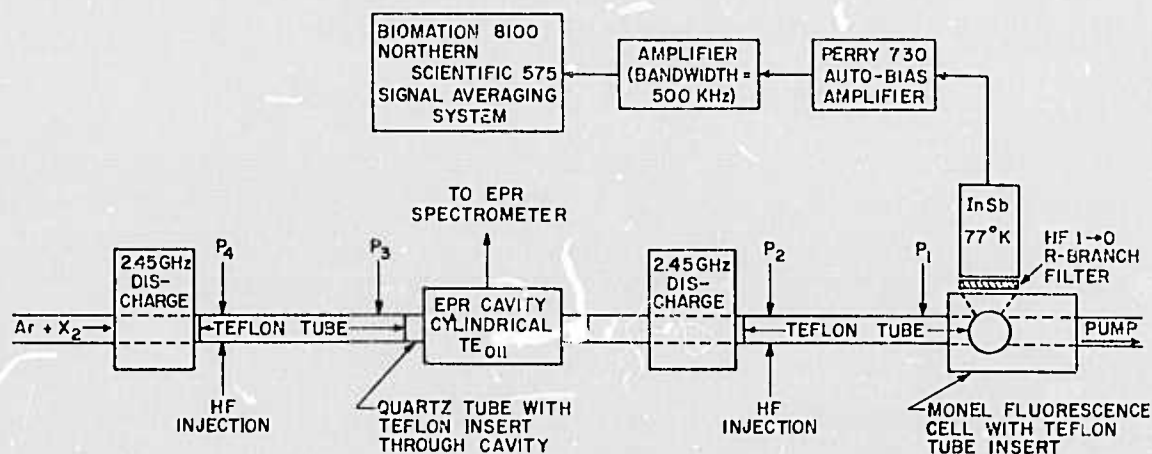
_13 t_

Fig. 1. A schematic diagram of the experimental apparatus.

InSb PV detector. A narrow band interference filter passed only the HF $1 \rightarrow 0$ R-branch emission. The overall response of the system was less than 0.5 μsec. The laser power was reduced to avoid overpumping the HF and thus eliminating the problems of V–V transfer and heating of the gas due to V–R,T energy transfer processes. The resultant loss in signal to noise was made up by the Biomation 8100 - Northern Scientific 575 signal averaging system.

A complete block diagram for the EPR spectrometer is not shown in fig. 1. A detailed description of this system will be given elsewhere. This technique for measuring absolute concentrations of gas phase radicals is well known and described by Westenberg [11].

The gas flow is along the axis of the high Q cylindrical cavity in a 10 mm i.d. quartz tube. The thin-walled Teflon tube insert substantially reduces or eliminates wall recombination and hence non-uniformities in the atom concentration without significantly affecting the sensitivity of the spectrometer. Taking the sine-squared dependence of the microwave magnetic field into account, the 3.5 cm long EPR cavity gives a resolution of about 2 cm over which the average atom concentration is determined. The usual problems of saturation of the spin system by high power microwave fields and broadening due to large amplitude magnetic field modulation were scrupulously avoided.

The following gas samples were used: F_2: Air Products technical grade (purity $> 98\%$); O_2: Linde

UHP (purity $> 99.99\%$); H_2: Matheson UHP (purity $> 99.999\%$); Ar: Matheson Purity (purity $> 99.9995\%$); He: Matheson Purity (purity $> 99.9999\%$); HF: Matheson (purity $> 99.9\%$).

Further purification involved passing each gas (except HF) through a liquid nitrogen cold trap. The HF was purified by trap to trap distillation between $77°K$ and $195°K$.

3. Results

For F_2 and O_2 in an argon diluent, the pertinent energy transfer processes in the deactivation of $HF(v = 1)$ are:

$$HF(v = 1) + HF(v = 0) \overset{k_{11}}{\rightarrow} 2HF(v = 0), \tag{1}$$

$$HF(v = 1) + X_2(v = 0) \overset{k_{12}}{\rightarrow} HF(v = 0) + X_2(v = 0), \tag{2}$$

$$HF(v = 1) + Ar \overset{k_{13}}{\rightarrow} HF(v = 0) + Ar. \tag{3}$$
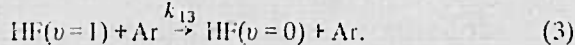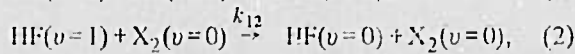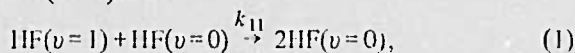
These apply while the microwave discharge is off, and the decay time of the fluorescence is given by:

$$1/\tau_0 = k_{11} [HF] + k_{12} [X_2] + k_{13} [Ar]. \tag{4}$$

This assumes that $[HF(v = 1)]$ is small.

When the microwave discharge is turned on, some of the X_2 is dissociated giving an additional channel for deactivation:

$$HF(v = 1) + X \overset{k_{1d}}{\rightarrow} HF(v = 0) + X. \tag{5}$$
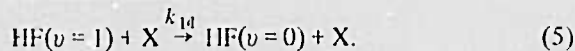
In this case, the decay time of the fluorescence is

277

given by:

$$1/\tau_D = k_{11}[HF] + k_{12}([X_2] - \tfrac{1}{2}[X])$$
$$+ k_{13}[Ar] + k_{14}[X]. \tag{6}$$

The difference between (6) and (4) gives:

$$k_{14} = \frac{1}{[X]}\left[\frac{1}{\tau_D} - \frac{1}{\tau_0}\right] + \tfrac{1}{2}k_{12}. \tag{7}$$

The rates used for k_{12} were: for O_2, $k_{12} = 400$ sec^{-1} torr^{-1} [4,5] and for F_2, $k_{12} = 100$ sec^{-1} torr^{-1} [6]. These turn out to be negligible corrections.

The importance of using the EPR spectrometer for measuring [X] is that it allows one to determine the absolute concentration of the atomic species in a fast flow system without the need to alter the flow (as in titration or catalytic probe methods) or even to know what the flow rates are. For F and O atoms, the absolute accuracy of the EPR measurement of concentration is better than 10%.

Another source of error is in measuring the change in the total fluorescence decay rate. For O and F atoms, the change is significant and hence the error

is small (10%). A typical run showing the change in decay rate of HF($v = 1$) in a mixture of O, O_2, Ar and HF as a function of O atom partial pressure (P_O) is shown in fig. 2. Similar results were obtained with fluorine.

Using eq. (7), one can plot $(\tau_D^{-1} - \tau_0^{-1})$ as a function of atom partial pressure. The result should be a straight line of slope equal to the atom deactivation rate k_{14} and intersecting the origin. The results of such a plot for the F and O atom data are shown in fig. 3. The rates determined from these data are:

$$k_{F-HF} = (0.9 \pm 0.2) \times 10^4 \text{ sec}^{-1} \text{ torr}^{-1},$$
$$k_{O-HF} = (1.0 + 0.2) \times 10^5 \text{ sec}^{-1} \text{ torr}^{-1}.$$

For the case of H atoms, the energy transfer is complicated by the near resonance of the first vibrational levels of H_2 and HF. This gives rise to a double exponential decay [7]. The fast decay is due to V–V transfer from HF to H_2 and HF self-relaxation, and the slow process is related to the decay of the H_2–HF vibrational energy pool through V–R,T transfer from HF($v = 1$). The atoms would be expected to effect

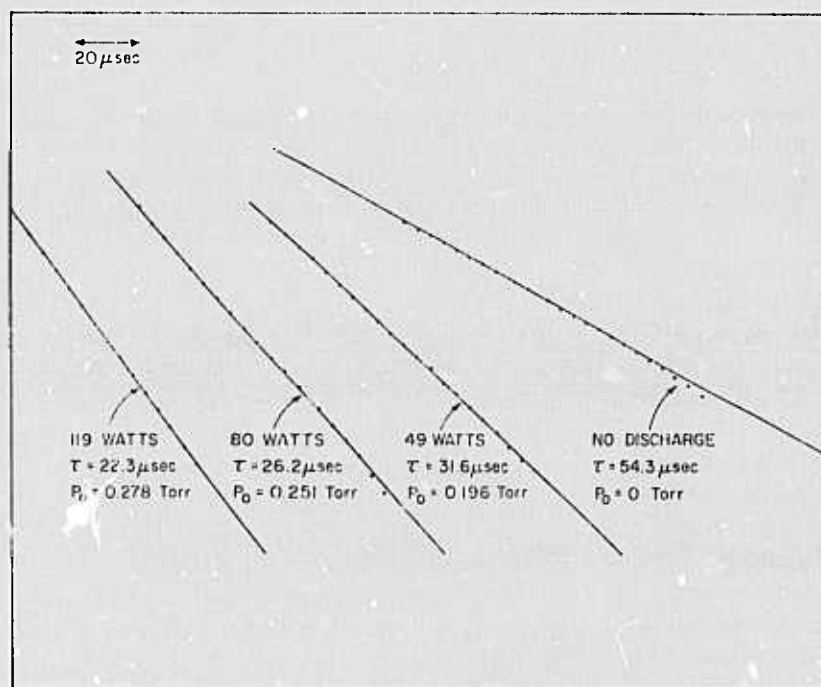| 119 WATTS | 80 WATTS | 49 WATTS | NO DISCHARGE |
| $T = 22.3\,\mu$sec | $T = 26.2\,\mu$sec | $T = 31.6\,\mu$sec | $T = 54.3\,\mu$sec |
| $P_0 = 0.278$ Torr | $P_0 = 0.251$ Torr | $P_0 = 0.196$ Torr | $P_0 = 0$ Torr |

Fig. 2. Semilog plot of relative intensity as a function of time for different discharge conditions in Ar + O_2.

13 d

this slow rate by deactivating both $H_2(v = 1)$ and $HF(v = 1)$. The former rate is known to be [12]:

$$k_{H-H_2} = (1.0 \pm 0.5) \times 10^4 \ \text{sec}^{-1} \ \text{torr}^{-1}.$$

However, under no circumstances was there any change observed due to the presence of H atoms.

The only safe thing that one can say in this case is that the hydrogen atoms are not as effective as H_2 in relaxing $HF(v = 1)$. This puts an upper limit on the atom deactivation rate of [7]:

$$k_{H-HF} < \tfrac{1}{2}(k_{H_2-HF}) < 0.5 \times 10^3 \ \text{sec}^{-1} \ \text{torr}^{-1}.$$

4. Conclusion

These and other preliminary results of this laboratory (D. N on $HF(v=1)$ [13]; O, Cl, H on $CO_2(001)$ [14]) lend support to the non-adiabatic theory of Nikitin [15] which is based on a vibronic to translational energy transfer mechanism. Briefly, as it applies to our experiments, atoms with electronic orbital angular momentum degeneracy would be expected to be more efficient in transferring vibrational energy from $HF(v=1)$. During a collisional encounter, the degeneracy which exists at infinite separation is split and electronic transitions are possible between these states. When the frequencies of the electronic transition in the atom and the vibrational transition in HF become equal, there is a large increase in the cross section for energy transfer.

This says nothing of the possibility for fast relaxation caused by atom exchange or abstraction reactions which could predominate under favorable conditions. This certainly appears to be true in the case of O and H atoms "deactivating" vibrationally excited HCl [16]. However, it does not appear to be important for the F and H atom encounters with $HF(T = 300°K)$. This is supported in part by the recent calculations of O'Neil et al. [17] which suggest a minimum barrier height for the exchange reaction:

$$F + HF(v=0) \rightarrow FH(v=0) + F \text{ of } 18 \text{ kcal/mole}.$$
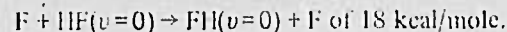
Previous high temperature results for the deactivation of $HF(v = 1)$ by F-atoms have been reported [2,8,9]. We choose to compare our results with those of Blair et al. [2]. This is shown in the Landau–Teller plot of fig. 4. The rather substantial temperature range of
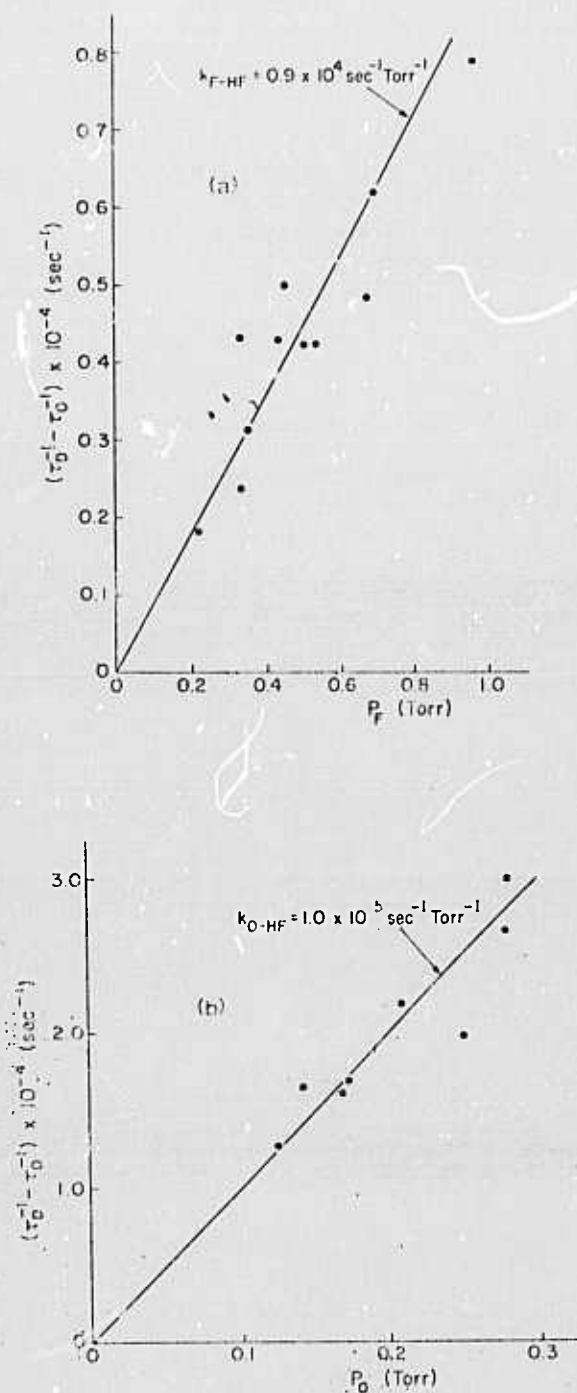
Fig. 3. Distribution of data points as calculated from eq. (7) about the measured atom deactivation rates for (a) F on $HF(v = 1)$ and (b) O on $HF(v = 1)$.
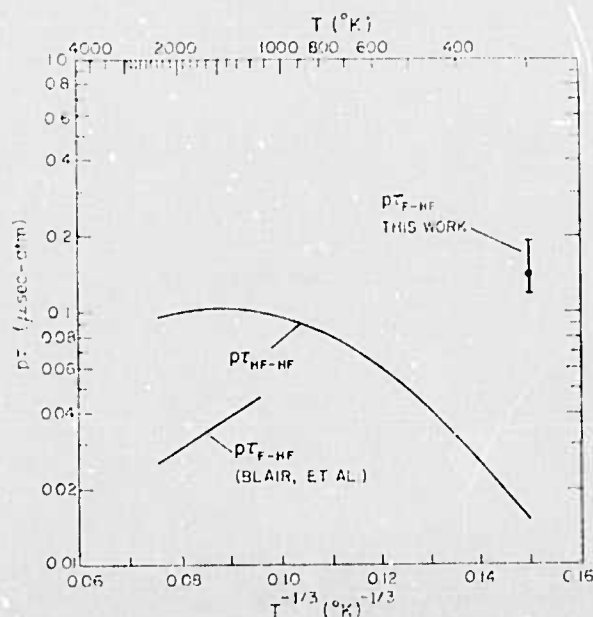
Fig. 4. Landau–Teller plot of the temperature dependence of the F atom deactivation of $HF(v=1)$.

$1000°K$ over which there is no rate measurement precludes the drawing of any but the most speculative conclusions. This figure does show however that the trend established at high temperatures, for the decreasing effect of F atoms on $HF(v=1)$ with decreasing temperature, persists at least to room temperature $(300°K)$. The temperature dependence of the pure HF relaxation rate [2] is shown for comparison.

Clearly, more rate measurements are needed above and below room temperature before anything definitive can be said about the effects of long range forces or chemical bonding on the efficiency of reactive atoms in deactivating $HF(v=1)$.

References

[1] R.A. Lucht and T.A. Cool, J. Chem. Phys. 60 (1974) 1026.

[2] L.S. Blair, W.D. Breshears and G.L. Schott, J. Chem. Phys. 59 (1973) 1582.

[3] R.M. Osgood Jr., P.B. Sackett and A. Javan, J. Chem. Phys. 60 (1974) 1464.

[4] W.H. Green and J.K. Hancock, IEEE J. Quantum Electron. QE-9 (1973) 50.

[5] J.F. Bott and N. Cohen, J. Chem. Phys. 58 (1973) 4539.

[6] S.S. Fried, J. Wilson and R.L. Taylor, IEEE J. Quantum Electron. QE-9 (1973) 59.

[7] J.K. Hancock and W.H. Green, J. Chem. Phys. 57 (1972) 4515.

[8] W.C. Solomon, J.A. Blauer, F.C. Jaye and J.G. Hnat, Intern. J. Chem. Kinetics 3 (1971) 215.

[9] J.F. Bott and N. Cohen, J. Chem. Phys. 55 (1971) 5124.

[10] L.O. Hocker, M.A. Kovacs, C.K. Rhodes, G.W. Flynn and A. Javan, Phys. Rev. Letters 17 (1966) 233.

[11] A.A. Westenberg, Progr. Reaction Kinetics 7, Part I (1973) 23.

[12] R.F. Heidner and J.V.V. Kasper, Chem. Phys. Letters 15 (1972) 179.

[13] G.P. Quigley and G.J. Wolga, to be published.

[14] M.I. Buchwald

[15] E.E. Nikitin, Opt. Spectry. 9 (1960) 8.

[16] D. Arnoldi and J. Wolfrum, Chem. Phys. Letters 24 (1974) 234.

[17] S.V. O'Neil, H.F. Schaefer III and C.F. Bender, Proc. Natl. Acad. Sci. USA 71 (1974) 104.

Vibrational Deactivation of Carbon Monoxide by Atomic Oxygen

Prof. R.A. McFarlane

Introduction

In chemical laser systems where CO molecules are the active species, modelling and optimization of laser performance require that information be available on the rates at which vibrationally excited CO molecules are deactivated by collisions with any other species present. The past contract period has been devoted to measurements of such rates using laser induced fluorescence techniques similar to work on other molecules being carried out in this laboratory.

Of particular importance in situations where the active CO molecules are produced in the reactions

$$O + CS_2 \rightarrow CS + SO$$
$$O + CS \rightarrow CO^* + S$$
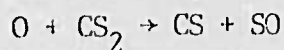
is the role that atomic oxygen could play in the removal of vibrational energy from CO^*. There are two possible routes by which this can occur, a direct V-T process and an atom exchange process and it is to be expected that both of these will make significant contributions to the total loss rate of CO^* molecules. An alternative process where CO_2 molecules are produced as a result of chemical reaction is known to be slow and is not expected therefore to be a significant loss mechanism in the laser system.

Our efforts have therefore been directed toward the measurement of the deactivation rates of $CO(v=1)$ molecules by atomic oxygen and this report will describe the development of the necessary laser source for CO excitation, the gas handling system and fluorescence cell, the design and construc-

tion of an E.P.R. system for absolute atom concentration determination, some preliminary data on the O + CO* rate and the direction of our ongoing activities.

General System Description

The excitation of CO molecules in either a static or flowing situation is accomplished by using the second harmonic of a pulsed CO_2 TEA laser. The overall block diagram of the experiment is shown in Figure 1. The TEA laser operates on the P(24) transition of the $00°1 \rightarrow 02°0$ band of CO_2 at 1043.154 cm^{-1} and is frequency doubled in a tellurium crystal to provide radiation which coincides with the P(14) transition of CO v=1 to v=0 at 2086.325 cm^{-1}. The pulse duration of this excitation is 300 nanoseconds and the subsequent fluorescence of the CO(v=1) molecules is monitored by an InSb photoconductive detector which observes spontaneous emission in a direction perpendicular to both the exciting beam and the direction of gas flow.

The laser excitation on P(14) directly populates the $J = 13$ level of v=1. To minimize the effect of laser light scattered directly into the detector a short pass filter is placed in front of the InSb detector to reject the P(14) frequency 2086.325 cm^{-1} and to pass only emission on R-branch transitions near R(12). The output of the detector is coupled to a Perry Model 720-84 amplifier which provides the necessary zero bias and this drives a Model 450-AG post-amplifier modified to drive a 50 ohm load. The frequency response of the detector amplifier combination limits observations to pulse risetimes of about 2 μsec. The fluorescence decay times which are obtained in the present experiments are substantially longer than this and are consequently faithfully reproduced. To enhance S/N ratios

of single pulse signals, each pulse waveform is digitized with a Biomation Model 8100 Waveform Digitizer and digital information for each of 2000 points in time during each pulse is accumulated in a Northern Model 575 Signal Averager. Typical runs accumulate data from 250 pulses. At the completion of each run the data is read from the signal averager to a magnetic cassette in a T.I. Model 733 A.S.R. data terminal. To obtain a measure of the fluorescence decay rate the data are processed using a Least Squares computer program to derive both a value for the decay rate and an estimate of its uncertainty. Computer programs are now operating for single and multiple exponential fits and to avoid the present requirement for punching the data manually onto computer cards we are presently arranging direct communication between our data terminal and the Cornell IBM 370 computer using an acoustic coupler and the time sharing capability of the 370. The entire 2000 data points will be available for curve fitting rather than the approximately 100 now processed on cards and significant reductions in uncertainties of fit will be possible. The realization of this interaction with the computer is essentially completed.

The TEA Laser

For this experiment a laser operating at 9.59 μ is required which is capable of operation in a selectable rotational transition, which can produce peak outputs on the order of 0.5 Mw for efficient harmonic generation and which can operate at one p.p.s. repetition rates reliably over extended periods.

A u.v. preionized laser with an active discharge region 3 cm x 3 cm x 40 cm is driven by discharging a 0.2 μfd low inductance capacitor into

the flowing gas column. An E.G.&G. HY-5 hydrogen thyratron is employed as a switch and plane parallel transmission line geometry is used to minimize circuit inductance and thereby increase the speed of the discharge. Typical operation is at 25 kV and uniform discharges are obtained in CO_2, N_2, He gas mixtures at total pressures as high as 500 Torr.

The laser cavity is formed by a concave reflector with 20% output coupling and a plane diffraction grating for selection of the operating wavelength. Single line operation in the $00°1 \rightarrow 10°0$ band and the $00°1 \rightarrow 02°0$ band of CO_2 is possible over a range of rotational lines up to $J = 40$ and output energies on the order of 100 - 200 mJ are available.

Optics and Harmonic Generator

The output from the laser is transmitted via a folded optical system to a crystal of tellurium mounted in a gimbal led holder for control of both the orientation of the beam direction with respect to the crystal C axis and the rotation of the crystal about the beam direction.

The first concave mirror in the optical path focuses the 2 cm diameter 10 μ beam onto the tellurium crystal. Care is taken to avoid placing the entrance plane of the crystal exactly at the focus since energy densities sufficiently large to cause surface damage can occur. Beam diameter at the crystal is controlled at about 1 mm. The second harmonic signal is optimized by adjusting the crystal orientation while monitoring the output of a Au:Ge detector on the far side of the fluorescence cell. A sapphire window rejects the fundamental signal.

Typical outputs at 5 μ of 10 μJ have been measured which is adequate for the fluorescence measurements. Larger pulse energies should be available considering the energy at the fundamental and a new boule of tellurium has

been cut to provide a larger clear aperture system which is expected to increase the energy at 5 μ by five to ten times.

Gas Handling System

A two stage Roots blower backed by a mechanical pump is used to exhaust the fluorescence cell and associated vacuum system. The blower is rated at an ultimate pressure of less than 10^{-5} Torr and is capable of a volumetric pumping rate of 100 cfm in the pressure range of 0.1 to 10 Torr . The maximum pumping capability is not required for most of the experiments on flowing gas mixtures. In addition, high quality ball valves are placed at each end of the flow-mixing tube, shown in Figure 2 and provide the capability for sealed-off operation with completely negligible leak rates.

Provision is made to introduce NO_2 into the fluorescence cell for titration determination of the atomic oxygen concentration resulting from the microwave discharge in O_2 farther upstream. A teflon tube between the microwave discharge and the fluorescence cell minimizes atomic recombination.

Absolute pressures and pressure gradients are measured using oil monometers and combined with flowmeter information adequate data is available to specify the concentration of atomic oxygen in the region of the fluorescence cell. For measurements on other atomic species an E.P.R. system has been constructed to provide atom concentration measurements but has not yet been used with the flow mixing system.

E.P.R. System

A block diagram of the E.P.R. system constructed during this contract period is shown in Figure 3. As a generator of X band radiation a Gunn diode oscillator replaces the reflex klystron used in the other E.P.R. systems in

the laboratory. The present oscillator produces about 10 mw at frequencies near 9400 MHz and can be grossly tuned mechanically and fine tuned by changes in the operating current. This latter capability is exploited to provide stabilization of the oscillator frequency to the resonant frequency of the TE_{11} mode of the E.P.R. cavity. This brings about a substantial reduction of noise over the unstabilized situation.

The system in Figure 3 is entirely conventional and need not be described in detail with the exception of the electronics system for stabilization. A block diagram of this is shown in Figure 4. Superimposed on the main D.C. voltage driving the Gunn oscillator is placed a small a.c. component at 70 kHz. This results in a frequency modulation of the 9400 MHz signal and if the center frequency is different from the TE_{11} mode resonant frequency, a 70 kHz component appears in the output of the balanced mixer. A tuned amplifier and an integrated circuit multiplier (Analog Devices Model AD530J) provide for phase sensitive detection of this signal and a high stability integrator (Analog Devices Model 45J) produces a correction voltage to be added to the D.C. level set control value. This correction is of such a sign as to return to a zero 70 kHz signal level which means the Gunn oscillator and cavity frequency are the same. The 70kHz derives from an Intersil Type 8038 integrated circuit waveform generator and the necessary phase shift control is provided for optimum locking adjustment.

The electromagnet is powered by a Hewlett-Packard 0-15 ampere D.C. supply. It was determined that the current stability of this supply alone was inadequate and a high precision secondary current stabilization system was constructed. Provision is made in the secondary system for field set and field sweep capabilities.

Experimental Results

To verify the proper operation of the laser induced fluorescence system, initial static measurements were made of the rate constant for the deactivation of $CO(v=1)$ by collisions with O_2 and H_2 molecules. The first of these represents a V-V process and the latter a V-R,T process. Our results are compared with the recent literature in Table No. 1

Table 1
k in $sec^{-1}torr^{-1}$

$CO(v=1)$ deactivator	Present Work	Green & Hancock[a]	J.G. Stephenson[b,c]
$CO-O_2$ V-V	2.65	2.75	2.88
$CO-H_2$ V-R,T	18.1	14.6	16.4

(a) J. Chem. Phys. 59, 4326 (1973).
(b) J. Chem. Phys. 60, 3562 (1974).
(c) Appl. Phys. Lett. 22, 576 (1973).

Good agreement is obtained with the results of other workers and this verifies the proper functioning of the fluorescence measurement system.

In experiments using oxygen atoms it is necessary to correctly balance the experimental conditions in light of two conflicting requirements. The gas flow rate must be fast enough to avoid complete O atom recombination before they reach the fluorescence cell but the CO* molecule residence time in the fluorescence cell must not be too short in order that some increment in loss rate due to O atom collisions be apparent. We have found this increment can be easily measured even when the volumetric pumping rate of CO* molecules is a significant fraction of the total CO* loss rate in the absence of O atoms.

At the present time the major source of error in our measurement of the rate of O atom deactivation of CO* (v=1) arises from NO_2 titration difficulties. This of course impacts our O atom concentration determination. Unless the flowmeter in the NO_2 line is scrupulously clean, sticking of the float gives inaccurate and irreproducible results. This problem will not be present when our E.P.R. apparatus is incorporated into the system.

The destruction rate of CO* via

$$CO^* + O \rightarrow CO + O + \Delta E$$
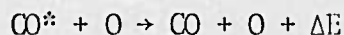
was measured over a range of [O] values and from the slope of destruction rate of CO* vs [O] a very preliminary value for the $p\tau$ product was derived. We find

$$p\tau = 0.55 \text{ } \mu sec \text{ atmospheres}$$

and estimate from our range of [O] atom uncertainties, maximum and minimum limits of 13 μsec atmospheres and 0.34 μsec atmospheres respectively. The extrapolation to room temperature of the shock tube data of R.E. Center would give a value near 2.2 μsec atmospheres. A calculation reported by Kelley at the 1974 St. Louis Conference on Molecular Lasers indicated a theoretical value of 20 μsec atmospheres including both atom exchange and inelastic collisions.

Future Work

A new fluorescence cell has been built with larger windows with the hope of minimizing scattered light at P(14) and a new tellurium crystal is being installed for increased harmonic generation efficiency. A photomulti-plier detector is being set up for a more precise NO_2 titration endpoint determination. With these improvements further data on O atom deactivation of CO* will be taken to reduce our above uncertainties.

A high temperature/low temperature flow mixing section is being installed in the region between the pole faces of the E.P.R. magnet. This will replace the unit in Figure 2 and has incorporated into it a single jacket which surrounds the fused quartz tubing. There are provision for flowing liquid N_2 along the entire section and heating coils, driven from a thermostatically commanded source, will permit stable operation at any temperature above that of liquid nitrogen. Materials of construction should permit operation as high as 300°C or greater.

Measurements over this temperature range will be made of $CO^*(v=1)$ deactivation by oxygen atoms as well as other species whose concentrations cannot be determined by titration but do require the E.P.R. capability.
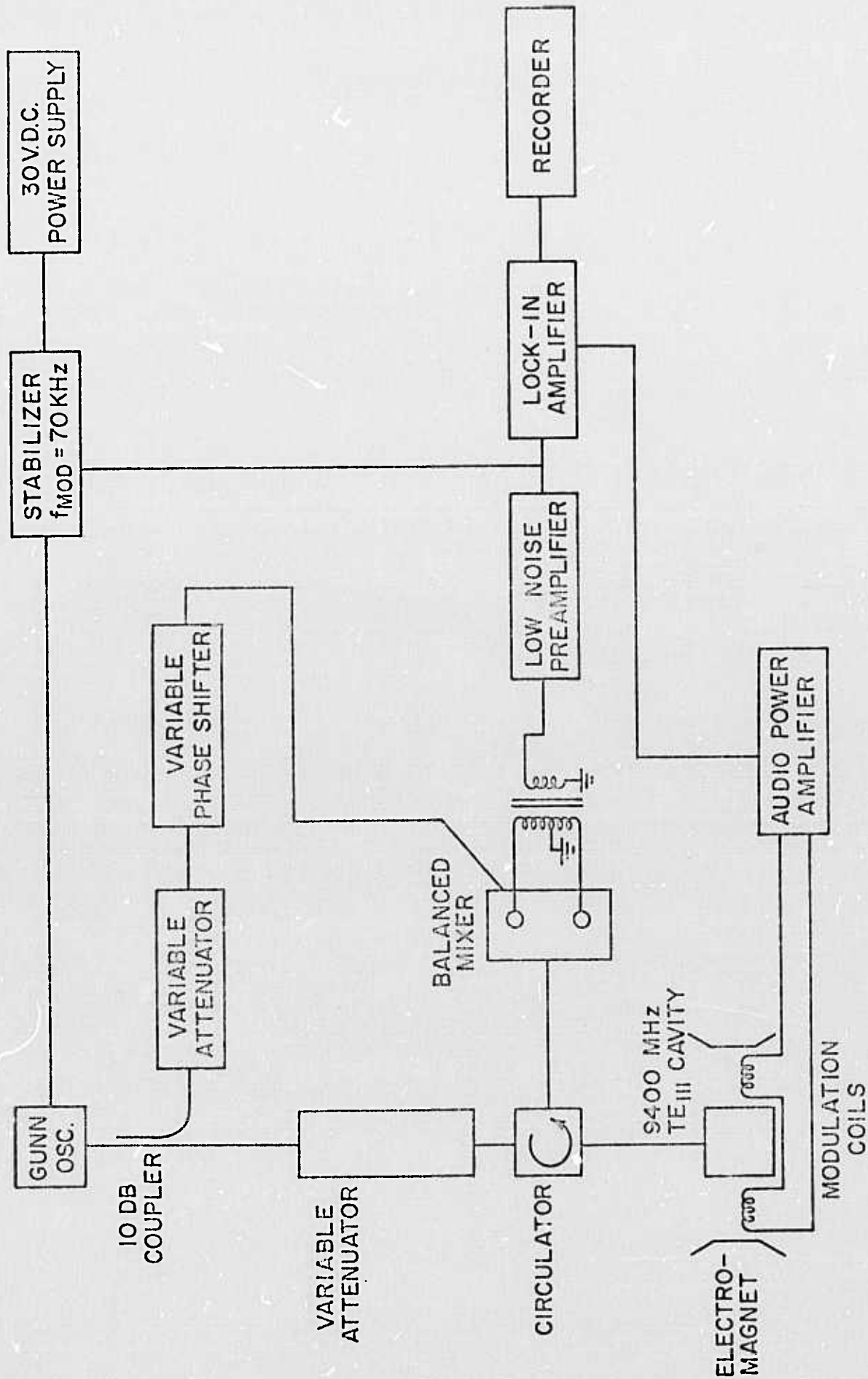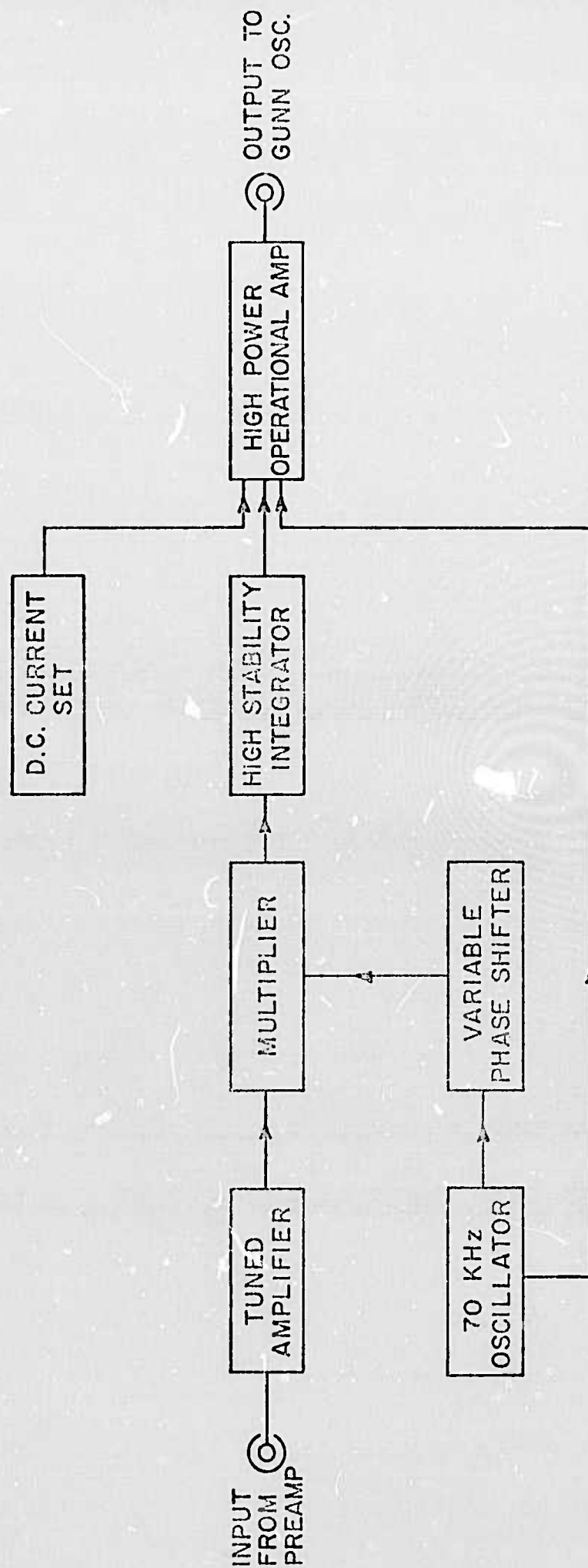
GUNN OSCILLATOR FREQUENCY STABILIZER
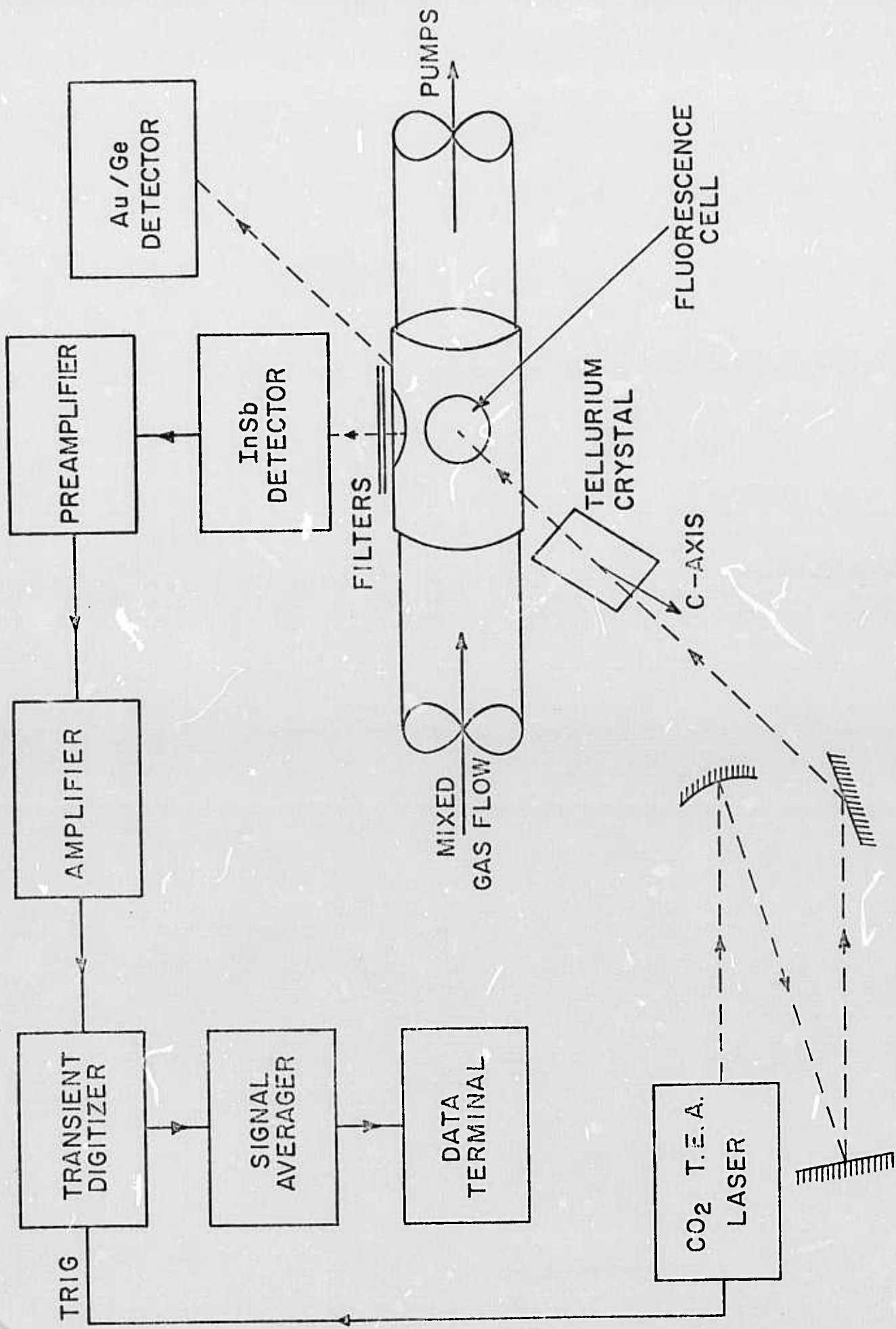
SCHEMATIC DIAGRAM OF LASER INDUCED FLUORESCENCE EXPERIMENT

SCHEMATIC DIAGRAM OF FLOW MIXING TUBE
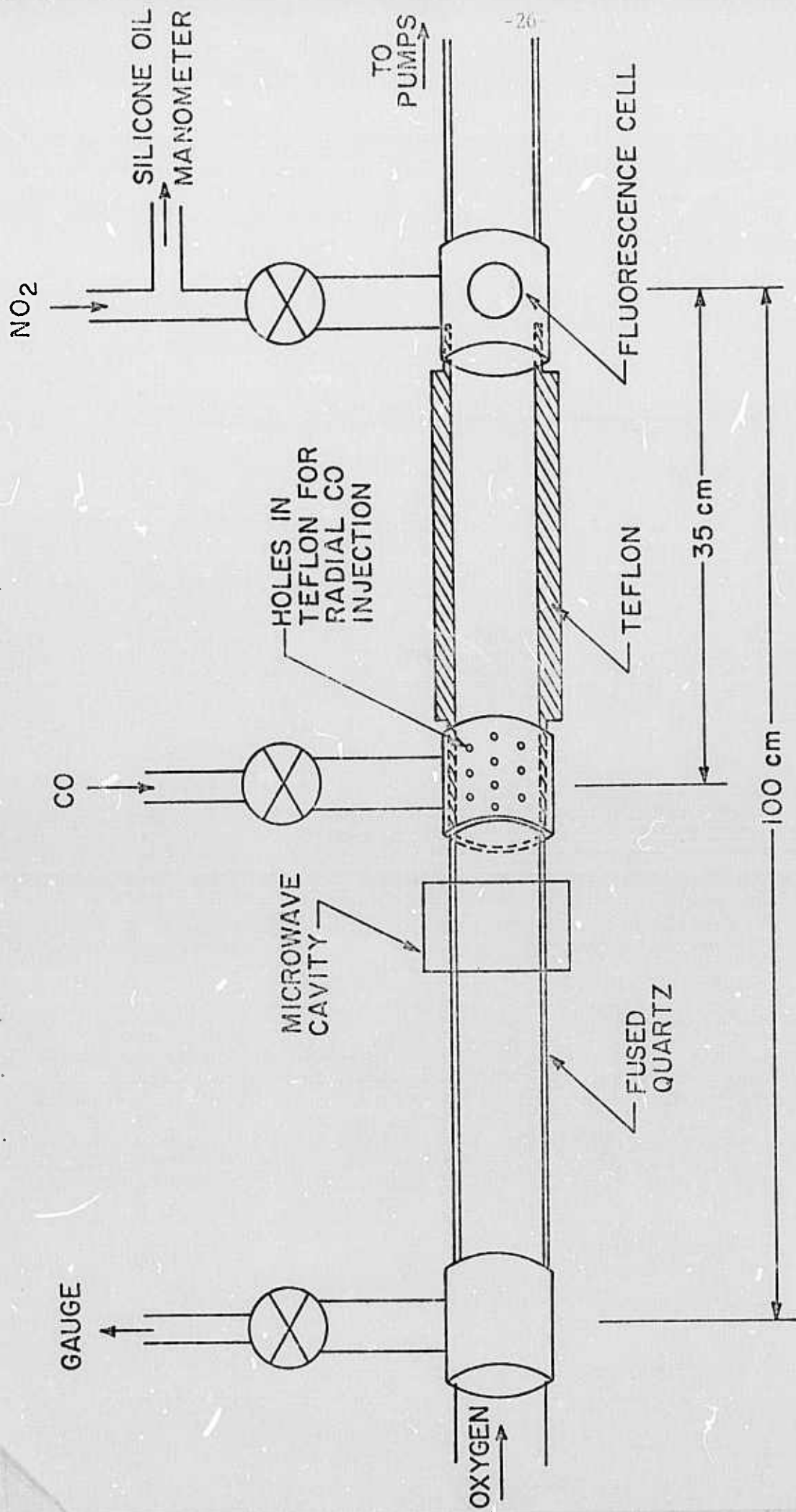
ALL GASES DELIVERED THROUGH CALIBRATED FLOWMETERS

New Chemical Laser Systems

Professor S.H. Bauer

The following summary of accomplishments consist of brief reports and preprints of two papers submitted for publication.

I. Bending Mode Relaxation of CO_2

The results of Peter Walsh's experiments were presented at the April ACS Meeting, in Los Angeles. Emission from an $HF^{\ddagger}$ laser $[SF_6 + H_2 + He$, electrically pulsed] at 2.8 μm is partially absorbed by carbon dioxide. HF lines at 3622.71, 3577.8 and 3644.16 μm pump the (02^o1) level, that at 3693.50 μm pumps the (11^11) level, and the two lines at 3593.80 and 3577.80 pump the (03^11) level of CO_2. Line center frequency mismatching is rectified partially by pressure broadening the absorber with argon or with mixtures which incorporate other collision partners of interest. At CO_2 concentrations above 2%, collisions with the (00^o0) state rapidly degrade the pumped states so as to overpopulate the (00^o1) and $(0n^{\ell}0)$ states, from which fluorescence is observed at 4.3 μm and 15.0 μm, respectively. The latter emission showed an early growth, followed by a fluorescence decay; the total fluorescence intensity could be represented by a superposition of two exponentials.

The longer period was associated with v-T de-excitation of CO_2, from which the values:

$$k(CO_2\text{-Ar}) = 41 \text{ sec}^{-1}\text{torr}^{-1}, \text{ and } k(CO_2\text{-}CO_2) = 227 \text{ sec}^{-1}\text{torr}^{-1}$$

were deduced. These check reasonably well with extrapolated shock tube measurements and ultrasonic data. The rate constants for pumping $(0n^00)$ proved to be about twice the literature values for the (00^01) de-excitation: $\approx 120 \text{ sec}^{-1}\text{torr}^{-1}$ for CO_2-Ar and $660 \text{ sec}^{-1}\text{torr}^{-1}$ for CO_2-CO_2. As yet the explanation for this is not clear. Corresponding values were also measured for two additional collision partners, CS_2 and COS.

This work did not receive ARPA support through salary recovery.

II. CS_2-O_2-He Chemical Laser

The assembly of kinetic data and the preparation of an extended computer program to model the CS_2-O_2-He chemical laser was completed. There is general consensus that the dominant pumping reaction which produces CO lasing is:

$$CS^{(o)}[\Sigma^+] + O[^3P_2] \rightarrow S[^3P_2] + CO^{(v)}[^1\Sigma^+],$$
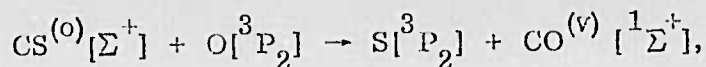
and that in the chain reaction, CS radicals are produced via a rapid abstraction of S by O from CS_2, with regeneration of oxygen atoms in the reaction $S + O_2 \rightarrow SO + O$. To develop an adequate but tractable mechanism we sought a minimum set of auxiliary steps; that is, those reactions which if omitted would affect to a measurable extent the concentrations of the important species: $CO^{(v)}$, O, S, and CS. After a thorough search of literature and the introduction of plausible rate parameters for all possible reactions, a sequence of computer
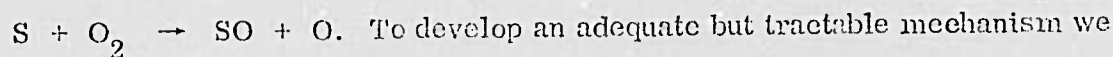
trials were run with our fully developed kinetics program, which incorporates v-T and v-v transfer rates as well as the adiabatic condition, for the time evolution of the state and species populations, following the pulsed discharge. Then, by successive approximations some of the reactions were eliminated and others inserted until a self consistent set of steps was developed.

An adequate computer model conforms to the following criteria. It incorporates:

(i) all chemical reactions and their inverses that significantly affect $[CO^{(v)}]_t$;

(ii) all (v-T) and (v-v) processes and their dependence on vibrational state, temperature and collider species;

(iii) state population changes due to radiative processes; and

(iv) it permits the computation to be made either on an isothermal or adiabatic basis. The adequacy of such a program can be ascertained by subjecting it to a series of tests which include checks on: (α) internal consistency; and (β) agreement with literature values for various rate constants --- i.e. chemical and energy transfer coefficients to within their specified error limits. The primary function of a model is to predict (for all transitions) laser gain vs time following the initiation of reaction. Also, it should account quantitatively for chemiluminescence $[I(\nu, t)]$ as it is affected by initial composition, discharge voltage, added reagents, etc.

The reactions finally accepted in the model are indicated in Table I which is in matrix form with the numbered reactions above the line being employed. On the basis of these and an extended series of preliminary runs, in which the concentrations of the various species were computed for

TABLE I

INDEX OF CHEMICAL REACTIONS

R_1 \ R_2	CS_2	CS	O_2	O	S	SO	SO_2	O_3	OCS	S_2	CO	S_2O	CS_3	S_2O_2	SO_3
1 CS_2	193			1,2											
2 CS		192		17–32	4									63	
3 O_2	147 166	138 161		5	10	14						7			
4 O		107	184	101	102	13		6	3	11		8,9	61	66	
5 S	162	106	186	103	112			15					60		
6 SO		164		104								12	62	69	
7 SO_2		148 165		109	110a	16 34									
8 O_3	182	183			134 197		140	139							
9 OCS		149	168 185	131	133	135 163		142							
10 S_2		152	167 196	111	113			130		114					
12 CO		137 153	143	105	108	144		141							
38 S_2O		198	199	115	153			159	202	203	160		206		
39 CS_3	210							200 201	215	216 217	204	205			
40 S_2O_2					211		212	213 214	215	216 217	218 219	220	207 208	221–223	
41 CO_2						151									
42 SO_3		154 155	157	132	145	136		156		157	146		209	224	

typical reaction conditions, the eight most important reactions and 17 of lesser significance (listed on the following page) were selected.

All available theoretical and experimental reports on CO relaxation by the variety of species present in the lasing plasma were reviewed. Thus covered were v,v and v, T processes for $CO^{(v)}$ with itself and with He, O, S, O_2, CS, SO_2, SO, OCS, and CS_2. Approximately 20 test runs were made using the overall model. First, note that this model is self-consistent as demonstrated by the many preliminary computational runs wherein reactions were selectively int duced or omitted, and the results compared with cases where the corresponding reactions were omitted or inserted. On the basis of their net contribution to the time dependent concentration of the vibrationally excited CO (we now believe) any subsequent reasonable changes in the magnitudes of the specific rate constants will not affect the selection of reactions. Second, the principal check was made by showing that the model reproduces the time evolution of $[CO^{(v)}]_t$ as derived from our chemiluminescent measurements. [S. Tsuchiya, N. Nielsen and S.H. Bauer, J. Phys. Chem., 77, 2455 (1973)]. A complete report documenting this model is available.

MOST IMPORTANT REACTIONS

			$k_f(400°K)$	$k = Ae^{-E_a/RT}$	
				A	E_a (kcal/mole)
1.	$O + CS_2$	$\rightleftharpoons CS + SO$	2.8×10^{12}	1.03×10^{13}	1.03
2.	$O + CS_2$	$\rightleftharpoons S + OCS$	3.0×10^{11}	1.1×10^{12}	1.03
3.	$O + OCS$	$\rightleftharpoons SO + CO^{(o)}$	6.8×10^{10}	4.08×10^{13}	5.08
10.	$S + O_2$	$\rightleftharpoons O + SO$	9.0×10^{11}	9.0×10^{11}	0.0
13.	$O + SO + M$	$\rightleftharpoons SO_2 + M$	3.2×10^{17}	3.2×10^{17}	0.0
14.	$SO + O_2$	$\rightleftharpoons O + SO_2$	7.0×10^{7}	2×10^{13}	10.0
17-32.	$O + CS$	$\rightleftharpoons S + CO^{(y)}$	1.5×10^{13}	1×10^{14}	1.5
33.	$O + CS_2$	$\rightleftharpoons CO^{(o)} + S_2$	1.5×10^{11}	5.6×10^{11}	1.03

NEEDED --- but, LESS IMPORTANT REACTIONS

			$k_f(400°K)$
4.	$S + CS_2 + M \rightleftharpoons CS_3 + M$		1.8×10^{17}
5.	$O + O_2 + M \rightleftharpoons O_3 + M$		1.9×10^{14}
6.	$O + O_3$	$\rightleftharpoons O_2 + O_2$	2.9×10^{10}
7.	$O_2 + S_2O$	$\rightleftharpoons SO + SO_2$	1.0×10^{8}
8.	$O + S_2O$	$\rightleftharpoons SO + SO$	1.0×10^{11}
9.	$O + S_2O$	$\rightleftharpoons O_2 + S_2$	1.0×10^{10}
11.	$O + S_2$	$\rightleftharpoons S + SO$	2.0×10^{12}
12.	$SO + S_2O$	$\rightleftharpoons S_2 + SO_2$	1.0×10^{9}
15.	$SO + O_3$	$\rightleftharpoons O_2 + SO_2$	1.1×10^{11}
16.	$SO + SO$	$\rightleftharpoons S_2O_2$	1.0×10^{10}
34.	$SO + SO$	$\rightleftharpoons S + SO_2$	6.9×10^{7}
60.	$S + CS_3$	$\rightarrow CS_2 + S_2$	1.2×10^{4}
61.	$O + CS_3$	$\rightarrow CS_2 + SO$	2.4×10^{4}
62.	$SO + CS_3$	$\rightarrow CS_2 + S_2O$	1.2×10^{3}
63.	$CS + S_2O_2$	$\rightarrow OCS + S_2O$	1.0×10^{11}
66.	$O + S_2O_2$	$\rightarrow O_2 + S_2O$	1.0×10^{12}
67.	$SO + S_2O_2$	$\rightarrow S_2O + SO_2$	1.0×10^{11}

III. <u>Alternate Hydrogen Sources for HF and DF Lasers</u>

The utility of formaldehyde [H_2CO and D_2CO] as a hydrogen source for an HF or DF laser, a source which does not require storage of the fuel in high pressure containers was tested. A report is summarized below.

INTRODUCTION

Laser radiation in the range 2.8 to 3.2 μm is most efficiently obtained from the combustion of hydrogen or hydrocarbon with fluorine atoms. Nearly all hydro-carbons and molecular hydrogen have the same exothermicity when combined with fluorine, but formaldehyde presents somewhat more exothermic combustion reactions:

$$F + H_2CO \rightarrow HF + HCO \qquad \Delta H^o = -44.4 \text{ kcal/mole}$$

$$F + HCO \rightarrow HF + CO \qquad \Delta H^o = -72.7 \text{ kcal/mole}$$
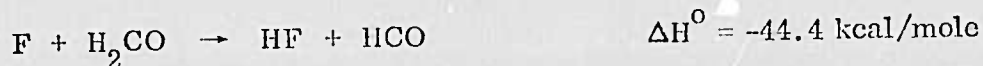
These should be compared with the "cold reactions":

$$F + H_2 \rightarrow HF + H \qquad \Delta H^o = -31.5 \text{ kcal/mole}$$

$$F + CH_4 \rightarrow HF + CH_3 \qquad \Delta H^o = -32 \quad \text{kcal/mole}$$

In addition to the possibility that the HF may leave in a higher state of vibrational excitation were formaldehyde used as a source of hydrogen, the other product of combustion could be vibrationally excited CO. This would lead to a new route for the production of excited CO, with minimal contamination from the ground state. Even if excited CO were not a direct product of reaction, there was the possi-bility that energy transfer from $DF^{(v)}$ to CO (near resonance) would pump the

latter. Finally, one should not overlook the possibility of a chain reaction:

$$F_2 + HCO \rightarrow HF + F + CO \qquad \Delta H^o = -84.28 \text{ kcal/mole}$$

$$F_2 + HCO \rightarrow HFCO + F \qquad \Delta H^o = -81.09 \text{ kcal/mole}$$

$$F + HFCO \rightarrow HF + FCO \qquad \Delta H^o = -35.5 \text{ kcal/mole}$$

$$F_2 + FCO \rightarrow F + F_2CO \qquad \Delta H^o = -92.5 \text{ kcal/mole} \qquad .$$
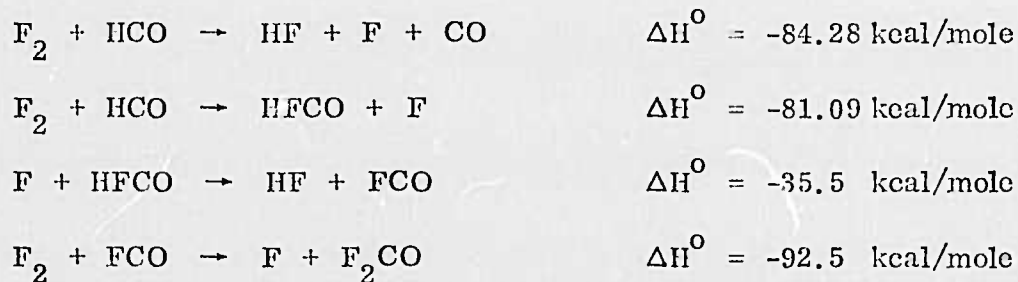
EXPERIMENTAL APPARATUS

Preliminary to experiments with a cw flow system the utility of H_2CO and D_2CO was evaluated in a TEA configuration, where these reagents were mixed with He and SF_6 and lasing initiated by an electrical discharge. A rectangular tube was used; it has a cross section of about 6.5 cm^2 and is 1.2 meters long. It is fitted with Brewster angle windows (KBr). The optical cavity is 1.5 meters; the output mirror was either a 50% transmitting germanium flat or a 2 m focal length gold mirror, with a 1 millimeter coupling hole (5% output). The back reflector was a two meter focal length gold coated surface. The electrical energy was deposited through 240 pins to a grounded rod (1 cm diameter); the discharge path is 15 mm; a 0.045 μf capacitor raised to voltages ranging from 14 to 33 Kv was used. This combination gave a pulse with a half width of about 0.1 μs. The repetition rate was 1 per 3 seconds; this assured complete removal by gas flow of all products produced in each pulse.

The flow rate of materials was calibrated by timing the pumpdown time from a measured volume of gas at the pressures used. At 10 to 80 torr the flow was found to be 0.71 millimole torr^{-1}. Relative intensities were measured as a function of system parameters; these were recorded as the oscilloscope output from a gold doped germanium detector, maintained at 77°K; output resistor 10 K. The

different wavelength regions were selected by narrow band pass infrared filters placed in front of the detector port. The total energy output was measured with a CDC 100 thermopile, and a Keithley microvoltmeter.

Pressures were measured with a mercury monometer and with a Wallace and Tiernan gauge (full range: 50 torr). The gases were mixed thoroughly during the 30 second elapsed time for flow from the injection region to the laser cavity. The monomer was swept into the laser tube by a nitrogen stream. The H_2CO monomer liquid was prepared prior to use by decomposing paraformaldehyde in an oil slurry at $120^{\circ}C$. It was trapped at $-67^{\circ}C$ as a liquid, and was redistilled (for purification) to prolong the time in which it remains as a monomer. Repolymerization is catalyzed by water, acid and particles in any form.

EXPERIMENTAL RESULTS

Laser output was measured as a function of impressed voltage, and the partial pressures of the hydrogen and deuterium atom sources. The results are summarized in Table I and displayed graphically in Figures 1-4. The remarkable observation is that when H or D atoms were generated from H_2CO or D_2CO as monomers the flow required was 1/15 (in millimoles per minute) of that for gaseous H_2 or D_2 to reach the optimum output energy. This was recorded as the partial pressure of the formaldehyde source, and cross checked by weighting the paraformaldehyde polymer consumed. With H_2CO, the maximum power attained was several percent greater than with H_2 using the same quantities of SF_6, He and input electric energy. However, with D_2CO mixtures the maximum was one half as large as that which could be obtained under the same conditions with D_2.

The formaldehyde gave a different shape curve for pressure vs output than did the hydrogen sources. In Figures 1a and 1b the output reaches a maximum quickly and stays flat with increasing pressure beyond 0.2 torr whereas for hydrogen the maximum is attained later at 15 times the formaldehyde pressures (Figures 2a,b); subsequently the power slowly decreases at larger pressures, where presumably the hydrogen becomes a charge carrier for the high voltage pulses. With formaldehyde the optimum output power is attained at lower driving voltages. The curves in Figure 3 show that with H_2CO the maximum is reached at 21 Kv, whereas with H_2 the power slowly continues to rise to 25 Kv. Figure 4 a similar graph for D_2CO vs D_2.

Prior to testing for lasing from CO, utilizing the formaldehydes as the source, the cavity was rechecked for alignment. The reagents SF_6, H_2CO and He were mixed, with partial pressures for each varied from 0.1 to 50 torr. The formaldehyde was introduced as a gas, from the liquid monomer maintained at $-22.9^{\circ}C$, where it has a vapor pressure of 600 torr. In another arrangement, the SF_6 and He mixtures flowed over the solid polymer (H_2CO or D_2CO) which was stored in a trap, heated to $60-120^{\circ}C$ with an oil bath. In experiments with the H_2CO an IR filter (#1) which has 80% transmittance from 4.0 to 6.5 μm, and completely absorbs all HF output between 2.7 and 3.1 μm, was used. Under all conditions tested no radiation was observed over the interval 4.9 to 5.1 μ, as would be expected were CO lasing achieved.

To detect possible CO chemiluminescence, adjacent to DF laser emission over the region 3.7-4.1 μ, a combination filter was prepared and its transmission checked. It incorporated a thin layer of D_2O liquid. The net transmission with

cutoff filter #2 is shown in Figure 5. This gave a narrow band centered at 5 μ (70% maximum); sapphire windows with a D_2O liquid thickness of 0.025 mm proved best. Neither the H_2CO nor the D_2CO showed pure fluorescence emission, as was checked by removing the output mirror. For the latter tests a front surface off axis 20 cm focal length parabolic mirror was inserted to focus the light from the cavity upon the detector. In neither case was any CO radiation observed. It is interesting to note that Shortridge and Lin [4th Conference on Chemical and Molecular Lasers, October 1974, Abst. MB5] observed very little CO emission from the reaction:

$$O(^3P) + CHF \rightarrow \{HFCO^{\ddagger}\} \rightarrow HF^{\ddagger} + CO^{(v)} \qquad \Delta H^O = -181 \text{ kcal/mole}$$
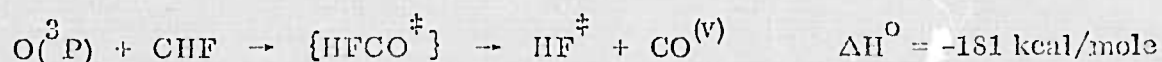
Nevertheless, they measured the vibrational state distribution for the product CO and found excitations up to $v = 11$, but no inversion.

The cw flow experiments were conducted in the apparatus described by Rosen, Sileo and Cool [IEEE Journal Quantum Electronics, $\underline{9}$, 163 (1973)]. The oxidizer stream consists of premixed F_2 and He gases, which pass through a 1 kw, 2450 MHz microwave discharge. The fuel gas (H_2CO, etc.) is injected into the flow through a row of 40 tubes, each with seven 0.127 mm holes, set perpendicular to the flow direction; CaF_2 windows were set at their Brewster angle. The optical cavity can be translated along the output windows, starting at the injector position, and downstream for 17 cm. The cavity mirrors consisted of a 1 meter radius gold reflectors, separated by 0.5 meter. Coupling was made through 0.25 and 1.0 mm diameter holes. Occasionally dielectric coated germanium mirrors were used; these transmitted 0.5, 5.0 and 10% of the output. Under all conditions of flow, at all cavity positions downstream, there was no HF lasing with

H_2CO, even though the system was well aligned and produced substantial levels of HF laser radiation from $H_2 + F_2$. Since the optimum H_2 pressure into the injectors was 50 torr, liquid polymer was prepared and its vapor was injected at flow rates up to 150 torr; still no lasing was observed. In an additional test for possible lasing, a mixture of H_2 and F_2 was initially set up, and then the pressure of H_2 was decreased while that of H_2CO was increased. There was no enhanced lasing; furthermore, as the hydrogen pressure decreased the total laser output also decreased. Thus it appears that while formaldehyde constitutes an excellent source of hydrogen in TEA-pulsed operation, and eliminates the need for carrying high pressure hydrogen at a fuel source, we have not yet found conditions wherein formaldehyde can be used as a source of hydrogen in a cw configuration.

TABLE I

	H_2	H_2CO	D_2	D_2CO	C_2H_4
λ range (μm)	2.7-3.1	2.7-3.1	3.7-4.2	3.7-4.2	2.7-3.1
Half-width	2 μs	2 μs	4 μs	4 μs	2 μs
Relative Power	0.78	0.81	1.0	0.5	0.21
Joules	0.017	0.019	0.047	0.023	0.005
Watts	1700	1900	2300	1150	500
Best V (Kv)	27	22	27	21	
Best P[‡] (Torr)	3.2	0.2	3.0	0.2	

[‡] Of fuel [SF_6 = 31 Torr; He = 16 Torr].

FIGURE LEGENDS

Figure 1.   Dependence of relative power on fuel pressure.

(a) H_2CO (b) D_2CO

Figure 2.   Dependence of relative power on fuel pressure.

(a) H_2 (b) D_2

Figure 3.   Dependence of relative power on impressed voltage.

$p(SF_6)$ = 35 torr $p(H_2)$ = 3 torr

$p(He)$ = 18 torr $P(H_2CO)$ = 0.3 torr

Figure 4.   Dependence of relative power on impressed voltage.

$p(SF_6)$ = 31 torr $p(D_2)$ = 1 torr

$p(He)$ = 16 torr $p(D_2CO)$ = 0.3 torr

Figure 5.   Transmittance spectra for filters.

RELATIVE POWER

H₂ PRESSURE (Torr)

(read upper scale)

(read lower scale)
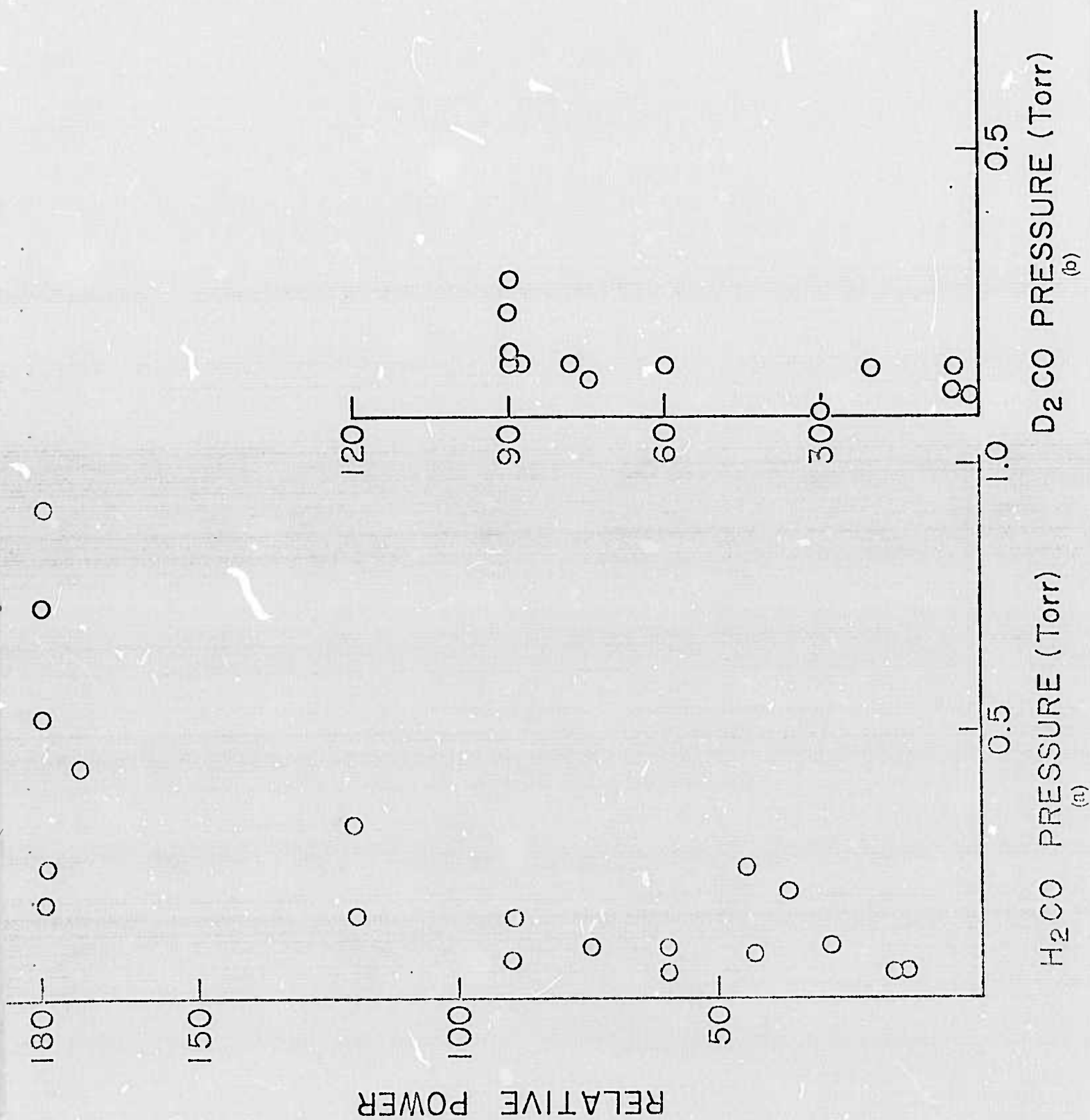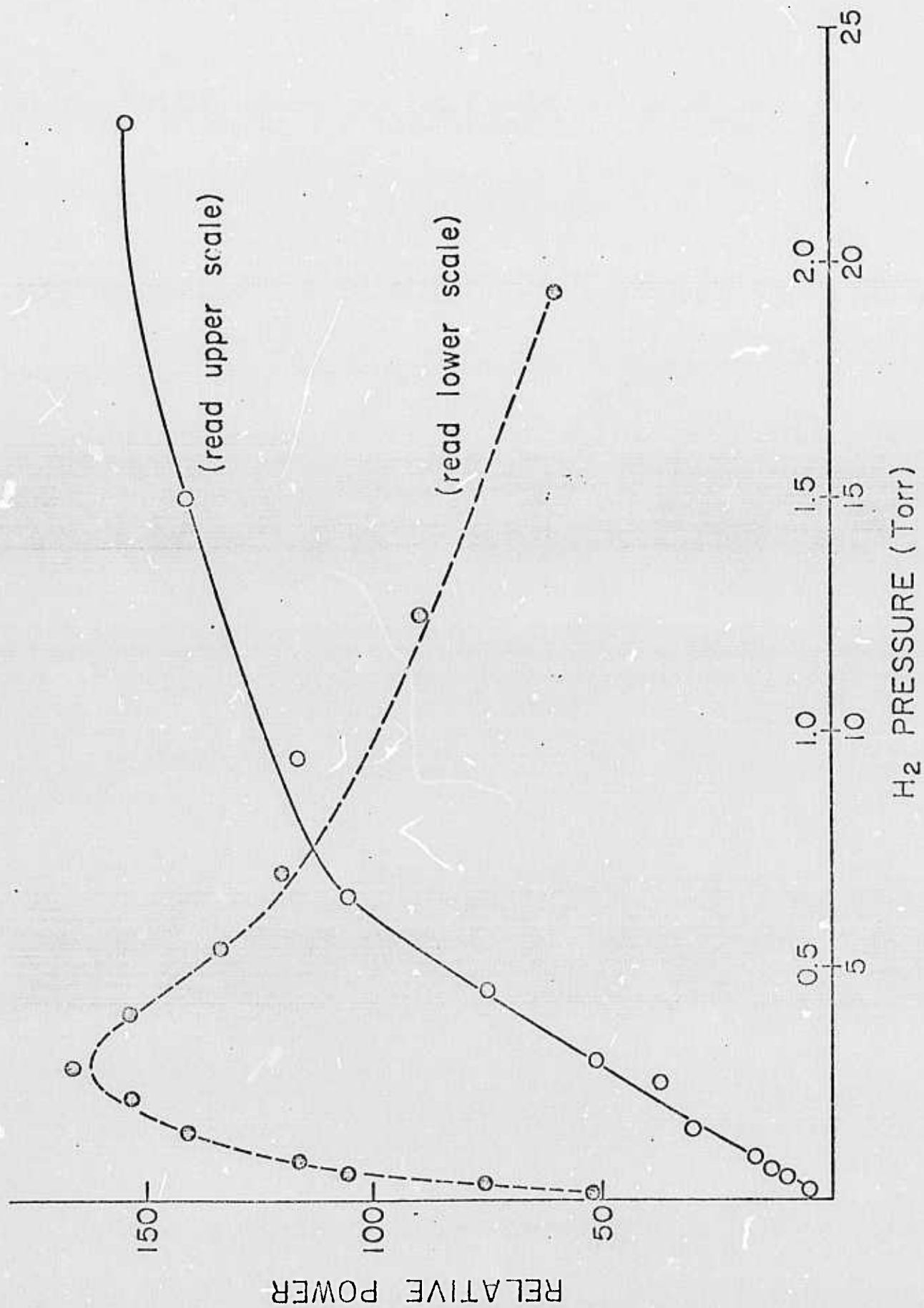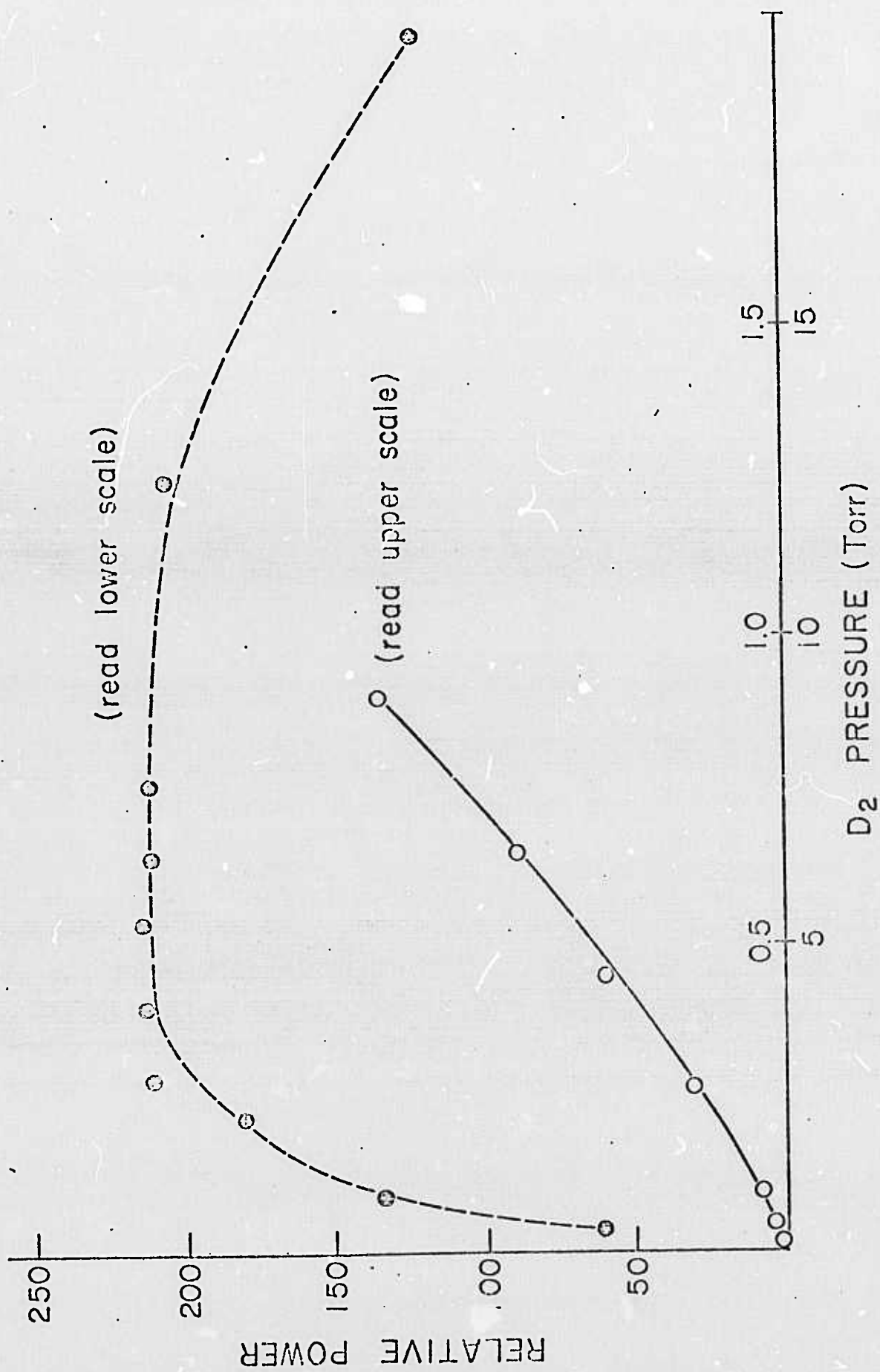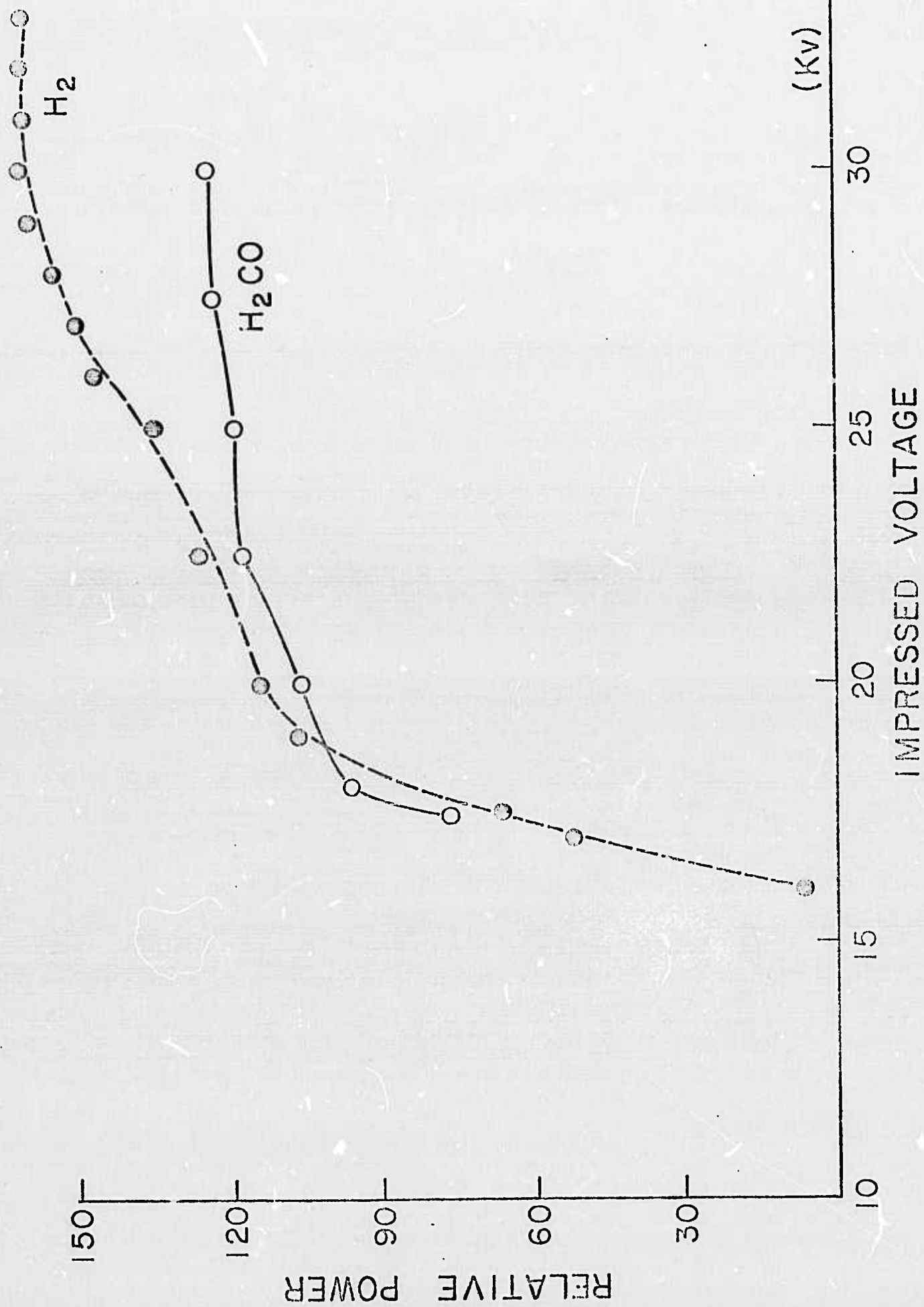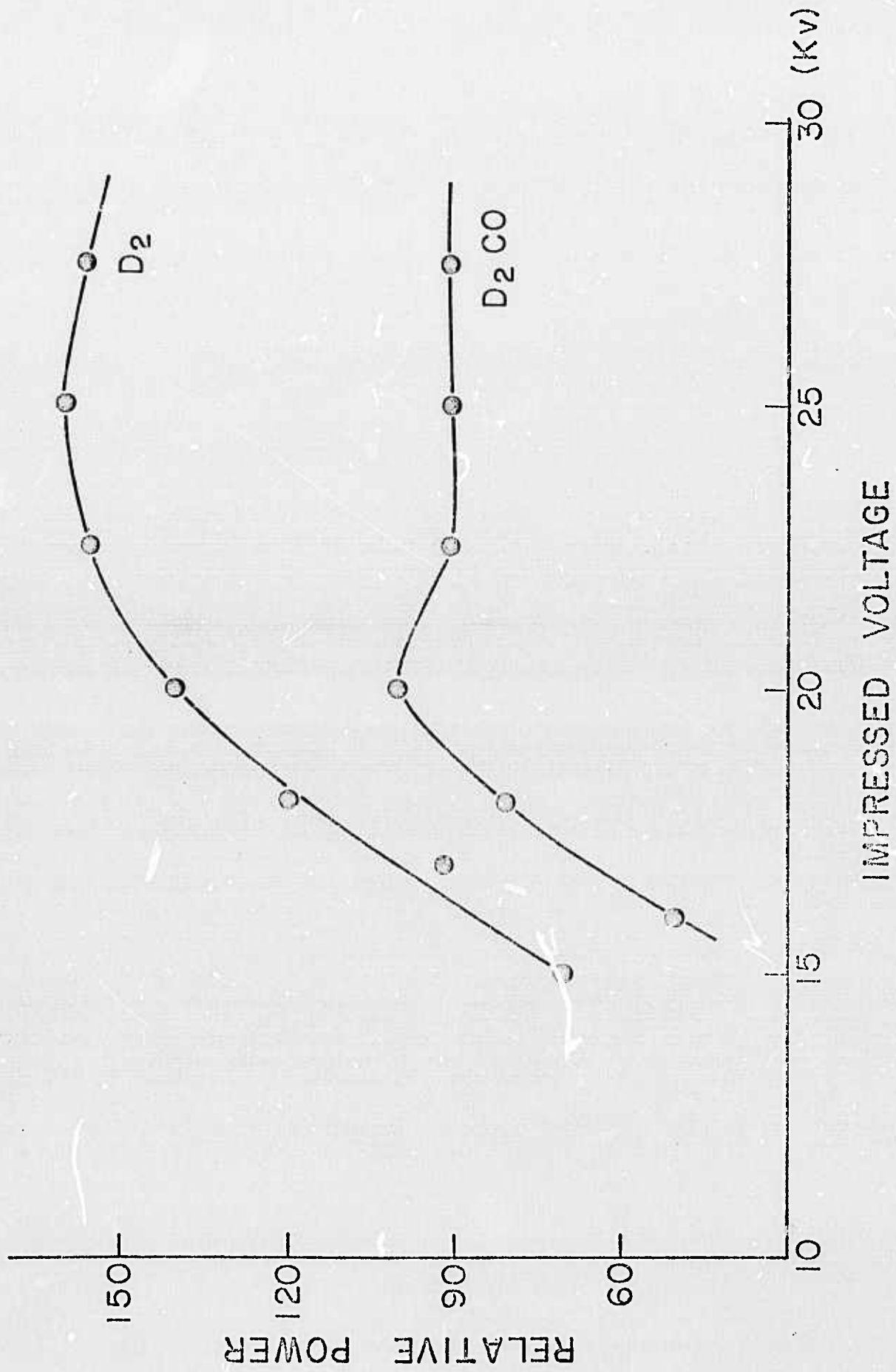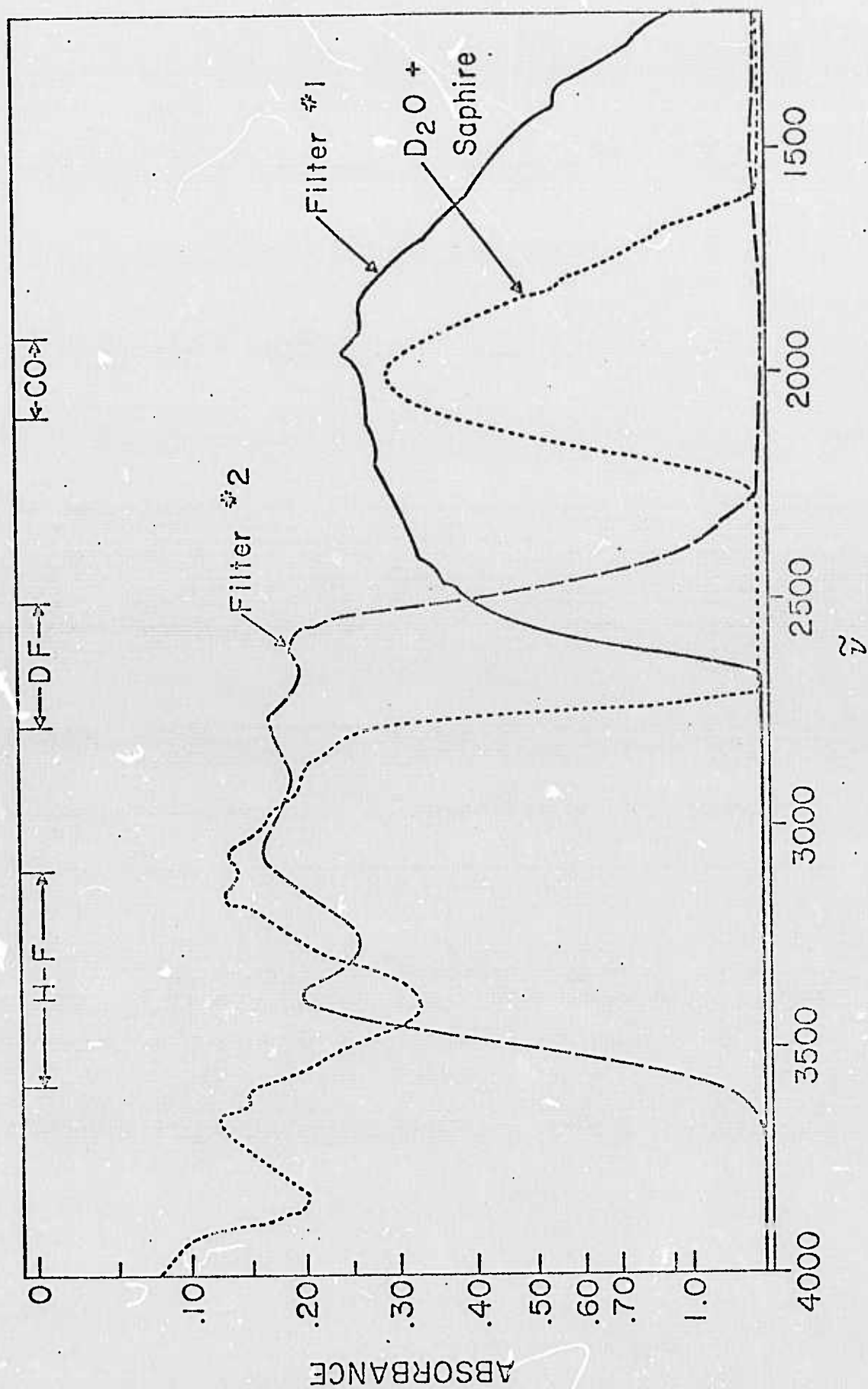
IV. Laser Heating Initiated Chemical Reactions

Construction of an adequate high intensity pulsed CO_2 laser ($\approx$25J/pulse) has taken much more effort and time than we had anticipated, even though a well designed unit had been described by Seguin. Indeed, there is a big gap between the bare description which appears in a journal article and the fully functioning device. After three periods of "restructuring" of the laser we hope that the present version will be operational at the 55 kV level, and its discharge characteristics properly controlled. Our objective is to use pulses developed by this laser (beam diameter approximately 4 cm) to generate a line focus with a cylindrical lens, which will be projected along the axis of a cell that contains a mixture of SF_6, B_2H_6 and NO_2. The light generated from this concurrent pyrolysis-oxidation reaction should be intense enough and of a quality that may provide essential information for the construction of a visible laser. This system will be studied in the near future.

V. CO v=1-0 Pulsed Chemical Laser

The conditions under which $CO(1 \rightarrow 0)$ lasing occurs in the CS_2-O_2-He pulsed chemical laser were discovered. The results of this work have been described in a short publication, accepted by Chemical Physics Letters [copy attached].

VI. $C_3O_2 + O_2$ — He Chemical CO Laser

Our studies of the [$C_3O_2 + O_2 + $He] pulsed laser consist of four parts. First, both literature and experimental surveys were made of preparative methods, in search for an efficient route for generating substantial quantities of the suboxide. In this

we were only partially successful. Yields of up to 15% were obtained, compared to conventional yields of about 8%. The second part consisted of a parametric study of reagent composition and of discharge conditions to maximize laser output for an axial discharge configuration, and the recording of relative lasing intensities and delays for onset of lasing as a function of the upper vibrational state. The effect of added cold CO was also investigated. In the third part, relative populations of excited states, as present at a sequence of delays after pulse initiation, were obtained from chemiluminescence data, in the absence of lasing.

A mechanism was developed which accounts semi-quantitatively (via our computer program) for the time evolution of lasing, as dependent on the upper state vibrational quantum number. This lasing system is much weaker than $CS_2 + O_2$ because (we believe) of strong absorption of $CO^{(v \rightarrow v-1)}$ radiation by the reagents: C_3O_2 at low v's and C_2O at $v \sim 7, 8$. Intracavity losses, therefore, remain high until these reagents are substantially depleted. Absorptions by C_3O_2 and C_2O have been measured over a range of v's for $CO^{(v \rightarrow v-1)}$ radiations. Our model also accounts for the long delay times for the onset of lasing (following pulse discharge), characteristic of the axially initiated configuration.

V. STIMULATED CO EMISSION OF THE (1 → 0) BAND IN A PULSE INITIATED (CS$_2$ + O$_2$) CHEMICAL LASER

Josef Stricker and S. H. Bauer

Department of Chemistry, Cornell University, Ithaca, New York 14850

Laser emission by CO on the $v = 1 \to 0$ transition have been reported by Gregg and Thomas[1] and by Djeu[2]. The first investigators initiated lasing in CS$_2$ + O$_2$ mixtures by flash photolysis. They reported typical delay times of 12-20 μs and emission pulses which lasted for 15 to 60 μs, depending on the gas composition and flash lamp energy. Djeu found a single line from the $v = 1 \to 0$ band when a continuous discharge was sent through H$_2$, N$_2$, Xe and CO mixtures, at liquid nitrogen temperatures. Here we report on lasing at the fundamental band of CO, generated in CS$_2$-O$_2$-He mixtures when initiated by an electric pulse of ≈ 0.7 μs duration. The mechanisms for producing the inverted populations are clearly different in these three cases.

A slowly flowing mixture of helium (3.25 torr), O$_2$ (0.40 torr), and CS$_2$ (0.08 torr) was subjected to an axial 13 Kv pulse (ring electrodes) in a one meter tube; C = 0.0051 μf.[3] Rotational lines ranging from P(14)...P(10) for the (1 → 0) transition were recorded using a Au-Ge detector (LN), viewing the laser emission through a PE 98 grating monochromator. Spectroscopic resolution for line identification was 0.9 cm^{-1}; for recording time dependence of individual lines, the slit was opened to 3.6 cm^{-1}. Delay times for onset of lasing were ≈ 160 μs, while pulse durations were between 600 and 800 μs. In contrast, typical values for $v = 13 \to 12$ transitions, lasing pulses lasted ≈ 200 μs after a delay of ≈ 20 μs. To establish that the radiation was produced by a transition to the ground vibrational state, a

cell 8.8 cm long was filled with CO at 0.17 torr (room temperature) and interposed between the laser and the monochromator. There was a marked decrease in the transmitted energy. The $\ln(I/I_0)$ values observed [4.0 for P(10), 2.3 for P(11), and 1.9 for P(12)] checked within acceptable error limits with the values calculated from Young and Eachus[4] vibrational matrix elements [3.2, 2.9, and 2.5, respectively]. This CO filled cell was almost transparent to all the other laser lines. We could not obtain lasing on the $1 \to 0$ transition in a TEA configuration using similar compositions, voltages and capacitances.

Optimum operating conditions for maximum power output on the P(10) line were determined by parametric variation of partial pressures and discharge voltages. The maximum appears at $p(He) \approx 3.25$ torr; $p(O_2) \approx 0.3$ torr, and $p(CS_2) = 0.08$ torr, using ≈ 11.3 Kv discharges (Fig. 1). Corresponding delay times, are also shown in Figure 1; they are inversely related to the discharge voltages. The net trends are as expected, based on the extent of fragmentation by the initiating electrical pulse. To eliminate populating the lower states by induced transitions from the upper states, intensities were remeasured with a grating tuned cavity. The relative powers as a function of discharge voltage are shown in Figure 2 (upper) and the corresponding delay times in the lower portion. Note that the latter values are about three times longer than for the free running configuration. It is also interesting to note that at specific grating positions the laser output consisted of two bell shaped peaks separated by 430-470 μs, depending on the discharge voltage. The peak centered at 850 μs was completely absorbed by cold CO, while that at 420 μs was unaffected. These were later identified as P(10) for $2 \to 1$, at 2077.14 cm^{-1} and P(16), $v = 1 \to 0$ at 2077.65 cm^{-1}, respectively.

The above observations indicated that under the specific conditions of these experiments, in contrast to the higher discharge voltages used in our first report[3], the initial population generated chemically in the low v levels does not rise; it is likely that under present conditions, the low v states are uniformly populated, as proposed by Powell and Kelly[5], or possibly decrease as initially proposed by Hancock, Morley and Smith[6]. Hence when the cavity is free running a partial inversion relative to $2 \rightarrow 1$ and $1 \rightarrow 0$ occurs sooner, due to the stimulated transitions, while in a tuned cavity lasing conditions are attained later because of the time required for v-v de-excitations. This assumption was checked with the Nielsen-Bauer model[7] for the $CS_2 + O_2$ system. The following assumptions were introduced: (a) For $p(CS_2) = 0.1$ torr; $p(O_2) = 0.3$ torr, and $p(He) = 3.25$ torr, we assumed that 60% of the total electrical energy in the capacitor was used for dissociation [2.2% of the O_2; 12% of the CS_2 and 8.5% of CS]. (b) The reacting system is adiabatic, with an initial temperature of about $400^{o}K$. The computer program was run three times, each with a set of relative reaction rate constants, corresponding to the three proposed initial vibrational state distributions for the pumping reaction: $CS + O \xrightarrow{k^v} CO^{(v)} + S$. While no positive gain was computed for the $v = 1 \rightarrow 0$ transition on the basis of the branching ratios given in reference 3, comparable delay times and gains were found for the distributions given in references 5 and 6 (Table I). Thus, on the basis of the present observations no choice can be made between the latter two distributions for this laser operation.

ACKNOWLEDGMENT

REFERENCES

1. D. W. Gregg and S. J. Thomas, J. Appl. Phys., <u>39</u>, 4399 (1968).

2. N. Djeu, Appl. Phys. Lett., <u>23</u>, 309 (1973).

3. S. Tsuchiya, N. Nielsen and S. H. Bauer, J. Phys. Chem., <u>77</u>, 2455 (1973).

4. L. A. Young and W. J. Eachus, J. Chem. Phys., <u>44</u>, 4195 (1966).

5. H. T. Powell and J. D. Kelley, J. Chem. Phys., <u>60</u>, 2191 (1974).

6. G. Hancock, C. Morley and I. W. M. Smith, Chem. Phys. Lett., <u>12</u>, 193 (1971).

7. N. Nielsen and Bauer, in preparation.

TABLE I

	Inversion starts			Max Inversion		
	Optimum J	Delay Time (μsec)	gain (arb.units)	Optimum J	Delay Time (μsec)	gain (arb.units)
Powell and Kelley[5]	15	180	0.40	12	300	3.5
Hancock, et.al.[6]	14	180	0.25	11	340	5.6

LEGENDS FOR FIGURES

Figure 1.   Relative powers and delay times for several mixtures, as a function

of discharge voltage (conventional cavity).

Figure 2.   Relative powers and delay times for P(10), P(11) and P(13),

$v = 1 \rightarrow 0$ transition, as a function of discharge voltage (grating

runed cavity).

Fig 1

$P_{He} = 3.30$ torr
$P_{O_2} = 0.45$ torr
$P_{CS_2} = 0.10$ torr
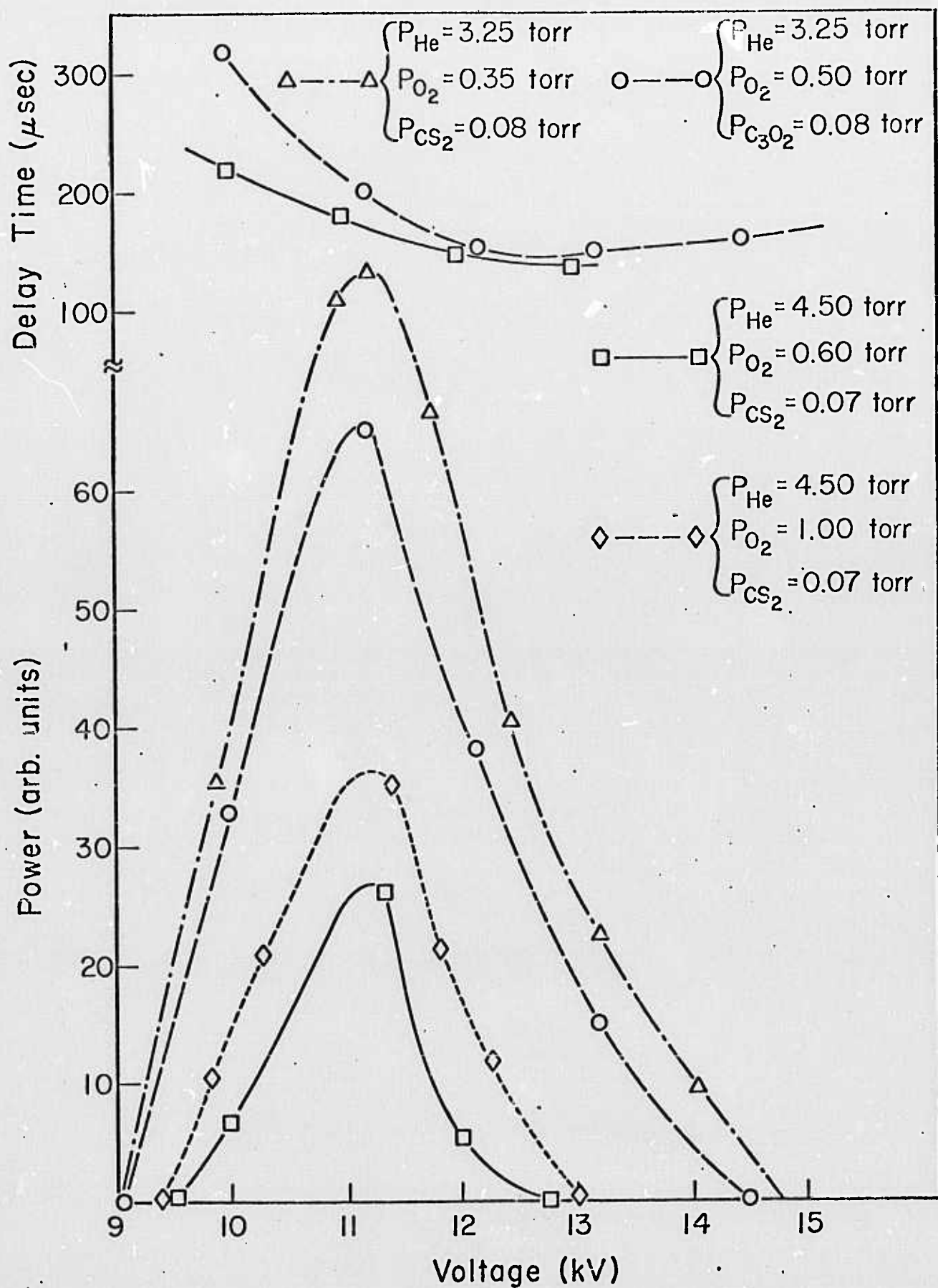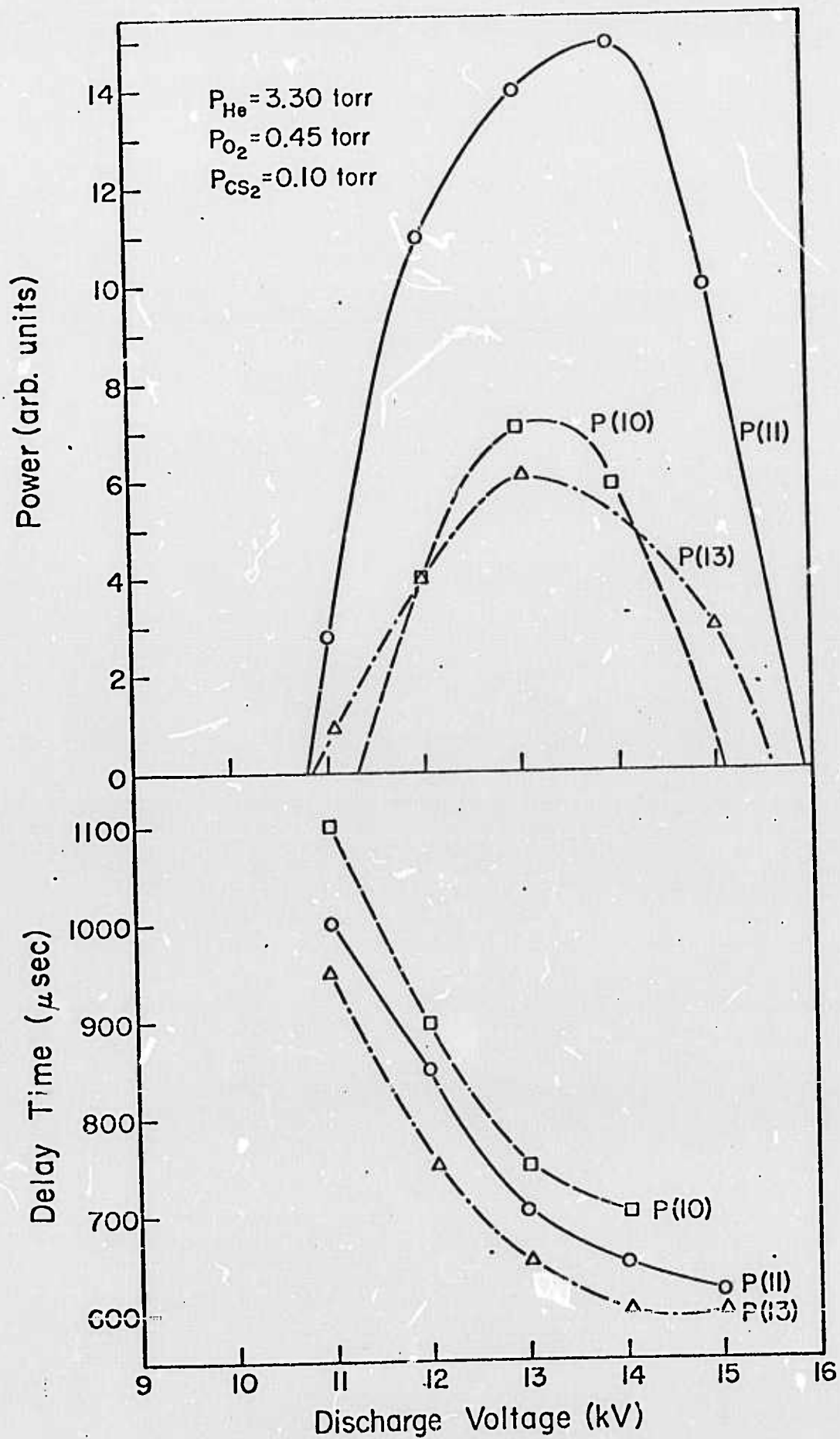
VI.   MODEL FOR THE $\{C_3O_2 + O_2 + He\}$ LASER

The apparatus utilized in these experiments was essentially identical with that used for the $\{CS_2 + O_2 + He\}$ system. The results of a series of parametric studies have been previously reported by David Sheasley [Laboratory of Plasma Studies Report of November 1, 1973]. To test the model, the following situation was simulated: discharge voltage = 12 Kv; capacitor 0.051 μf; assume that half of the available electrical energy is utilized for dissociation of the reagents. The gas mixture consisted of 0.19 torr C_3O_2, 0.55 torr O_2, and 3.75 torr He. This corresponds to an optimum combination for CO lasing. Initial conditions for the computer program were: 5% of the C_3O_2 dissociated into $C_2O + O$; 0.8% of the O_2 was dissociated into atomic species; of the C_2O initially produced 3.5% was further dissociated into $CO + C$. That a substantial fraction of the C_3O_2 was dissociated by the pulsed discharges is supported by the reported fragmentation patterns obtained in mass spectrometers with incident electron voltages of 250 ev. The relative intensities of the various mass peak showed that the most abundant fragment is C_2O^+; the parent ion only 7/10 of C_2O^+, and C^+ was produced at a level 0.4 of C_2O^+. The thermochemical data inserted in the program are listed in Table I. The heat of formation of C_2O was taken as 92 kcal/mole, on the basis of K, T & W [Z. Phys. Chem., 68, 321, (1969)] in contrast to the value given in the JANAF Tables [68.8 kcal/mole].

Of 78 possible reactions involving the species C, C_2O, C_3O, O, O_2 and CO, only 21 were found to make a significant contribution to the production of $CO^{(v)}$. These were selected on the basis of the following criteria. In the first step all reactions were included in the program; then the net rate of formation of each

TABLE I. Thermochemical Data

No.	Specie	Initial Mole Fraction	C_p (a)		ΔH_f^o (b)	
1	C	7.382E-05	4.974		1.712E	02
2	CO_2	0.0	1.028	01	-9.408E	01
3	C_2	0.0	9.177		2.009E	02
4	C_2O	2.035E-03	1.131	01	9.230E	01
5	C_3O_2	4.007E-02	1.862	01	-2.153E	01
6	O	1.954E-03	5.108		5.980E	01
7	O_2	1.211E-01	7.313		0.0	
8	O_3	0.0	1.088	01	3.402E	01
9	C_3	0.0	9.068		1.961E	02
10	He	8.326E-01	4.975		0.0	
11	$CO^{(0)}$	2.183E-03	7.067		-2.631E	01
12	$CO^{(1)}$	0.0	7.067		-2.018E	01
13	$CO^{(2)}$	0.0	7.067		-1.413E	01
14	$CO^{(3)}$	0.0	7.067		-8.152E	00
15	$CO^{(4)}$	0.0	7.067		-2.251E	00
16	$CO^{(5)}$	0.0	7.067		3.575E	00
17	$CO^{(6)}$	0.0	7.067		9.326E	00
18	$CO^{(7)}$	0.0	7.067		1.500E	01
19	$CO^{(8)}$	0.0	7.067		2.060E	01
20	$CO^{(9)}$	0.0	7.067		2.613E	01
21	$CO^{(10)}$	0.0	7.067		3.158E	01
22	$CO^{(11)}$	0.0	7.067		3.696E	01
23	$CO^{(12)}$	0.0	7.067		4.227E	01
24	$CO^{(13)}$	0.0	7.067		4.750E	01
25	$CO^{(14)}$	0.0	7.067		5.266E	01
26	$CO^{(15)}$	0.0	7.067		5.775E	01
27	$CO^{(16)}$	0.0	7.067		6.276E	01
28	$CO^{(17)}$	0.0	7.067		6.770E	01
29	$CO^{(18)}$	0.0	7.067		7.270E	01
30	$CO^{(19)}$	0.0	7.067		7.770E	01

TABLE I (Continued)

No.	Specie	Initial Mole Fraction	C_p [a]	ΔH_f^o [b]	
31	$CO^{(20)}$	0.0	7.067	8.270E	01
32	$CO^{(21)}$	0.0	7.067	8.770E	01
33	$CO^{(22)}$	0.0	7.067	9.270E	01
34	$CO^{(23)}$	0.0	7.067	9.770E	01
35	$CO^{(24)}$	0.0	7.067	1.027E	02
36	$CO^{(25)}$	0.0	7.067	1.108E	03

(a) in cal/mole-degree at 450^oK.

(b) in cal/mole at 450^oK.

specie via a given reaction was compared at short and long times, and for high and low levels of dissociation, with the rates of formation from all reactions. If the rate of formation of a selected specie in a particular reaction was found to be less then the sum rate by a factor of 10^{-4} that reaction was discarded.

The two reactions which generate CO in excited vibrational states are: $C_3O_2 + O \rightarrow CO^{(v)} + C_2O$, and, $C_2O + O \rightarrow CO^{(v)} + CO$. In Table II all the reactions included in the program and their rate constants are listed with the corresponding enthalpies; references to the literature are cited in the extended report.

Of primary interest to this project are the values assumed for the vibrational relaxation of the chemi-excited $CO^{(v)}$. The specific rate constants for most of the species which appear in this system have been presented in the report on the $\{CS_2 + O_2 + He\}$ system. The atomic species deactivate CO via v-T processes, while the molecular species are involved both in v-T and v-v steps. The latter, of course, are most effective when the energy discrepancy is small, of the order of kT or less. The rates which have been presented previously will not be discussed. Attention is called to the following. The relaxation of $CO^{(v)}$ by C was neglected, since the rate constants for deactivation by atomic carbon were equal to those for atomic oxygen and the concentration of the former is very small compared to that of the latter. The rate constant for vibrational relaxation of $CO^{(v)}$ by CO_2 at room temperature are given by Stephenson and Moore [J. Chem.Phys., 50, 1911(1969)], and by Rosser and Sharma [J.Chem.Phys., 54, 1196(1971)] for v = 1. Hancock and Smith [App.Opt., 10,1827(1971)] presented $k_{v,v-1}$ values for 4<v<13. The rate constants for the other vibrational states were obtained by interpolation of

TABLE II. Kinetic Parameters: $k = A \exp(-E_a/RT)$

No.	Reaction	$A \dfrac{cc}{mole \cdot sec}$	$E_a \dfrac{kcal}{mole}$	$k(T = 300^{\circ}K)$ -literature-	ΔH°_{300}
1	$C + CO_2 + M \rightleftharpoons CO + CO + M$	3×10^{13}	5.1	$< 6 \times 10^9$	-129.8
2	$C + C_2O \rightleftharpoons C_2 + CO$	6×10^{13}	0.6	–	-89.0
3	$C + O_2 \rightleftharpoons CO + O$	1.0×10^{14}	2.8	$1.5 \times 10^{12} < k$ $k < 2 \times 10^{13}$	-137.7
4	$C_2O + O_2 \rightleftharpoons CO + CO_2$	2.0×10^{12}	1.5	4.9×10^{11}	-212.7
5	$C_2O + O_2 \rightleftharpoons 2CO + O$	2.0×10^{12}	1.5	5.0×10^{11}	-85.1
6	$C_3O_2 + O \rightleftharpoons C_2O + CO_2$	2.0×10^{12}	2.2	$(2.5 \pm 1.2) \times 10^{10}$	-40.1
7	$O_3 + M \rightleftharpoons O + O_2 + M$	2.0×10^{15}	24.0	–	25.8
8	$O + O_3 \rightleftharpoons 2 O_2$	3.0×10^{13}	6.0	–	-93.8
9	$C_2 + O \rightleftharpoons CO + C$	1.0×10^{14}	3.0	–	-115.8
10	$C_2O + O \rightleftharpoons CO^{(o)} + CO^{(o)}$	1.72×10^{13}	0.6	$(5.7 \pm 3) \times 10^{13}$	-204.7
11	$C_2O + O \rightleftharpoons CO^{(1)} + CO^{(o)}$	1.02×10^{13}	0.6	–	-198.6
12	$C_2O + O \rightleftharpoons CO^{(2)} + CO^{(3)}$	4.69×10^{12}	0.6	–	-192.5
13	$C_2O + O \rightleftharpoons CO^{(3)} + CO^{(o)}$	2.34×10^{12}	0.6	–	-186.6
14	$C_2O + O \rightleftharpoons CO^{(4)} + CO^{(o)}$	1.17×10^{12}	0.6	–	-180.7
15	$C_2O + O \rightleftharpoons CO^{(5)} + CO^{(o)}$	6.64×10^{11}	0.6	–	-174.8
16	$C_2O + O \rightleftharpoons CO^{(6)} + CO^{(o)}$	1.95×10^{11}	0.6	–	-169.1
17	$C_2O + O \rightleftharpoons CO^{(7)} + CO^{(o)}$	1.56×10^{11}	0.6	–	-162.9
18	$C_2O + O \rightleftharpoons CO^{(8)} + CO^{(o)}$	0.0		–	-157.8
19	$C_2O + O \rightleftharpoons CO^{(9)} + CO^{(o)}$	0.0		–	-152.3
20	$C_2O + O \rightleftharpoons CO^{(10)} + CO^{(o)}$	0.0		–	-146.8
21	$C_2O + O \rightleftharpoons CO^{(11)} + CO^{(o)}$	0.0		–	-141.4
22	$C_2O + O \rightleftharpoons CO^{(12)} + CO^{(o)}$	7.81×10^{10}	0.6	–	-136.1
23	$C_2O + O \rightleftharpoons CO^{(13)} + CO^{(o)}$	3.13×10^{11}	0.6	–	-130.9
24	$C_2O + O \rightleftharpoons CO^{(14)} + CO^{(o)}$	1.64×10^{12}	0.6	–	-125.7
25	$C_2O + O \rightleftharpoons CO^{(15)} + CO^{(o)}$	1.41×10^{12}	0.6	–	-120.7
26	$CO_2 + C_2 \rightleftharpoons C_2O + CO$	7.0×10^{13}	6.0	–	-40.8
27	$C + C_3O_2 \rightleftharpoons 2CO + C_2$	1.0×10^{13}	4.0	–	-1.4
28	$C_2O + C_2O \rightleftharpoons 2CO + C_2$	4.0×10^{12}	3.0	–	-36.3
29	$C_2O + C \rightleftharpoons C_2 + O_2$	6.0×10^{13}	54.5	–	48.8
30	$C_2O + O \rightleftharpoons CO_2 + C$	2.0×10^{13}	3.6	–	-75.0
31	$C + C_2O \rightleftharpoons C_3 + O$	3.0×10^{13}	4.0	–	-7.6
32	$C_3 + C \rightleftharpoons C_2 + C_2$	1.0×10^{14}	36.0	–	34.4
33	$C_2 + C_2O \rightleftharpoons CO + C_3$	3.0×10^{13}	0.7	–	-123.3
34	$C_3 + O \rightleftharpoons CO + C_2$	6.0×10^{13}	0.7	–	-81.4
35	$C_3 + O_2 \rightleftharpoons 2CO + C$	5.0×10^{12}	1.5	–	-77.5
36	$C_3O_2 + O \rightleftharpoons CO^{(o)} + 2CO^{(o)}$	8.7×10^{12}	2.0	$(3.2 \pm 1.2) \times 10^{11}$	-117.2
37	$C_3O_2 + O \rightleftharpoons CO^{(1)} + 2CO^{(o)}$	5.8×10^{12}	2.0	–	-111.1
38	$C_3O_2 + O \rightleftharpoons CO^{(2)} + 2CO^{(o)}$	2.1×10^{12}	2.0	–	-105.0
39	$C_3O_2 + O \rightleftharpoons CO^{(3)} + 2CO^{(o)}$	1.1×10^{12}	2.0	–	-99.0
40	$C_3O_2 + O \rightleftharpoons CO^{(4)} + 2CO^{(o)}$	6.8×10^{11}	2.0	–	-93.1

TABLE II (Continued)

No.	Reaction	$A \frac{cc}{mole \cdot sec}$	$E_2 \frac{kcal}{mole}$	$k(T = 300^oK)$ -literature-	ΔH^o_{300}
41	$C_3O_2 + O \rightleftharpoons CO^{(5)} + 2CO^{(o)}$	2.8×10^{11}	2.0	-	- 87.3
42	$C_3O_2 + O \rightleftharpoons CO^{(6)} + 2CO^{(o)}$	1.5×10^{11}	2.0	-	- 81.6
43	$C_3O_2 + O \rightleftharpoons CO^{(7)} + 2CO^{(o)}$	1.7×10^{11}	2.0	-	- 75.9
44	$C_3O_2 + O \rightleftharpoons CO^{(8)} + 2CO^{(o)}$	5.3×10^{11}	2.0	-	- 70.3
45	$C_3O_2 + O \rightleftharpoons CO^{(9)} + 2CO^{(o)}$	2.6×10^{11}	2.0	-	- 64.8
46	$C_3O_2 + O \rightleftharpoons CO^{(10)} + 2CO^{(o)}$	1.9×10^{11}	2.0	-	- 59.3
47	$C_3O_2 + O \rightleftharpoons CO^{(11)} + 2CO^{(o)}$	9.2×10^{10}	2.0	-	- 53.9
48	$C_3O_2 + O \rightleftharpoons CO^{(12)} + 2CO^{(o)}$	0.0		-	- 48.6
49	$C_3O_2 + O \rightleftharpoons CO^{(13)} + 2CO^{(o)}$	0.0		-	- 43.4
50	$C_3O_2 + O \rightleftharpoons CO^{(14)} + 2CO^{(o)}$	0.0		-	- 38.2
51	$C_3O_2 + O \rightleftharpoons CO^{(15)} + 2CO^{(o)}$	0.0		-	- 33.1

these data. The final values used are given in Table III. The temperature dependence of $k_{1 \to 0}$ for CO_2 on CO was given by Stephenson and Moore; the rate constant changes linearly with temperature, in contrast to the SSH theory, which predicts a much stronger temperature dependence. Thus, at $600^{\circ}K$ the SSH value is larger by a factor of 3.5 than the value given by S & M. In our program the linear temperature dependence was used for all v values.

With reference to C_2O, note that one of its fundamental vibrational frequencies is 1978 cm^{-1}; this falls between the v = 7 and v = 8 for CO. In such a case of nearly exact resonance one should not anticipate a strong temperature dependence. The vibrations of OCS molecules are also in resonance with CO at the 4th vibrational level. For C_2O we used the OCS values for $k_{v,v-1}$ given by Hancock and Smith, but the values were scaled in order to bring the largest $k_{v,v-1}$ to v = 7. These are listed in Table IV.

C_3O_2 has a characteristic normal mode vibration at 2200 cm^{-1}, which is close to the spacing for the fundamental transition of CO. Hence $k_{v,v-1}$ should be large for v = 1, and its magnitude should decrease for higher v's. We assumed that $k_{v,v-1}$ to be the same for C_3O_2 as for N_2O on CO, since one of the normal modes of N_2O is 2224 cm^{-1}. The rate constants for $4 \leq v \leq 13$ were taken from Hancock and Smith; the other values were interpolated from these data (Table V).

The computed concentrations of C_2 as a function of time, under laser operating conditions, are shown in Figure 1. Note that its magnitude rises very rapidly and attains a maximum at about 33 μs; then it decreases gradually. The reactions that produce C_2 are (2), (27), (28), and (34); reaction (29) proceeds in reverse direction thus reducing the C_2 concentration. Reactions (2) and (34) are exoergic, sufficiently to excite C_2 to the A state, the upper level in the Swan band

TABLE III

Rate Constants, $k_{v,v-1}$ ($cm^3 mole^{-1} sec^{-1}$) for

Deactivation of $CO^{(v)}$ by CO_2

v	$k_{v,v-1}$
1	4.13×10^4
2	3.30×10^4
3	2.50×10^4
4	1.80×10^4
5	1.00×10^4
6	9.50×10^3
7	9.00×10^3
8	9.50×10^3
9	1.25×10^4
10	2.00×10^4
11	3.20×10^4
12	5.10×10^4
13	6.70×10^4
14	9.00×10^4
15	1.10×10^5
16	1.25×10^5
17	1.40×10^5

TABLE IV

$$k_{v,v-1} (C_2O) \ (cm^3 mole^{-1} sec^{-1})$$

v	$k_{v,v-1}$
1	6×10^5
2	1.5×10^6
3	3.6×10^6
4	6×10^6
5	1.3×10^7
6	2.4×10^7
7	3.6×10^7
8	3.4×10^7
9	2.2×10^7
10	7.9×10^6
11	4.2×10^6
12	2.3×10^6
13	1.8×10^6
14	1.1×10^6
15	6×10^5
16	2.4×10^5
17	1.2×10^5

TABLE V

$$k_{v,v-1} (C_3O_2) (cm^3 mole^{-1} sec^{-1})$$

v	$k_{v,v-1}$
1	6×10^5
2	5.4×10^5
3	4.4×10^5
4	3.0×10^5
5	1.5×10^5
6	9.0×10^4
7	5.8×10^4
8	5.1×10^4
9	5.1×10^4
10	6.0×10^4
11	6.0×10^4
12	6.0×10^4
13	5.6×10^4
14	5.6×10^4
15	4.8×10^4
16	4.2×10^4
17	3.6×10^4

Fig 1
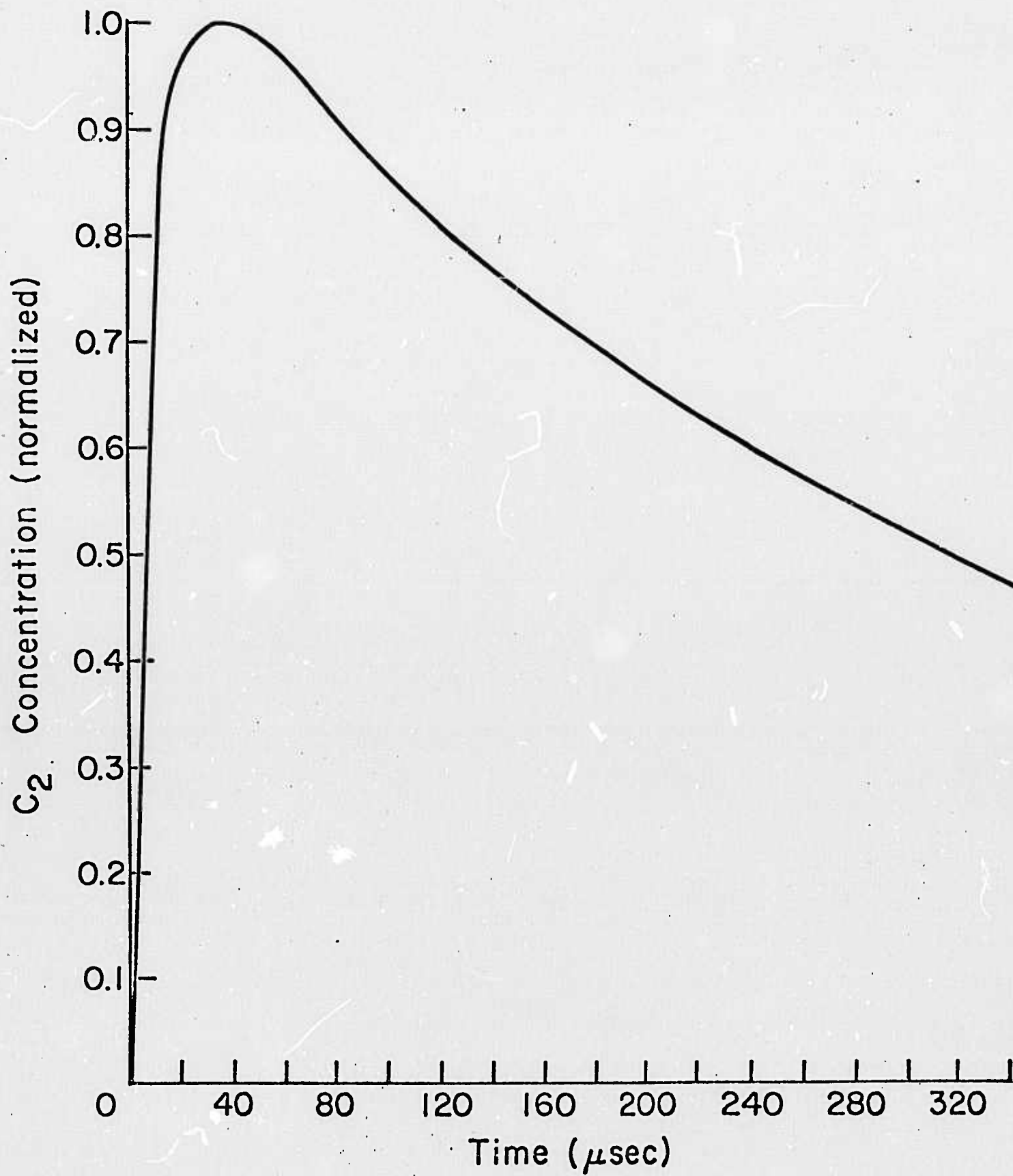
system $[A^3\Pi_g - X^3\Pi_u]$. The rates of production of C_2 by these reactions (in moles $cm^{-3} sec^{-1}$) are summarized in the following table.

Reaction No.	Reaction	delay times (μsec)			
		2	17	33	43
2	$C + C_2O \rightarrow C_2 + CO$	1.3×10^{-13}	1.6×10^{-14}	2.0×10^{-15}	9.0×10^{-16}
34	$C_3 + O \rightarrow CO + C_2$	7.0×10^{-17}	6.0×10^{-16}	7.0×10^{-16}	6.0×10^{-16}
27	$C + C_3O_2 \rightarrow 2CO + C_2$	1.1×10^{-14}	2.2×10^{-15}	5.0×10^{-16}	2.7×10^{-16}
28	$C_2O + C_2O \rightarrow 2CO + C_2$	2.1×10^{-14}	1.2×10^{-14}	5.9×10^{-15}	3.8×10^{-15}

During the first 30 μs the most important contributor to the production of C_2 is step (2). This is supported by the measured Swan band radiations as a function of the oxygen present in the discharge; the results are shown in Figure 2 for the indicated v-v transitions. Clearly, the relative intensities of the Swan bands depend strongly on the oxygen pressure; they decrease sharply with increasing partial pressure. This is compatible with our assumption that the principal mechanism for C_2 production is (2). When oxygen is introduced the amount of C_2O and C available for this reaction are reduced, causing the sharp decrease in intensity. Additional support is provided by literature reports on the thermal decomposition of C_3O_2; C_2 is produced. Klemenc, et.al. [Z. Elektrochem., 40, 488 (1934)] suggested that the overall reaction is: $C_3O_2 \rightleftarrows CO_2 + C_2$; Kunz [J. Chem. Phys., 46, 4157 (1967)] proposed that the reaction (2) produces C_2 in the $(A^3\Pi)$ state. The calculated and observed vibrational state populations of $CO^{(v)}$, at several delay times, are shown in Figure 3. The solid lines are the experimental results
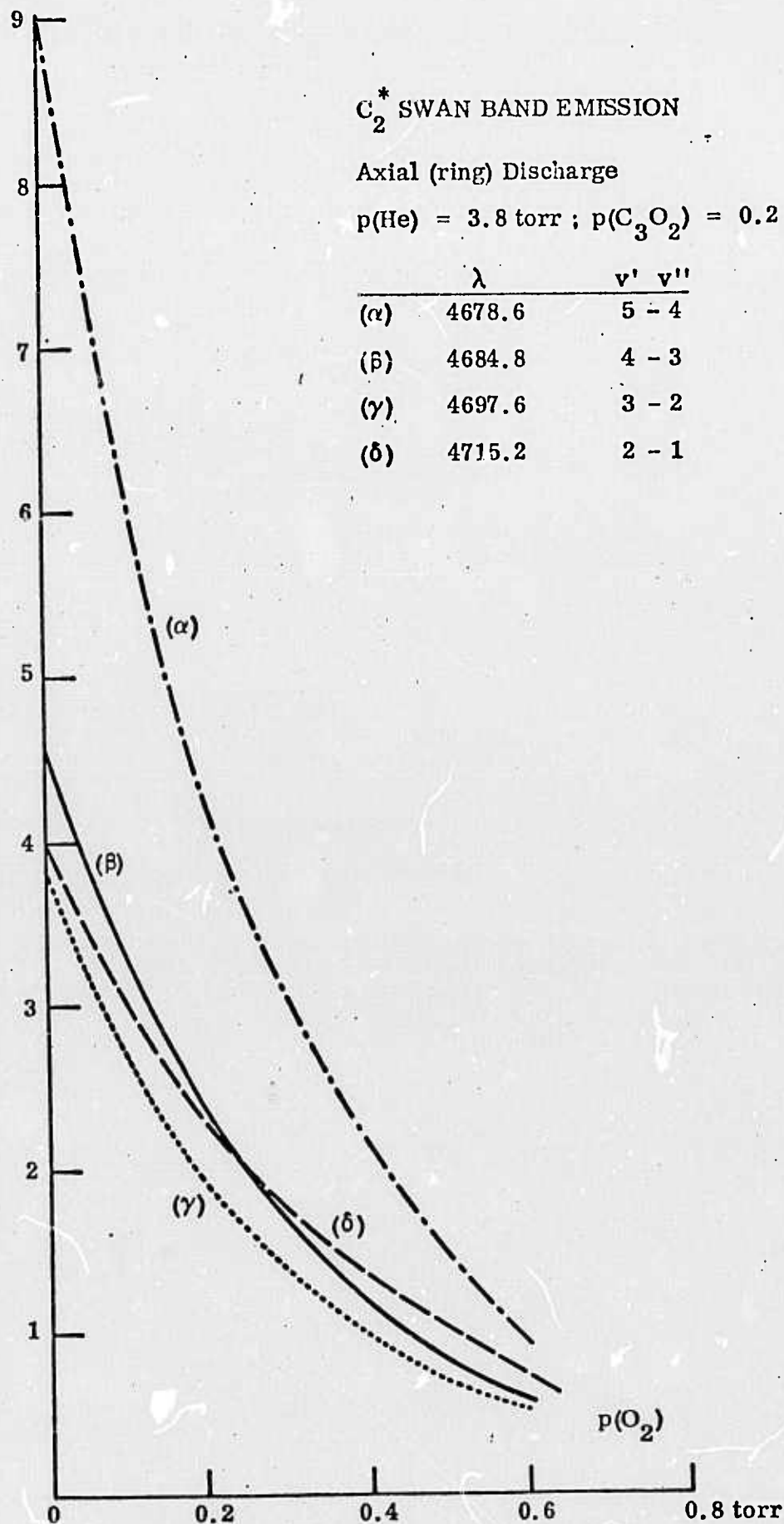
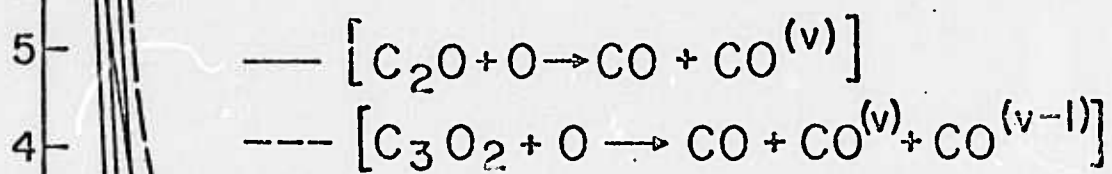C$_2^*$ SWAN BAND EMISSION

Axial (ring) Discharge

p(He) = 3.8 torr ; p(C$_3$O$_2$) = 0.2 torr

	λ	v' v''
(α)	4678.6	5 – 4
(β)	4684.8	4 – 3
(γ)	4697.6	3 – 2
(δ)	4715.2	2 – 1
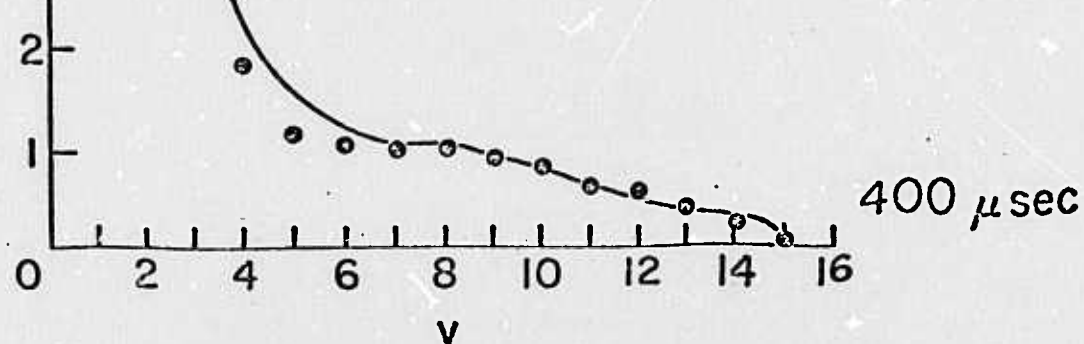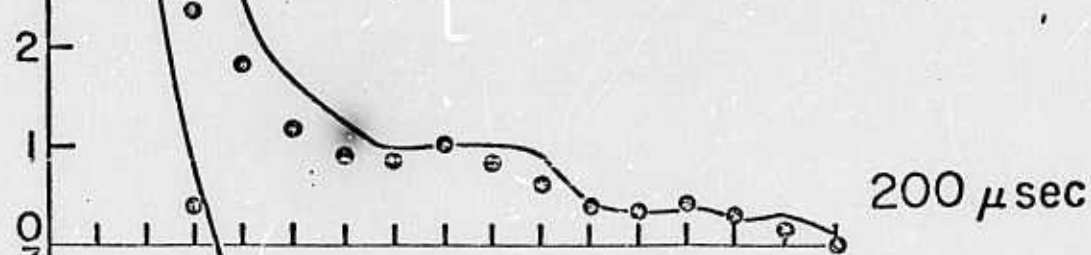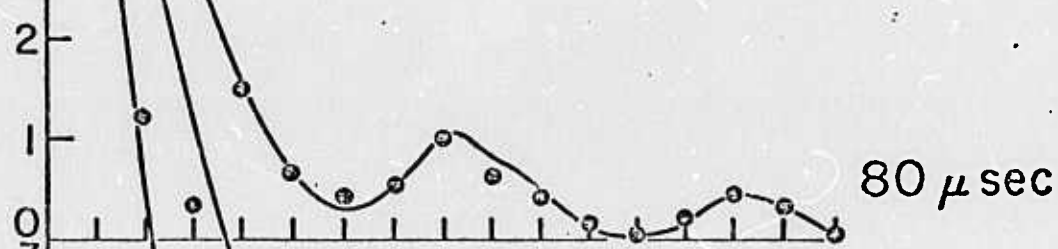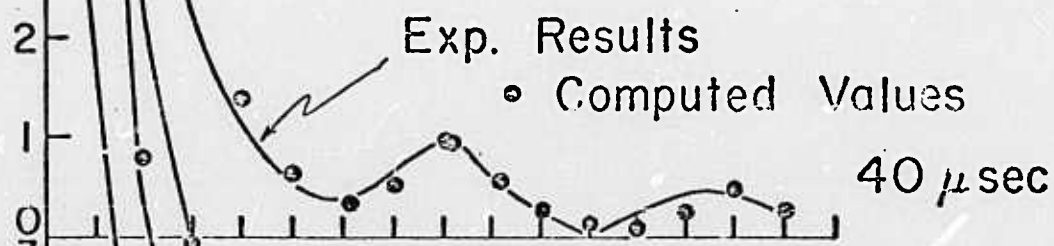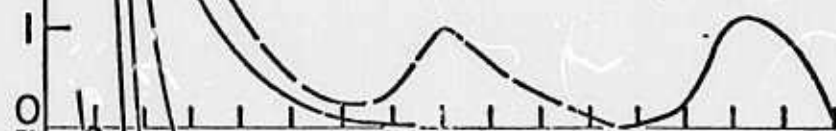
(Sheasley), and the points were computed; in each case, the magnitudes were normalized to unit value at $v = 8$. On comparing the vibrational populations derived experimentally from the chemiluminescence intensities, with those computed (Figure 4), we find the agreement is fairly good, except for the distribution at the 40 μsec delay time. In this case the model shows higher values by a factor of about 2. The reason could be the low chemiluminescence intensity emitted at this early delay time, and the need to use a wide monochromator slit. The two maxima in the $CO^{(v)}$ distribution (at $v = 8$ and $v = 13, 14$) are compatible with the Clough, Schwartz and Thrush experiments [Proc. Roy. Soc. London, A317, 575 (1970)]. Our model shows that the first peak at $v = 8$ is primarily produced by the $C_3O_2 + O \rightarrow 3\,CO$ reaction, which is sufficiently exothermic to pump 3CO to the $v = 6$ state. The second maximum at $v = 13, 14$ is primarily produced by the $C_2O + O \rightarrow 2CO$ reaction; this is sufficiently exothermic to pump 2CO to about $v = 18$.

Gain coefficients at different delay times were computed for $v' = 2, 3, \ldots\ldots 11$; for each v' level we computed the gain for P(1)...(P20) rotational lines. The gain for a P-branch transition $[v, J-1 \rightarrow v-1, J]$ is given by:

$$ g = \frac{8\pi^3 c}{3kT \sqrt{\dfrac{2\pi kT}{m}}} \; \varkappa_{v,v-1} \, J \left[N_v B_v e^{-\dfrac{F_v(J-1)hc}{kT}} - N_{v-1} B_{v-1} e^{-\dfrac{F_{v-1}(J)hc}{kT}} \right] $$

where $\varkappa_{v,v-1}$ is the vibrational contribution to the transition matrix element; m is the mass of CO; $F_v(J)$ is the rotational term value for the v' vibrational level; $F_v(J) = B_v(J+1) - D_v J^2 (J+1)^2$. The rotational constants were taken from Patel [Phys. Rev., 141, 71 (1966)]. $\varkappa_{1 \rightarrow 0}$ is given by Young and Eachus [J. Chem. Phys.,

(b) Theoretical Results

(a) Experimental Results

40 μsec
80 μsec
200 μsec
400 μsec

[C(v)] (arbitrary units)
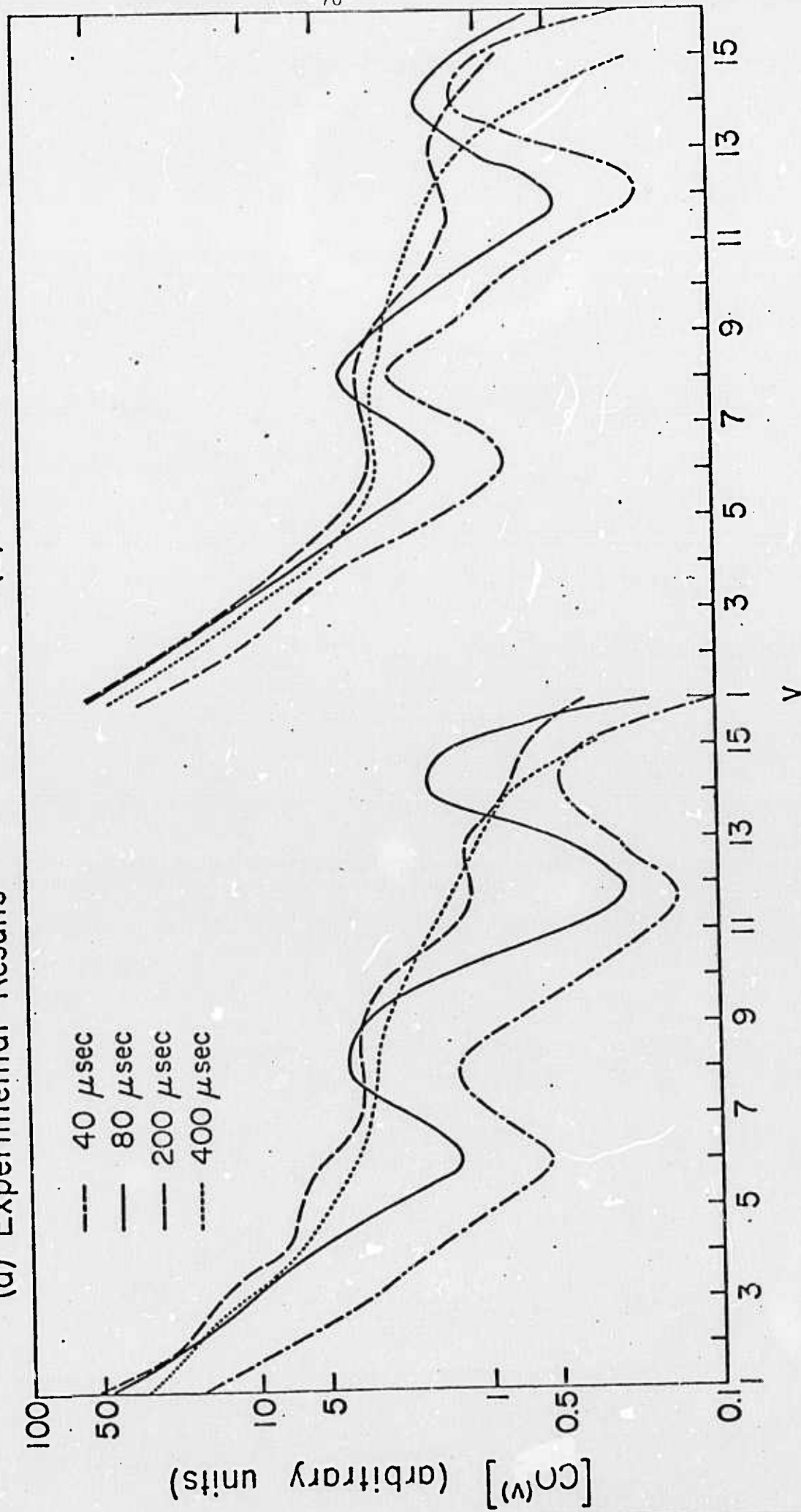
44, 4195 (1966)], and ratios of matrix elements for v up to 9 are given in

Journal of Molecular Spectroscopy, 10, 182 (1963). The ratios of matrix elements

for v' = 10 and v' = 11 were calculated via:

$$\frac{\varkappa_{v,v-1}}{\varkappa_{1,0}} = \frac{A_{v,v-1}}{A_{1,0}} \left(\frac{\nu_{1,0}}{\nu_{v,v-1}} \right)^3$$

This gives for v' = 8, 9, 10 and 11 the ratios: 2.8004, 2.9547, 3.1065 and 3.2504. The
model shows/positive gain is attained for v' = 6, 7 ... 11, as summarized in Table VI.
that

Note that the model predicts lasing at the correct vibrational lines and at correct

delay times for v' = 6, 9 and 10. The calculated delay times for v' = 7 and 8 are

very short, compared with those observed. We propose that this is due to the fact

that v' = 7 and 8 lines are absorbed within the system during the early times by

the incompletely reacted reagents. To check this assumption we measured the

absorption of v' = 7 → 6, P(13) line by the laser plasma (no cavity mirrors) at

several delay times. C_2O is one of the principal species in the system which could

absorb CO radiation. The wave numbers for the laser transitions v = 7 → 6 and

8 → 7 are compared with C_2O rotational lines of the (001) band (Table VII),

computed by assuming:

$$E_v(\nu_3) = 1978.0 \text{ cm}^{-1} \quad ; \quad B = 0.4085 \text{ cm}^{-1}$$

$$D \approx 4B^3/E_v(\nu_1)^2 = 2.36 \times 10^{-7}, \text{ where } E_v(\nu_1) = 1074.0 \text{ cm}^{-1}$$

B and D are the rotational constant needed   to calculate the corresponding

term values: $F(J) = BJ(J+1) - DJ^2 (J+1)^2$. The last column of Table VII shows the

fraction of C_2O molecules in the absorbing level. Note the small discrepancy

between the frequencies for C_2O and the CO. By measuring the net absorption at

about 300 μsec, when the C_2O concentration is very low, approximately 10^{-13} of

TABLE VI. Summary of Delay Times

v'	Inversion Starts (μsec)			At 400 μs $T = 533^{\circ}K$		At 400 μs $T = 300^{\circ}K$		At 400 μs $T = 400^{\circ}K$	
	τ	Gain (rel)	J_{opt}	Gain (rel)	J_{opt}	Gain (rel)	J_{opt}	Gain (rel)	J_{opt}
6	240	0.18	20	0.4	19	1.4	14	1.13	17
7	<40	1.8	12	1.8	13	4.2	11	4.3	13
8	<40	10.5	11	1.9	15	4.9	11	4.4	13
9	320	0.2	20	0.5	19	1.8	15	1.5	17
10	400	0.1	20	0.1	20	1.03	16	0.8	18
11	320	0.08	20	0.2	19	1.4	15	1.1	18

TABLE VII. Computed Frequencies for C_2O Rotational Lines

C_2O ; $E_v(\nu_3) = 1978$ cm^{-1}			CO lines with short τ			C_2O Population at 500°K $N(J)/N$
P(J)	ν(cm^{-1})	$\nu_{C_2O} - \nu_{CO}$	v'-v''	P(J)	ν(cm^{-1})	
37	1947.82	0.30	7–6	10	1947.52	4.5×10^{-2}
47	1943.76	0.22		11	1943.54	3.8×10^{-2}
52	1935.65	0.16		13	1935.49	3.3×10^{-2}
57	1931.61	0.20		14	1931.41	2.7×10^{-2}
62	1927.57	0.27		15	1927.30	2.3×10^{-2}
67	1923.55	0.39		16	1923.16	9.7×10^{-3}
84	1909.93	0.05	8–7	13	1909.88	6.5×10^{-3}
94	1901.99	0.22		14	1901.77	3.1×10^{-3}

its initial concentration, we can estimate the CO contribution. Then by sub-stracting this magnitude from the measured absorption, obtain the net absorption by C_2O at $v' = 7$ and 8. This indicated that the assumption that C_2O was the only absorber was not adequate. Were this the case the ratio of the net absorption co-efficient divided by the C_2O concentration would not vary significantly with the delay time, which it does. We suspect that the remaining absorption is due to the undecomposed C_3O_2, but the complete explanation for this discrepancy is not now available, nor do we have an explanation as to why the J's for the optimum transitions, as calculated, do not agree with those observed.

We calculated the gain at different delay times when cold CO was introduced into the gas mixture. The measured delay times at which gain first attains positive values, as a function of the pressure of the added CO, are shown in Figure 5. The initial conditions inserted in the program are the same as used previously, except the total pressure is higher due to the increase in the added CO. The computed values are compatible with the experimental observations (Table VIII). (a) The delay times become shorter as more cold CO is added; (b) for $v' = 6, 7$ and 9 the absolute value for the gain reaches a maximum at approximately $P_{CO} \approx 0.12$ torr; (c) for $v = 8$ the gain is reduced as a function of the added CO whereas for $v' = 10$ and 11 the gain goes up with added CO.
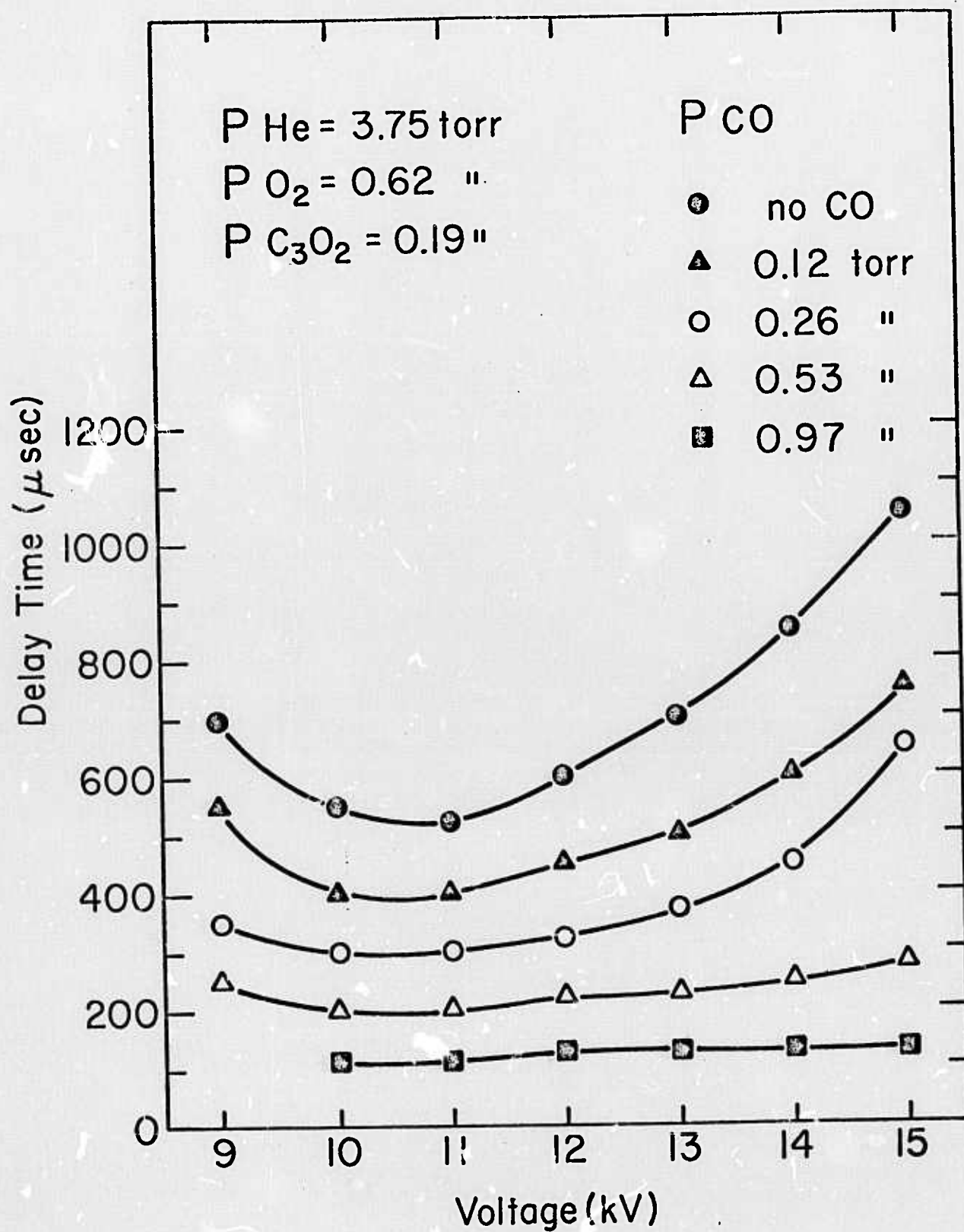
FIG.5

TABLE VIII. Effect of Added "Cold" CO

v'	p(CO) = 0.0 torr		p(CO) = 0.12 torr		p(CO) = 0.8 torr	
	Gain	Delay (μs)	Gain	Delay (μs)	Gain	Delay (μs)
6	0.46	620	1.4	260	0.86	160
7	4.1	160	4.3	120	2.9	80
8	12	80	9.9	80	6.1	40
9	1.0	640	1.4	600	0.95	360
10	0.6	640	0.97	560	1.2	320
11	0.33	440	0.83	440	1.6	280

VII. Laser Initiated Reactions in Mixtures of B_2H_6

Conditions for operating <u>boron atom laser</u> were discovered. This material is described in the attached report, which has been submitted for publication in <u>Chemical Physics Letters</u>.

The exploratory work with the CO_2 laser initiated reactions in mixtures of B_2H_6 with one of the following oxidizers [O_2, N_2O, NO_2, PF_3] led to interesting results. In these the admixed SF_6 serves as an absorber and heat transfer agent. The rapid heating of mixtures of B_2H_6, NO_2 and SF_6 produced high levels of luminosity. In most of these experiments the cell was filled with about 15 torr of SF_6, 13 torr B_2H_6 and 25 torr of the oxidizer; it was exposed to a 10 watt cw-CO_2 laser oscillating on the P(28) line. Very bright yellow-green flashes were observed, particularly when the oxidizer was molecular oxygen or NO_2; weaker illuminosities were produced when the oxidizer was N_2O or PF_3. The spectra of the light emitted were photographed with a Spex three-quarter meter grating instrument, and the plates read with a microdensitometer. A large number of bands were thus recorded, ranging from $\lambda 5875$ to $\lambda 3818$. These bands are superposed on a substantial background which appears to be a continuum but not of uniform intensity. The brightest regions of the spectrum appeared at 5800, 5400, 5200, 4900, 4500, and 4000 Å. Some of these can be assigned to diatomic emitters, such as BO, BS, BF and H_2; BO_2 is a very prominent emitter. Several bands correlate well with spectra from H_2 and H_2O, however, these assignments have not been checked and at present we can only say that the system appears to have a very high radiative temperature. As yet the relative intensities of these bands have not been quantitatively ascertained, since we do not have the sensitometric calibration for the film used in these studies. It is clear, however, that the most

intense band appears at 5875 Å; this could be due to BO, second order, for 2935 Å. There is a dense system of red-degraded double-head bands between $2700 \rightarrow 4500$ Å which belong to the BO α series $[A^2\Pi \rightarrow X^2\Sigma]$. If this interpretation is correct then we must look for a reaction which is capable of generating 97 kcal/mole to provide the exothermicity for exciting BO to emit at these short wavelengths. The only such reactions known to us are the following:

$$BH_2 + O \rightarrow BO + H_2 \qquad \Delta H^o = -108(\pm 17) \text{ kcal/mole}$$

$$BO + O_2 \rightarrow BO_2 + O \qquad \Delta H^o = -109(\pm 4) \text{ kcal/mole}$$

This interesting system clearly merits further study.

To help unscramble the mechanisms of pyrolysis and oxidation of boron containing systems, preliminary measurements were made utilizing a mass spectrometer and a rapid gas flow reactor to measure the rate of reaction between oxygen atoms and several boron hydrides. Hand and Derr [Inorg. Chem., 13, 339 (1974)] described a similar experiment in which oxygen atoms were allowed to react with B_2H_6. The rate constant they found is $(4.21 \pm 2.7) \times 10^{-15}$ cm^3 molecules^{-1}sec^{-1} at room temperature; it has an apparent activation energy of 4.8 ± 0.5 kcal/mole^{-1}. We confirmed their value and then measured the corresponding rate between oxygen atoms and BH_3CO. A much larger rate constant was found, as expected: $k = (6.1 \pm 0.6) \times 10^{-13} cm^3$molecules^{-1}sec^{-1}, at room temperature. The rates of reaction of the boranes with molecular oxygen are too slow to be measured with his apparatus. In another experiment which sheds a light on this mechanism, he recorded the emission spectra produced on mixing H_3BCO with oxygen atoms in a flow system. He found red-degraded, double-headed bands, and assigned the

highest transition to v', v'' = 12,0 at 2700 Å. This corresponds to 104 kcal/mole above the ground state. In the absence of molecular oxygen no BO_2 emission was seen. It is suspected that the three body reaction $BO + O + M \rightarrow BO_2 + M$ does not lead to high levels of excitation of BO_2. On the other hand, when molecular oxygen was added, a very intense green band system from BO_2 was observed, presumably produced in the reaction $BO + O_2 \rightarrow BO_2^* + O$.

We conclude that a combination of techniques, such as the use of fast flow reactors with a mass spectrometer/ the photographic recording of spectra in low
diagnostics,
pressure flow systems, when one of the reagents is excited by a microwave discharge, and parallel studies of laser heated initiation reactions, will be needed to develop adequate mechanisms, and lead to optimum conditions for generating chemiluminescence in the visible.

-80-

AN ATOMIC BORON LASER ---

PUMPING BY INCOMPLETE AUTOIONIZATION,

OR ION-ELECTRON RECOMBINATION

J. Stricker[‡] and S. H. Bauer

Department of Chemistry, Cornell University, Ithaca, New York 14850

ABSTRACT

Pulsed lasing was obtained from discharges in mixtures of He ($\approx$10 torr) and a number of boron containing species ($\approx$ 25 mTorr). Discharge conditions for optimizing the output are briefly described. Laser emission appears at 2777 ± 1.6 cm^{-1}, with 20-50 μs delay after passage of the discharge pulse ($\approx$1 μs half width). The emitters are boron atoms. Among the term values for B I and B II only one pair of levels for B I have a separation close enough to the observed frequency to be considered. One possible mechanism is based on excitation to a metastable level above the first ionization limit. A distant collision may induce transition to captured-electron states at the limit (incomplete autoionization), which constitute the upper lasing levels; lasing them occurs by induced transitions to the lower level, 7s, $^{2}S_{1/2}$, which is rapidly depleted. Another possibility is the capture of an electron by B^{+} into a very large Rydberg orbit, at the ionization limit, which are the upper lasing states.

[‡] Permanent address: Department of Aeronautics, The Technion, Haifa, Israel

Our search for a BH elimination laser so far has proved illusive, but we did discover laser emission from atomic boron, when low concentrations of certain boron bearing species, diluted in helium, are subjected to a pulse discharge. The following is a brief description of the experiment.

The reactor tube is a 1" I.D. pyrex pipe, 120 cm long, fitted with rock salt windows at their Brewster angle. The discharge is impressed by two aluminum co-axial ring electrodes, placed about 1 meter apart. A modest helium flow is maintained at the desired pressure, while the test gas is admitted several meters upstream for complete mixing. Pulses from a 5.13 nf condenser are repeated at 6 Hz, at set voltages; they are less than 1 μs in half-width. The cavity consists of a 3 m radius gold mirror at one end and a gold flat with a 1 mm hole at the other, set about 160 cm apart. With this arrangement laser emission from Ar [$\approx$5 torr He, $\approx$5 torr Ar, $\approx$11 Kv] is easily excited. This emission starts with the discharge and declines rapidly; half-time $\approx$10 μs. Its wavelength is 2.205 $\pm$ .005 μ, which corresponds to the reported ArI laser line at 2.20245 μ $\{3d[1/2]_0^0 \rightarrow 4p'[3/2]_1\}$. Cavity alignment is greatly facilitated with this pulsed emission.

The following gases produce laser radiation [the rationale for their selection is indicated below]: $^nB_2H_6$ [^nB represents boron with normal isotopic abundance], $^nB_2D_6$, $H_3{}^nBCO$, $^nB_5H_9$, $^{10}B_2H_6$ and $^nBBr_3$. No lasing was obtained with $^nBC\ell_3$ and $^nB(C_2H_5)_3$. The purity of these gases was checked by mass spectroscopy and their infrared spectra. No differences in laser operation could be detected when Airco (commercial) He was replaced by high purity (Matheson) He. Very slight amounts of oxygen completely quenched lasing; H_2 is not quite so drastic

for quenching; the addition of Ar reduced laser output power. Lasing conditions were very sensitive to the pressure of the lasing gas; either too much or too little was detrimental, with the optimum pressure ≈ 25 mTorr.

By a suitable combination of filters that spanned the range $1 \rightarrow 11$ μm, we established that the radiation appeared only between 2 and 4 μm; a gold doped germanium detector, cooled to liquid nitrogen, was used. We did not test for radiations outside the 1 to 11 μm range. With a calibrated 25 cm f. ℓ. Spex grating monochromator fitted with a 25 μm slits, a single line was found at 2777 ± 1.6 cm^{-1}; its width was less than or equal to the resolution of our intrument. This frequency was unaffected by the reagents used. The absence of any H/D isotope shifts eliminated BH, BH_2 and BH_3 as emitters; later confirmed by the observed lasing from BBr_3-He mixtures. The possibility that the emitter is BHe^+ was eliminated by the absence of any $^{10}B/^{11}B$ isotope shift. We conclude that the emitter is atomic boron. Indeed, absorption spectra of B and B_2 were previously recorded[1] following flash photolysis in H_3BCO. The fact that neither $BC\ell_3$ nor $B(C_2H_5)_3$ lased can be rationalized in terms of their respective average bond dissociation energies[2] and our observation that the density of boron in the discharge is very critical. The following sequence suggests that boron hydrides are the best sources for boron atoms.

⟨D⟩ values: B-B (70 kcal/mole); B-H (78); B-N (92); B-Br (103); B-C (106);

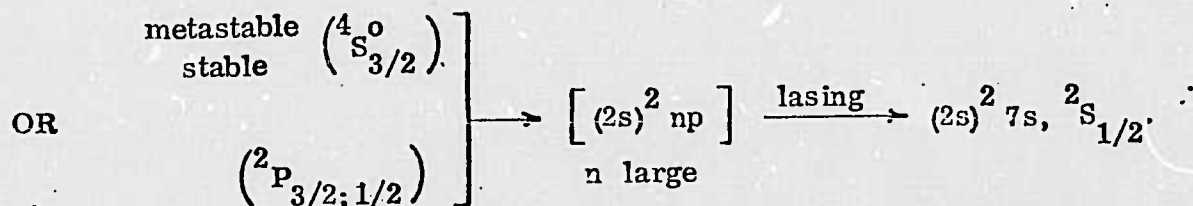B-Cℓ (127); B-F (181) and B-O (187).

Indeed, B_5H_9 gave somewhat more intense emission than did B_2H_6. The optimum discharge voltage for BBr_3 was several kilovolts higher than that for the boron hydrides, reflecting its higher average bond dissociation energy.

The shape of the output pulse is shown in Fig. 1. We present a dual trace to illustrate the reproducibility of the laser output. Delays ranging from 20 μs to 50 μs were observed, depending on the He pressure and discharge voltage [Fig. 2]. The width of the pulse at half maximum is somewhat less than the delay time ($\approx$30 μs for a 40 μs delay). When the pressure is low the delay time is shorter, suggesting that while He is necessary to sustain the discharge it may also quench the radiating species. The pulse duration decreases with increasing He pressure.

The output power of the laser depends both on the He pressure and the discharge voltage. For a sequence of fixed pressures, the voltage dependence passes through a maximum [Fig. 3]. Over the range of conditions covered in these experiments, the maximum output using B_2H_6 as precursor appears at 11.5 Kv with He pressures 10-12 Torr. Increasing the voltage beyond this value reduces the concentration of lasing species and/or modifies the electron energy distribution toward an unfavorable shape.

The appearance of a delay in the 20-50 μs range for an atomic laser is indicative of a multistep collisional mechanism. This was supported by our search for coincidence spacings among the term values for B I and B II. Reference to Moore's Tables[3] and the later work by Edlén, et. al.[4] uncovered a single combination in the B I set which was close enough to be considered. The limiting ionization level for the doublet states is 66,928.10 $\pm$ 0.1 cm^{-1} [nf ^{2}F series][4], while (2s) ^{2}7s, $^2S_{1/2}$ occurs at 64,156 $\pm$? cm^{-1}; i.e. 2772 $\pm$? cm^{-1} lower. The fact that two well characterized states were observed above the ionization limit [2s 2p^2, $^2P_{3/2;1/2}$ at 72,547 and 72,535 cm^{-1}; 2p^3, $^4S^o_{3/2}$ at 97,037 + x cm^{-1}] suggests that pumping may start by excitation to a metastable state above the ionization limit. Then, due to some perturbation such as a distance collision, de-excitation to the

ionization limit occurs but with the electron still captured (incomplete auto-ionization). Lasing occurs by induced transition to $1s^2 2s^2 7s$, $^2S_{1/2}$.

$$\left.\begin{array}{c} \text{metastable} \\ \text{stable} \end{array} \left(^4S^o_{3/2}\right) \atop \left(^2P_{3/2;\,1/2}\right)\right] \longrightarrow \left[\underset{n \text{ large}}{(2s)^2 np}\right] \xrightarrow{\text{lasing}} (2s)^2 7s,\ ^2S_{1/2}.$$

OR

Such a sequence of events accounts, in a qualitatively way, for our observation of a long delay time, and presents a novel pumping mechanism. Dr. T. A. Cool called our attention to a second matching interval. Extrapolation via a linear Ritz formula indicates a term value of $61,381$ cm^{-1} for the $1s^2 2s^2 5p$, $^2P_{3/2;\,1/2}$ state, which is 2775 cm^{-1} below $7s$, $^2S_{1/2}$. Thus the delay may be due to cascading from the incompletely autoionized states to $1s^2 2s^2 7s$, which is the upper lasing level, from which induced transitions are made to the 5p state.

Another possible route for populating states at the ionization limit is the capture of an electron by B^+ during a large impact-parameter encounter. The high sensitivity of lasing power to the pressure of B atom precursors suggests that populating the upper lasing level competes with other B atom or B^+ reactions.

REFERENCES

1. S. H. Bauer, G. Herzberg and J. W. C. Johns, J. Mol. Spec., 13, 256 (1964).

2. B. de B. Darwent, "Bond Dissociation Energies in Single Molecules", NSRDS-NBS 31, January 1970.

3. C. Moore, "Atomic Energy Levels", Vol. I, Circular No. 467, p.16, 1949.

4. E. Edlén, A. Ölme, G. Herzberg and J. W. C. Johns, J. Opt. Soc. Am., 60, 889 (1970).

LEGENDS FOR FIGURES

Figure 1.   Oscilloscope traces of detector signal for two pulses of radiation

at 2777 cm^{-1}; 20 μs/div.

Figure 2.   Delay (in μs) for onset of lasing, following the initiating pulse

discharge, for a range of He pressures.

Figure 3.   Relative power output as a function of impressed voltage, for a

sequence of He pressures.

(20 µs/div)

t →